MODELING OF SELECTIVE CATALYTIC REDUCTION (SCR) OF NITRIC OXIDE WITH AMMONIA USING FOUR MODERN CATALYSTS

A Thesis

by

GIRIRAJ SHARMA

Submitted to the Office of Graduate Studies of
Texas A&M University
in partial fulfillment of the requirements for the degree of

MASTER OF SCIENCE

August 2004

Major Subject: Mechanical Engineering

MODELING OF SELECTIVE CATALYTIC REDUCTION (SCR) OF NITRIC OXIDE WITH AMMONIA USING FOUR MODERN CATALYSTS

A Thesis

by

GIRIRAJ SHARMA

Submitted to the Office of Graduate Studies of
Texas A&M University
in partial fulfillment of the requirements for the degree of

MASTER OF SCIENCE

Approved as to style and content by:

Jerald A. Caton (Chair of Committee)	A. Beskok (Member)
D. W. Goodman (Member)	Dennis O'Neal (Head of Department)

August 2004

Major Subject: Mechanical Engineering

ABSTRACT

Modeling of Selective Catalytic Reduction (SCR) of Nitric Oxide with Ammonia Using Four Modern Catalysts. (August 2004)

Giriraj Sharma, B. Tech., Indian Institute of Technology, Bombay

Chair of Advisory Committee: Dr. Jerald A. Caton

In this work, the steady-state performance of zeolite-based Cu-ZSM-5, vanadium based honeycomb monolith catalysts (V), vanadium-titanium based pillared inter layered clay catalyst (V-Ti PLIC) and vanadium-titanium-tungsten-based honeycomb monolith catalysts (V-Ti-W) was investigated in the selective catalytic reduction process (SCR) for NO removal using NH_3 in presence of oxygen. The objective is to obtain the expression that would predict the conversion performance of the catalysts for different values of the SCR process parameters, namely temperature, inlet oxygen concentration and inlet ammonia concentration.

The NO_x emission, its formation and control methods are discussed briefly and then the fundamentals of the SCR process are described. Heat transfer based and chemical kinetics based SCR process models are discussed and widely used rate order based model are reviewed.

Based on the experimental data, regression analysis was performed that gives an expression for predicting the SCR rate for the complete temperature range and the rate order with respect to inlet oxygen and ammonia concentration. The average activation energy for the SCR process was calculated and optimum operating conditions were determined for each of the catalyst.

The applicable operating range for the catalyst depends on the NO conversion as well as on the ammonia slip and the N_2O and NO_2 emission. The regression analysis was repeated for the applicable range and an expression was obtained that can be used to estimate the catalyst performance.

For the Cu-ZSM-5, the best performance was observed for 400^{o}C, 660 ppm inlet ammonia concentration and 0.1% inlet oxygen concentration. For the V based honeycomb monolith catalyst, the best performance was observed for 300^{o}C, 264 ppm inlet ammonia concentration and 3% inlet oxygen concentration. For the V-Ti based PLIC catalyst, the best performance was observed for 350^{o}C, 330 ppm inlet ammonia concentration and 3% inlet oxygen concentration. For the V-Ti-W based honeycomb monolith catalyst, the best performance was observed for 300^{o}C, 330 ppm inlet ammonia concentration and 3% inlet oxygen concentration. The conversion performance of all of these catalysts is satisfactory for the industrial application. At the operating conditions listed above, the N_2O emission is less than 20 ppm and the NO_2 emission is less than 10 ppm.

The results were validated by comparing the findings with the similar work by other research groups. The mechanism of SCR process is discussed for each of the catalyst. The

probable reactions are listed and adsorption and desorption process are studied. The various mechanisms proposed by the researchers are discussed briefly.

It is concluded that V-Ti-W and Cu-ZSM-5 catalyst are very promising for SCR of NO_x. The expressions can be used to estimate the conversion performance and can be utilized for optimal design and operation. The expressions relate the SCR rate to the input parameters such as temperature and inlet oxygen and ammonia concentration hence by controlling these parameters desired NO_x reduction can be achieved with minimal cost and emission.

DEDICATION

I would like to dedicate this thesis to my parents who have been a major influence in my life and have supported me wholeheartedly in all my endeavors. I would also like to dedicate the thesis to my two sisters, who have been among my best friends and whose encouragement has kept me going throughout my life as a student.

ACKNOWLEDGEMENTS

I would like to thank my advisor, Dr. Jerald A. Caton, for his constant support and encouragement throughout the course of this work. I would also like to thank Mr. S. Gupta and Mr. H. Oh for providing the necessary experimental data. Finally, and most importantly, thanks are due to my father, mother and sisters for their constant support and encouragement.

TABLE OF CONTENTS

Page

Page

LIST OF FIGURES

Page

Page

Page

LIST OF TABLES

Page

Page

Page

1. INTRODUCTION

The requirement for energy has grown exponentially over the past decades owing to industrialization and subsequent lifestyle changes. Much of this energy is generated by combusting fossil fuels such as coal, natural gas, gasoline and diesel. The combustion process releases the chemical energy contained in the fuels as thermal energy, which is used to run different power cycles depending upon the application. The combustion process involves complex chemical reactions; the reactants are fuel and air, and the products include various species such as water, oxides of carbon, nitrogen and sulfur, unburned fuel, organic compounds and particulate matter. Some of these species have a harmful effect on the living beings and environment and hence are termed as pollutants.

1.1 NO_x: A Severe Air Pollutant

Oxides of nitrogen, NO_x (NO and NO_2), pose a substantial environmental hazard. NO_x in combination with other air pollutants such as SO_2 and volatile organic compounds contributes to acid rain, ground-level ozone and photochemical smog [1] The term 'NO_x' usually refers to the two most common oxides of nitrogen; namely NO – nitric oxide and NO_2 – nitrogen dioxide. Among them, NO is of primary concern because of its high concentration relative to NO_2 in the exhaust. It is the oxidation of NO to NO_2 that forms a part of the process that results in the creation of ozone in the lower level of the atmosphere [2] Though ozone present in the upper-level of the atmosphere adsorbs the harmful ultraviolet rays from the sun, ground-level ozone causes human respiratory problems [3] Like CO, the oxides of nitrogen tend to combine with the hemoglobin in the blood. However, probably the most undesirable toxic effect of oxides of nitrogen is their tendency to join with the moisture in the air to from dilute nitric acid. Because the amounts formed are minute and dilute, the effect is very small but over a long period of time can be cumulatively undesirable, especially for humans having respiratory problems. Oxides of nitrogen are a component of photochemical smog. Low concentrations of NO_2 are sufficient to cause lung irritation, tissue damage and irritation of mucous membranes. It is a moderate irritant to the eyes and nose, and can cause coughing, frothy sputum, dyspnea (shortness of breath), chest pain, pulmonary edema, cyanosis, tachypnea, tachycardia (relatively rapid heart action), and eye irritation. NO modifies the function of lungs and irritates human mucous. Exposure to nitrous oxide (N_2O), a byproduct of reactive gases in the atmosphere and nitrogen dioxide (NO_2), causes reproductive impairment [4]

This thesis follows the format and style of Catalysis Today.

In view of these harmful effects on living beings and the environment, the emissions of NO_x have been regulated. Federal laws require that for power plants, the emission levels of NO_x be reduced by 73% by year 2018 while for heavy duty engines, the NO_x emission levels have to be reduced by 90% by year 2007 [5] Table 1.1 lists the current and upcoming NO_x emission standards for the heavy duty engines. The NO_x emission would have to be reduced drastically from 4 grams per bhp-hour to 0.2 grams per bhp-hour.

Table 1.1 NO_x Emission Standards for Heavy Duty Engines [5]

Current standards	2007 standards
4 g/bhp-hr	0.20 g/bhp-hr

Table 1.2 lists the current and upcoming NO_x emission standards for power plants. The NO_x emission would have to be reduced from a total of 5.1 million tons to 2.1 million tons per year by 2008 and then to 1.7 million tons per year by 2018.

Table 1.2 NO_x Emission Levels and Upcoming Standards for Power Plants [5]

Actual Emission (in 2000)	First Phase of Reductions (by 2008)	Second Phase of Reductions (by 2018)
5.1 million tons per year	2.1 million tons per year	1.7 million tons per year

The adopted emission regulations pose significant technological challenges. The conventional methods being used for emission control in the automotive and power sector will no longer be sufficient to reduce the emissions to such low levels. Large scale implementation of the new emission control technology such as SCR requires substantial research and development work. The NO_x formation mechanism must be understood and pre-combustion emission control techniques must be used to minimize the NO_x formation, and then post-combustion techniques can be employed to reduce the NO_x emission to acceptable levels.

1.2 NO_x Formation

Almost half of all anthropogenic NO_x emissions come from mobile sources, mainly internal combustion engines while the remainder comes from stationary sources, mainly combustion of fuels in power stations and industrial boilers [6]

NO_x formation mainly occurs through three mechanisms – Thermal NO_x, Fuel NO_x, and Prompt NO_x. In thermal NO_x process, reactions occurring at high temperatures during combustion processes generate both oxygen and nitrogen atoms by dissociation of respective molecules

which subsequently lead to the formation of NO [7] The quantity of NO_x formed depends on the reaction temperature, residence time, local stoichiometric composition and turbulence [8] Three main reactions leading to the formation of thermal NO are described by the Zeldovich mechanism as below:

$$O + N_2 \Leftrightarrow N + NO \quad (1)$$

$$N + O_2 \Leftrightarrow O + NO \quad (2)$$

$$N + OH \Leftrightarrow H + NO \quad (3)$$

Although the rate of formation of thermal NO_x is slow in comparison to the other processes, it is the largest contributor to the total NO_x formed [9]

In fuel NO_x process, reaction occurs with fuel bound nitrogen at relatively low temperatures [10] Between 20 and 80 percent of the bound nitrogen is typically converted to NO_x depending on fuel pyrolysis and subsequent reaction between many intermediate nitrogenous species and the oxidant species.

In the prompt NO_x process, chemical reactions in thin oxygen-poor flame layers of premixed combustion produce HC radicals which form cyanides together with nitrogen that ultimately form NO_x [11]

1.3 NO_x Control

Methods of NO_x control can be categorized as pre- and post-combustion methods. In applications involving internal combustion engines, NO_x control is achieved by a number of techniques such as modification of the compression ratio, equivalence ratio and the use of EGR (Exhaust Gas Recirculation). These methods try to keep the combustion temperature low and are classified as pre-combustion techniques. The amount of NO_x reduction achieved through these methods is extremely limited and is insufficient for compliance with the stringent regulations. Post-combustion methods (also known as after-treatment methods) are more effective in this regard and are therefore relatively more popular and are discussed in next few paragraphs [12]

1.3.1 Non-selective Catalytic Reduction (NSCR)

In this process, hydrogen, natural gas or naphtha reacts with the NO_x and the free oxygen in the exhaust gas over a platinum, rhodium or palladium catalyst. The nitrogen dioxide is reduced first and if the reduction is not taken further, the process merely decolorizes the gas (incomplete reduction of NO_2, NO is formed instead of N_2) according to the reactions: -

$$CH_4 + 2O_2 \rightarrow CO_2 + 2H_2O \quad (4)$$

$$CH_4 + 4NO_2 \rightarrow CO_2 + 2H_2O + 4NO \quad (5)$$

when methane is used.

$$2H_2 + O_2 \rightarrow 2H_2O \quad (6)$$

$$H_2 + NO_2 \rightarrow H_2O + NO \quad (7)$$

when hydrogen is used.

An excess of the reducing agent is required to reduce nitrogen oxides to nitrogen. This may result in a high temperature gas containing methane and naphtha and also, when hydrocarbons are used, the release of carbon monoxide and hydrocarbons into the atmosphere:-

$$CH_4 + 4NO \rightarrow O_2 + 2H_2O + 2N_2 \quad (8)$$

$$CH_4 + 4\ N_2O \rightarrow CO_2 + 2H_2O + 4N_2 \quad (9)$$

when methane is used.

$$2H_2 + 2NO \rightarrow 2H_2O + N_2 \quad (10)$$

$$H_2 + N_2O \rightarrow H_2O + N_2 \quad (11)$$

when hydrogen is used.

The exhaust gas has to be pre-heated to a minimum of 300°C with hydrogen or 550°C with methane for efficient operation of the NSCR catalyst. The reactant gas is mixed with the pre-heated exhaust gas and the mixture is passed into a reactor containing the catalytic bed [13]

The advantages of NSCR are: -

– Substantial N_2O reduction

– The low cost and the availability of the reducing agent (especially in a fertilizer plant)

– The possibility to act only as a decolorizing unit

The disadvantages are: -

– The release of ammonia and also carbon monoxide, carbon dioxide and unburned hydrocarbons if a hydrocarbon reducing agent is used

– The exhaust gas has to be preheated to high temperatures unless hydrogen is used as the

reducing agent

– The impossibility of starting the NSCR until the oxygen content has stabilized

1.3.2 Selective Catalytic Reduction (SCR)

In selective catalytic reduction ammonia reacts with nitric oxide and nitrogen dioxide. The reactions involved are:-

$$6NO + 4NH_3 \rightarrow 5N_2 + 6H_2O \quad (12)$$

$$4NO + 4NH_3 + O_2 \rightarrow 4N_2 + 6H_2O \quad (13)$$

$$6NO_2 + 8NH_3 \rightarrow 7N_2 + 12H_2O \quad (14)$$

Vanadium pentaoxide, platinum, iron/chromium oxides and zeolites are among the catalysts that can be used. The operating temperature is generally above 200°C and operating pressure has only a minor effect on overall efficiency.

The exhaust gas is pre-heated (if required) to a minimum temperature for good operation of the SCR catalyst. The reactant gas is mixed with the pre-heated exhaust gas and the mixture passed into a reactor containing the catalyst bed.

The advantages of the SCR system are:-

– A low NO_x content can be achieved

– Operating temperatures are lower

– Ammonia concentration in the exhaust is minimal

The disadvantages of the SCR system are:-

– High capital cost

– Catalyst aging and poisoning

1.3.3 Selective Non-Catalytic Reduction (SNCR)

Though selective in nature, this process is different from the SCR since a catalyst is not used. The NO_x are reduced while the reducing agent like HC and NH_3 are oxidized.

The two techniques, Selective Catalytic Reduction and Selective Non-Catalytic Reduction, are compared in table 1.3.

Table 1.3 Comparisons of the SCR and the SNCR Techniques [14]

Features	SCR	SNCR
NO_x removal efficiency (%)	70 – 90	30 – 80
Operating temperature (°C)	200 – 500	800 – 1100
NH_3/NO molar ratio	0.4 – 1.0	0.8 – 2.5
NH_3 slip (ppm)	< 5	5 – 20
Capital cost	High	Low
Operating cost	Moderate	Moderate

From the table, it can be concluded that in comparison with SNCR, the SCR process has the advantage of higher NO_x removal efficiency at relatively lower operating temperatures. The disadvantage with using the SCR technique is the high capital cost in comparison with SNCR. Though an SCR system is generally designed to reduce NO_x emissions by 70–90%, higher reductions are possible. In the SCR process, several different catalysts e.g. metal-supported zeolites, mono-crystal and mixed phase catalysts, etc. operating over varying temperature windows can be used.

2. SCR PROCESS

The computer simulation and mathematical modeling of the physical and chemical processes involved in catalysis has a wide range of uses. Firstly, mathematical modeling can be used to study the phenomena involved in a catalytic process and gain further understanding of the system without the need for costly, time-consuming experimentation. Secondly, it can be used to obtain values of physical parameters that are very difficult or impossible to obtain by experiment because they are present in highly convoluted form in the data. Thirdly, modeling can be used in the interpretation of experiments.

Prior to modeling the SCR process, it must first be understood in its entirety. Unlike an elementary single step of a gas phase chemical reaction, a catalytic reduction process involves several reaction steps that represent different physical and chemical processes. These processes can be independent, i.e. taking place in parallel, regardless of the other processes or dependent, i.e. taking place in series, one using up the product(s) of the process concluding before it. To model such a process requires a thorough understanding of the underlying chemistry, and of the chemical and mechanical engineering principles.

The role of a catalyst in the reduction process, the general catalytic reduction mechanism and elementary reaction steps in a catalytic process are discussed in the following subsections.

2.1 Role of a Catalyst

A catalyst is generally defined as a substance that alters the speed of a reaction but does not itself undergo any chemical change. The presence of a catalyst leads to a mechanism having a lower energy barrier than the barrier that exists when the reaction occurs in the absence of the catalyst. This is graphically illustrated with figure 2.1.

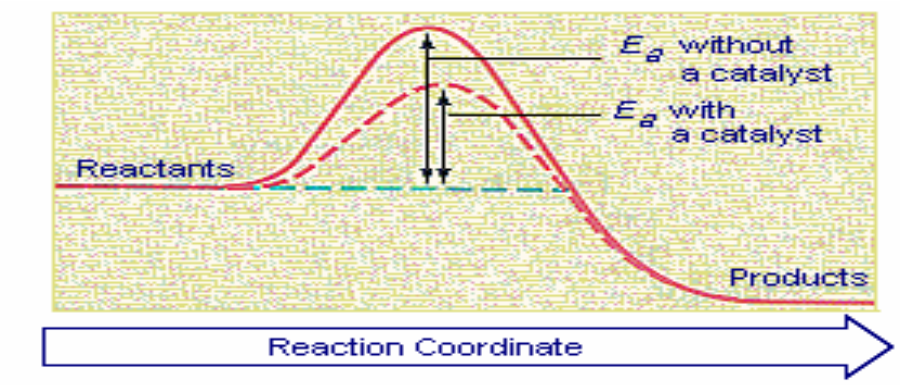

Fig 2.1 Altering of Chemical Pathway by Using a Catalyst

The primary role of the catalyst is to change the mechanism to one with lower activation energy hence enabling the reaction to take place at higher rates at lower temperatures.

2.2 Reduction Mechanism

Modern industry is characterized by the almost exclusive use of continuous processes. This type of operation calls for continuous flow reactors. The chemical reactions occur while the reacting stream is flowing through the reactor containing the catalyst. The conversion of the reacting stream through the reactor is proportional to the length of time the reacting mixture resides in the reactor, which in turn is proportional to the reactor volume. The process can be classified as adiabatic or isothermal, steady state or unsteady state or based upon particular mixing model assumed for the fluid within the reactor.

The development of models for catalytic reactors is based on the postulate that the following steps are required for a chemical reaction to occur:

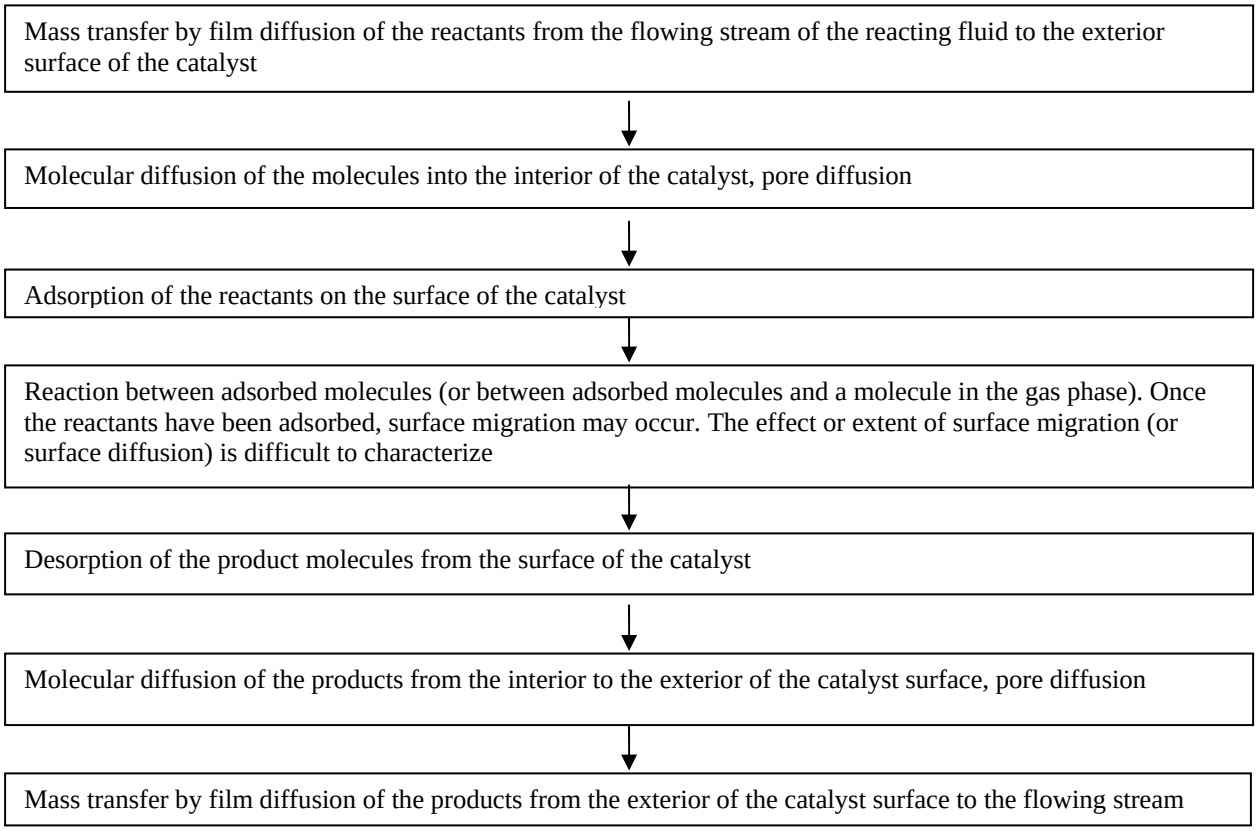

These seven steps occur in series, and for a flow process to be at steady state operation, the individual rates must be equal; provided that each rate is stated on the same basis.

2.3 Reaction Rates

Based on above discussion on the reaction mechanism, it might appear possible to develop a rate equation involving the individual rate constants (or resistances) for each step and the overall potential in a manner analogous to that used to develop the heat transfer equation:

$$\dot{Q} = UA\,\Delta T \tag{15}$$

Analogous to the term "ΔT" for the heat transfer process, the driving forces for a catalytic reduction process are the species concentration gradients and the difference in the energy levels of the products and the reactants. The heat transfer coefficient “U” corresponds to a reaction rate coefficient that will be determined by the resistance to the physical and chemical processes for a given catalytic reduction process. That resistance will be a function of physical and chemical parameters of the system such as binary diffusion coefficients and individual reaction rate coefficients [15]

However, it is generally impossible to obtain an expression parallel to (15) because of the impossibility of stating the individual rate expressions in the explicit forms. Because of the complexity of the process, working expressions for the reaction rates are commonly based on the rate expression for the “rate controlling step”, the step having the smallest rate constant. (This step is sometimes called the slowest rate in spite of the fact that the rates of individual steps are equal at steady state). The “rate controlling step”, that can be the diffusion rate or the adsorption rate or the chemical reaction rate. Depending upon the process to be modeled (with parameters like the gas composition, catalyst, temperature, flow rates, application, catalyst aging, pretreatment), various specifically tailored expressions have been proposed. A most probable mechanism for the process is assumed and then experiments are conducted to validate the assumptions, based on the outcome of these experiments, the postulates are refined and the expressions are modified till an acceptable level of accuracy is obtained.

3. OBJECTIVES

Although some of the previous studies have modeled the selective catalytic process, the catalytic reduction of nitric oxide with ammonia as a reducing agent in presence of oxygen over four catalysts, a Copper exchanged form of the zeolite ZSM-5 honeycomb monolith catalyst, henceforth referred as Cu-ZSM-5, Vanadium oxide based honeycomb monolith catalyst, henceforth referred as V and Vanadium, Titanium and Tungsten oxide based honeycomb monolith catalyst, henceforth referred as V-Ti-W and a Vanadium and Titanium based pillared inter layered clay catalyst, henceforth referred as V-Ti PLIC remains to be modeled.

For practical applications, it is desirable to have an expression for the catalytic reduction rate, an expression that would predict the conversion performance for different operating conditions such as temperatures and concentrations. The four different catalysts in consideration have shown great promise in reducing the NO_x emissions and are expected to be installed at various sites in the near future. If a rate expression is available then a converter system with any of these catalysts can be optimally controlled to minimize the cost and the emissions.

4. LITERATURE REVIEW

One of the many challenges of modeling catalytic converters is that the conversion performance and thermal response are coupled. The rates of chemical reactions in converters are highly nonlinear functions of temperature. Conversely, heat release during the reactions contributes to the thermal response. This coupling implies that a realistic converter model must solve the chemical and thermal problem simultaneously. Complex physical phenomenon occurring in a converter include the heat and mass transfer between the gas and the catalyst surface, convective heat and mass transport, chemical reactions and the attendant heat release, heat conduction in the substrate and the heat loss to the surroundings. To further complicate the situation, the problem is three-dimensional in nature; the converter structure itself is three-dimensional and so is the nature of the heat and mass transfer processes.

Hence, a model should include all three-dimensions. It should simulate the thermal and conversion characteristics of non-adiabatic monolith converters operating under flow misdistribution conditions. The model should account for convective heat and mass transport, gas-solid conduction, chemical reactions and the attendant heat release, and the heat loss to the surroundings. The transient regime of the catalytic conversion process should also be accommodated.

For the monolith catalytic converter, it is necessary to include energy and reaction species balances in the gas stream and the catalyzed wall during the exothermic chemical reactions. Outside the catalyzed monolith, the only phenomenon is heat conduction through the surrounding materials. Gas temperature, concentration and mass flux will be functions of position y and z at the monolith front face that depends on the assumed mixing model.

For most practical applications, the choice is between a plug flow model, perfectly mixed flow model, laminar flow model, partial axial mixing model and partial axial and radial mixing model. In the plug flow model, the mixing is assumed to be perfect in the radial direction and negligible in the axial direction. For perfectly mixed model, the properties are the same throughout the volume. In the laminar flow model, there is no mixing in the radial and axial directions.

The choice of the mixing model depends on the particular operating conditions of the catalytic converter. The plug flow or the laminar flow assumptions should give sufficiently accurate results for most practical setups, and if assumption of the flow profile leads to unacceptable model performance then more sophisticated models like the partial axial and partial radial mixing model can be used.

Preferably the mixing model should depict the physical system as accurately as possible but corresponding increase in model complexity and computational requirements limit how real the model can be. Knowledge of the physical system, the process and fluid mechanics can be applied to make simplifying assumptions on a case by case basis.

4.1 Mathematical Modeling

The basic principles of heat transfer, mass transfer and conservation can be applied to a given catalytic converter system and a mathematical representation of the physical system can be obtained. Two representative models will be documented and discussed in the following sections. The first model primarily applies the heat transfer fundamentals while the second model depends upon the chemical kinetics information to determine the catalytic converter behavior.

4.1.1 Heat Transfer Based Model

The heat conduction equation for the surrounding materials can be expressed as:

$$\rho \frac{\partial (CT)}{\partial t} = \lambda_x \frac{\partial T^2}{\partial x^2} + \lambda_y \frac{\partial T^2}{\partial y^2} + \lambda_z \frac{\partial T^2}{\partial z^2} \tag{16}$$

Subjected to the initial condition:

$$T(x,y,z,0) = T_o(x,y,z) \tag{17}$$

And the boundary condition for convection and radiation:

$$\lambda_n \frac{\partial T}{\partial n} = h_c (T - T_a) + h_r (T^4 - T_a^4) \tag{18}$$

For the reaction/transport phenomenon in the catalyzed monolith, this transient three-dimensional model includes the effects of transverse heat flux and non-uniform gas flow distribution. The mass and energy balances in the gas and solid phase are:

$$\varepsilon \rho_g \frac{\partial C_{g,i}}{\partial t} = -w \frac{\partial C_{g,i}}{\partial x} - \rho_g k_{m,i} S (C_{g,i} - C_{s,i}) \Big|_{y,z} \tag{19}$$

$$\varepsilon \rho_g C_{P_g} \frac{\partial T_g}{\partial t} = -w C_{P_g} \frac{\partial T_g}{\partial x} - hS (T_s - T_g) \Big|_{y,z} \tag{20}$$

$$\frac{M}{\rho_g} a(x) R_i (C_s, T_s) = k_{m,i} S (C_{g,i} - C_{s,i}) \Big|_{y,z} \tag{21}$$

$$(1-\varepsilon)\rho_s \frac{\partial (C_s T_s)}{\partial t} = (1-\varepsilon)\left(\lambda_x \frac{\partial T_s^2}{\partial x^2} + \lambda_y \frac{\partial T_s^2}{\partial y^2} + \lambda_z \frac{\partial T_s^2}{\partial z^2} \right) + hS (T_g - T_s) + a(x) \sum - \Delta H_i R_i (C_s - T_s) \tag{22}$$

The axial diffusion of mass and heat, and the chemical reactions in the gas phase are neglected. Moreover, the time derivative terms (in equation 22) involving the gas phase are discarded since the time constants involved are typically much smaller than that of the solid thermal response. Heat exchange between the substrate and the surroundings at the both inlet and the outlet faces of the monolith is neglected.

The appropriate initial and boundary conditions for the model become:

$$\mathrm{T_s}\,(\mathrm{x,y,z,0}) = \mathrm{T_{s_o}}\,(\mathrm{x,y,z}) \tag{23}$$

$$C_{g,i}(x_{in}, y, z, t) = C_{g,i}^{in}(y, z, t) \tag{24}$$

$$\frac{\partial T_s(x_{in}, y, z, t)}{\partial x} = 0 \tag{25}$$

$$w(x, y, z, t) = w^{in}(y, z, t) \tag{26}$$

$$\frac{\partial T_s(x_{out}, y, z, t)}{\partial x} = 0 \tag{27}$$

Heat and mass transfer coefficients between the bulk stream and the catalyst surface are estimated from the Nusselt and the Sherwood numbers for the fully developed laminar flow (no mixing between the adjacent layer of the fluid and invariant flow profile as a Function of time) with constant wall heat flux in the monolith channels. It is required to obtain the values for the D_i and λ_g, and then the expressions given below can be used to evaluate the heat and mass transfer coefficient values.

$$h = \frac{Nu_\infty \lambda_g}{2R_h} \tag{28}$$

$$k_{m,i} = \frac{Sh_\infty D_i}{2R_h} \tag{29}$$

The heat and mass transfer coefficients calculated above neglect the variance within the developing laminar flow regime near the monolith inlet because the length of this hydrodynamic entrance region is typically a small fraction of the total monolith length.

Thus the model comprises eleven coupled non-linear, three-dimensional partial differential equations (16 and 19-22). The numerical solution of these equations is a considerable challenge [16]

It was noted that the model equations are simplified versions of the more general heat conduction equations with a heat source function and hence can be expresses in a more compact form as:

$$\rho_s \frac{\partial(C_s T_s)}{\partial t} = \left(\lambda_x \frac{\partial T_s^2}{\partial x^2} + \lambda_y \frac{\partial T_s^2}{\partial y^2} + \lambda_z \frac{\partial T_s^2}{\partial z^2} \right) + F_1(T_s, T_g, C_s) \tag{30}$$

$$\frac{dC_g}{dx} = F_2(T_g, C_g, C_s)\Big|_{y,z} \tag{31}$$

$$\frac{dT_g}{dx} = F_3(T_g, T_s)\Big|_{y,z} \tag{32}$$

$$0 = F_4(T_g, T_s, C_g, C_s)\Big|_{y,z} \tag{33}$$

Where function F_1, F_2, F_3 and F_4 are algebraically determined from equations (19-22).

A one-dimensional model based on a similar approach was developed to reduce the calculations to manageable proportion [17] For this model, the equations for the gas phase reduce to:

$$-\varepsilon V_{avg} \rho_g C_{P_g} \frac{\partial T_g}{\partial x} - hS(T_g - T_w) = \varepsilon \rho_g C_{P_g} \frac{\partial T_g}{\partial t} \tag{34}$$

$$-\varepsilon V_{avg} \frac{\partial C_g}{\partial x} - k_m S(C_w - C_g) = \varepsilon \frac{\partial C_g}{\partial t} \tag{35}$$

The model equations for the solid phase:

$$-rS\Delta H + hS(T_g - T_w) = \rho_w C_{P_w} \frac{\partial T_w}{\partial t} \tag{36}$$

$$\frac{\rho_g k_m}{M_g}(C_g - C_w) = r \tag{37}$$

At steady state

$$\frac{dC_g}{dX^*} = \frac{Sh}{Le}\left(C_w - C_g\right) \tag{38}$$

Where

$$X^* = \frac{4x/D}{\mathrm{Re}\,\mathrm{Pr}} \quad \text{(Graetz number)} \tag{39}$$

For adiabatic temperature rise:

$$T_g^{i+1} = T_g^i + \frac{\Delta HC_g^i}{M_g C_{P_g}}\left(1 - \frac{C_g^{i+1}}{C_g^i}\right) \tag{40}$$

$$T_w^{i+1} = T_g^i + \frac{\Delta HC_g^i}{M_g C_{P_g}}\left(1 - \frac{C_g^{i+1}}{C_g^i}\right) + \frac{LeSh}{Nu}\left(\frac{C_g^{i+1} - C_w^{i+1}}{C_g^i}\right) \tag{41}$$

Another model similar to the one above also took into account the heat loss to the ambient and the gas-louver (both open ends of the converter casing) heat transfer. The natural convection and radiation dominate the heat transfer process between the converter external wall and the ambient. The heat loss to the ambient is less important in a radial flow converter and for an axial flow converter; it will depend on the radial distribution of temperature of the gas, the gas flow rate, the bed temperature, the ambient temperature and the air circulation around the converter. Heat resistance for this process is dominated by the air film adjacent to the external wall of the converter and by the thin layer of the catalyst adjacent to the inner wall of the converter. The calculations show that including the ambient heat loss in the model does not make a significant difference (±5 ppm, which is within the experimental error). If the catalyst has sufficiently high activity and moderate working temperature, the heat loss can be neglected.

Similarly the effect of gas-louver heat transfer can be ignored since increasing the heat transfer by a factor of 200 changed the outlet concentration values by less than 5 ppm [18]

4.1.2 Chemical Kinetics Based Model

Representative software “CRESLAF” marketed by Reaction Design, Inc., is used for modeling laminar, chemically reacting, boundary-layer flow in cylindrical or planar channels.

CRESLAF predicts the velocity, temperature, and species profiles in two-dimensional (planar or axisymmetric) channels. Applications of CRESLAF include chemical vapor deposition (CVD) reactors, heterogeneous catalysis on reactor walls, and corrosion processes. The application accounts for finite-rate gas-phase and surface chemical kinetics and molecular transport. The model employs boundary-layer approximations for the fluid-flow equations, coupled to gas-phase and surface species continuity equations.

CRESLAF solves the boundary-layer equations for the fluid flow coupled with species equations. These equations describe chemical species production and destruction, and both convective and diffusive transport. The applicability of the equations relies on the existence of a principal flow direction in which diffusive transport is negligible compared to convective transport [19]

The set of equations describing the CRESLEF model is presented below.

Momentum equation

$$\rho u\frac{\partial u}{\partial x}-\frac{\rho u}{\dot{m}}\left(\xi\frac{d\dot{m}}{dx}-\frac{d\dot{m}_l}{dx}\right)\frac{\partial u}{\partial \xi}+\frac{dP}{dx}=\frac{\rho u}{\dot{m}^2}\frac{\partial}{\partial \xi}\left(\rho u\mu y^{2\alpha}\frac{\partial u}{\partial \xi}\right)+g(\rho_i-\rho) \tag{42}$$

Species equation

$$\rho u\frac{\partial Y_k}{\partial x}-\frac{\rho u}{\dot{m}}\left(\xi\frac{d\dot{m}}{dx}-\frac{d\dot{m}_l}{dx}\right)\frac{\partial Y_k}{\partial \xi}=\dot{\omega}_k W_k-\frac{\rho u}{\dot{m}}\frac{\partial}{\partial \xi}\left(\rho y^{\alpha}Y_k V_{k,y}\right) \quad ; \quad k = 1,\ldots, K_g \tag{43}$$

Energy equation

$$\rho uC_p\frac{\partial T}{\partial x}-\frac{\rho uC_p}{\dot{m}}\left(\xi\frac{d\dot{m}}{dx}-\frac{d\dot{m}_l}{dx}\right)\frac{\partial T}{\partial \xi}=\frac{\rho u}{\dot{m}^2}\frac{\partial}{\partial \xi}\left(\rho u\mu y^{2\alpha}\frac{\partial T}{\partial \xi}\right)-\sum_{k=1}^{K_g}\dot{\omega}_k W_k h_k-\frac{\rho^2 u y^{\alpha}}{\dot{m}}\sum_{k=1}^{K_g}Y_k V_{k,y}C_{pk}\frac{\partial T}{\partial \xi} \tag{44}$$

State equation

$$P=\frac{\rho RT}{\overline{W}} \tag{45}$$

Two different transport models can be used. In case of multi-component transport model, the diffusion velocity is given by

$$V_{k,y}=\frac{\rho u y^{\alpha}}{X_k\overline{W}\dot{m}}\sum_{j\neq k}^{K_g}W_j D_{k,j}\frac{\partial X_k}{\partial \xi}-\frac{D_k^T}{\rho Y_k}\frac{\rho u y^{\alpha}}{T\dot{m}}\frac{\partial T}{\partial \xi} \tag{46}$$

While when mixture-averaged transport is used, the diffusion velocity is expressed as

$$V_{k,y}=\frac{D_{km}\rho u y^{\alpha}}{X_k\dot{m}}\frac{\partial X_k}{\partial \xi}-\frac{D_k^T}{\rho Y_k}\frac{\rho u y^{\alpha}}{T\dot{m}}\frac{\partial T}{\partial \xi} \tag{47}$$

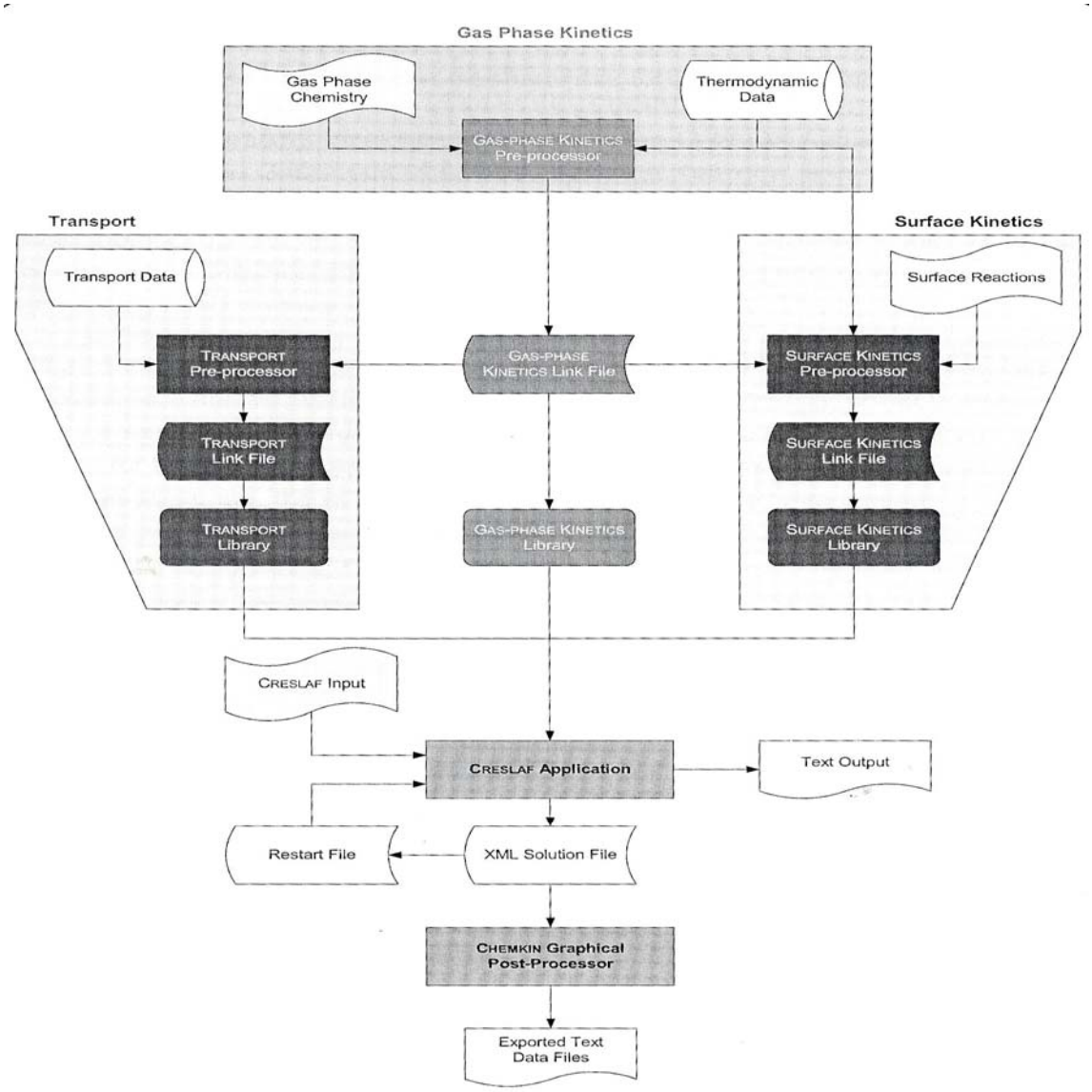

Fig 4.1 Flow Diagram for CRESLAF [19]

Initial and boundary conditions are applied and this set of differential/algebraic equation (DAEs) is solved using numerical software DASSL (Differential Algebraic System Solver, a software available in public domain). At the entrance to the reactor channel, the initial profiles of u, T and Y_k, the pressure and the surface site fraction z_k must be specified. The schematic flow diagram for the CRESLAF is presented in the figure 4.1.

The major limitation of this method is that the chemical kinetics data and the thermodynamic data required for the software is mostly unavailable. Any chemical species that appears in a problem must have thermodynamic data associated with it. For the calculation purposes, it is required to have the fits for specific heats, enthalpy and entropy for each and every

species. This data may or may not be available. The input file to the software requires the complete set of reactions taking place in the gas phase and at the surface, complete with the kinetics data such as three Arrhenius coefficients (pre-exponential factor, temperature exponent and activation energy) for each and every reaction. To conclusively determine a reaction mechanism for the catalytic process is itself a very involved process and then to come up with such detailed kinetics data for each of the species and reactions is almost impossible. That requires a comprehensive experimentation, analysis and data manipulation which means years of focused research work and even then the cumulative uncertainty may grow to undesirable levels.

4.1.3 Rate Order Based Models

Though comprehensive models are preferable, it is not always possible to find solutions to these models because of data unavailability, computational requirements, and non-convergence to state a few reasons. Fortunately certain assumptions can be made which suggests that the rate equation should model the process accurately enough for practical applications. Eng et al. (1997) found that that isothermality and other simplified assumptions could be justified for the SCR application under some conditions. For a power plant, if NO is reduced from 500 to 100 ppm, the maximum temperature rise will be 5.1^{o}C and for an automotive catalytic converter, assuming 100 percent conversion for a 1000 ppm inlet NO, the maximum temperature rise is 12.8^{o}C. Consequently, we can allow isothermality as a simplifying assumption that is an important step for the rate order modeling method [20] Most of the models are based on such simplifying assumptions and adopt a rate equation which is a function of the rate constants and the reactant concentrations.

For nitric oxide reduction by hydrocarbons over Cu-ZSM-5 monolith catalysts under lean conditions, the reaction rate is of first order as a Function of NO in the low concentration regime and is of zero order in the high concentration regime. During the experimentation, the temperature was varied from 200 to 600^{o}C, NO concentration was 230 ppm, oxygen concentration was 7% and 800 ppm of C_3H_6 or 1200 ppm of C_2H_4 was used. The rate expression given was R = k θ, where k and θ are decomposition rate and surface coverage of NO respectively. When adsorption equilibrium of Langmuir type is established on the surface, the reaction rate is given by $R = \frac{kKC}{1+KC}$, where K is the adsorption equilibrium constant and C is the gas phase concentration of NO [21]

A similar model based on experimental data with a pressure of 1.6 bar, temperatures of 200-300^{o}C, 500 ppm of NO, 600 ppm of NH_3, 2% oxygen and 10% water, adopted a Rideal type rate equation, $R_{NO} = k_c C_{NO} \frac{K_{NH_3} C_{NH_3}}{1 + K_{NH_3} C_{NH_3}}$, which is in line with mechanistic and kinetic

evidence concerning the role of strongly adsorbed ammonia in the catalytic reduction of NO when V-Ti-W oxide catalysts are used [22]

Another research group conducted experiments temperatures of 200-500^{o}C, 500 ppm of NO, 500 ppm of NH_3, 14% oxygen and 5% water and used slightly modified rate expressions for V_2O_5-WO_3/TiO_2 Catalyst:

$$-R_{NO} = \frac{k_{NO}C_{NO}K_{NH_3}C_{NH_3}}{1+K_{NH_3}C_{NH_3}} - \frac{k_{NH_3}K_{NH_3}C_{NH_3}}{1+K_{NH_3}C_{NH_3}} \tag{48}$$

$$-R_{NH_3} = \frac{k_{NO}C_{NO}K_{NH_3}C_{NH_3}}{1+K_{NH_3}C_{NH_3}} + \frac{k_{NH_3}K_{NH_3}C_{NH_3}}{1+K_{NH_3}C_{NH_3}} \tag{49}$$

And for the Cu-H-M catalyst the rate expressions were:

$$-R_{NO} = \frac{k_{NO}C_{NO}K_{NH_3}C_{NH_3}}{(1+K_{NH_3}C_{NH_3})(1+K_{NO}C_{NO})} \tag{50}$$

$$-R_{NH_3} = \frac{k_{NO}C_{NO}K_{NH_3}C_{NH_3}}{(1+K_{NH_3}C_{NH_3})(1+K_{NO}C_{NO})} + \frac{k_{NH_3}K_{NH_3}C_{NH_3}}{(1+K_{NH_3}C_{NH_3})(1+K_{NO}C_{NO})} \tag{51}$$

The kinetic parameters were estimated for honeycomb and packed-bed reactors. Fig 4.2 presents the plot of model prediction at different temperatures over a honeycomb reactor and a packed-bed flow reactor.

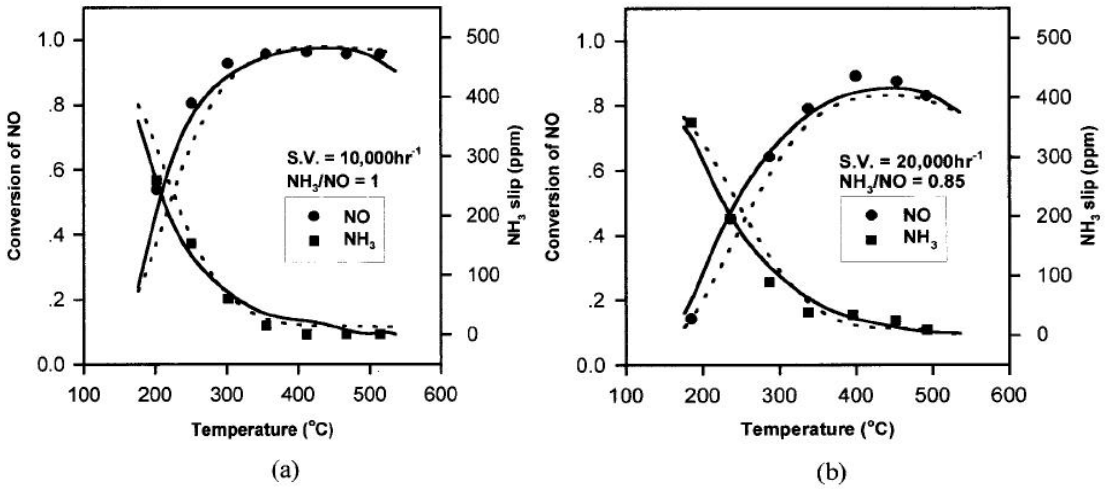

Fig 4.2 Prediction of the Model for the Extruded Honeycomb Reactor with the V_2O_5-WO_3/TiO_2 Catalyst (——, Prediction with the Parameters Estimated from the Experimental Data Over a Honeycomb Reactor; - - -, Prediction with the Parameters Estimated from the Experimental Data Over a Packed-bed Flow Reactor) [23]

A model for Vanadium based catalysts used the steady state assumption and came up with the expression W_1- W_2 –W_3 = 0. Where:

Rate of reversible NH_3 adsorption: $W_1 = k_1^+ C_{NH_3}(1-\theta) - k_1^- \theta$,

Rate of adsorbed ammonia interaction with NO: $W_2 = k_2 C_{NO_x} \theta$,

Rate of adsorbed ammonia oxidation: $W_3 = k_3 \theta$,

And θ is the adsorbed ammonia concentration.

The experiments were conducted with an operating temperature of 300-450^{o}C, NO concentration of 2-11 g/m^3 and ammonia water supply of 90-220 1/h. The values for the rate constant were obtained from the literature [24]

Another research group focusing on the SCR conditions over Cr_2O_3/TiO_2 performed experiments with fixed NO and NH_3 concentration of 1000 ppm, the temperatures varied from 400 to 485 K, water concentration varied from 1 to 6% and oxygen concentration varied from 0 to 12%. The following rate expression was proposed [25]:

$$r_1 = k_1 \left(np_{O_2} + \frac{K_{O_2} p_{O_2}}{1 + K_{O_2} p_{O_2} + K_w p_{H_2O}} \right) \left(\frac{1}{1 + K_{H_2O} p_{H_2O}} \right) p_{NO} \tag{52}$$

Where

$$K_i(T) = K_i^o(T_{ref}) \exp\left(\frac{-E_{A_i}}{R} \left(\frac{1}{T} - \frac{1}{T_{ref}} \right) \right) \tag{53}$$

and

$$K_{H_2O}(T) = K_{H_2O}^o(T_{ref}) \exp\left(\frac{-\Delta H_{H_2O}}{R} \left(\frac{1}{T} - \frac{1}{T_{ref}} \right) \right). \tag{54}$$

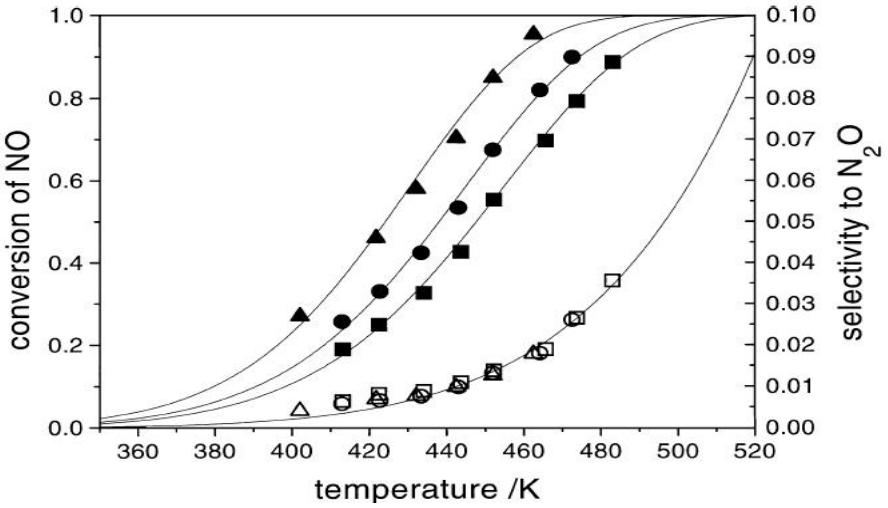

Fig 4.3 Model Performance for the Cr_2O_3/TiO_2 Catalyst [25]

Fig 4.3 presents the model performance for the Cr_2O_3/TiO_2 catalyst over a range of temperature.

Another paper modeled the process using three separate terms in the expression. The temperature was varied from 350 to 450°C, the NO concentration was varied from 0 to 500 ppm, the O_2 concentration was varied from 0.5 to 2% and the NH_3 concentration was varied from 100 to 500 ppm. For the H-ZSM-5, the SCR rate is first order in NO and O_2 and would be given by, $r_{SCR} = \frac{k_{SCR}[NO][O_2]}{1 + K_a[NH_3]}$, the rate of ammonia oxidation is a function of the ammonia coverage and is zero order in oxygen concentration hence the expression used was, $r_{ox} = \frac{k_{ox}K_a[NH_3]}{1 + K_a[NH_3]}$ and to account for the SCR in the absence of oxygen a term, $r_o = k_o[NO]$ was introduced. Combining all three terms gives an overall rate expression of the form [26]:

$$r_{N_2} = \frac{k_{SCR}[NO][O_2]}{1 + K_a[NH_3]} + \frac{k_{ox}K_a[NH_3]}{1 + K_a[NH_3]} + k_o[NO] \quad (55)$$

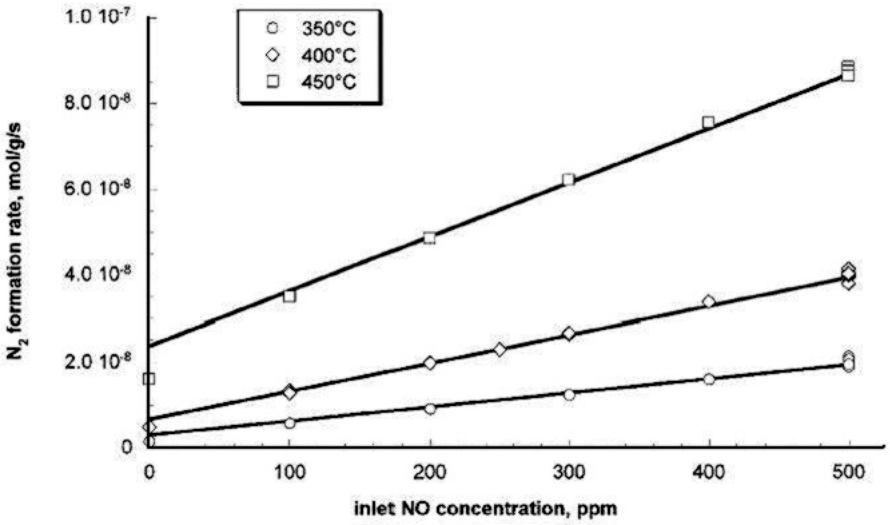

Fig 4.4 Model Performance for the H-ZSM-5 Catalyst [26]

Fig 4.4 presents the model performance for the H-ZSM-5 catalyst over a range of temperature.

5. PROCEDURE

The experimental data was obtained from the research work conducted at the Engines, Emissions and Energy Research Laboratory, Mechanical Engineering Department, Texas A&M University. The experimental data for the Cu-ZSM-5 and V based honeycomb monolith catalysts was taken from the work of S. Gupta [27] and the experimental data for the V-Ti based honeycomb monolith catalyst and the V-Ti-W catalyst based pillared inter layered clay catalyst was taken from the work of H. Oh [28] The experimental data consists of the concentrations of ammonia, oxygen, nitric oxide, nitrous oxide, nitrogen di-oxide and nitrogen before and after the catalyst and operating temperatures.

In this proposed research investigation, the SCR process will be modeled with a rate order expression. This kind of expression incorporates all the process parameters (temperature and concentrations of ammonia and oxygen) in a simplified and easy to use formula. It can be customized to accurately depict a specific process by performing a regression analysis of a comprehensive data set.

The selective catalytic reduction rate can be expressed as:

$$r = k_T^{'}[NH_3]^a[O_2]^b[NO]^c[H_2O]^d$$

Where $k_T^{'}$ is the rate constant for temperature T and a, b, c and d are reaction order of ammonia, oxygen, NO and water respectively.

The rate order with respect to NO has been measured to be 1 by many research groups i.e., c=1. The SCR rate dependencies on water concentration can be neglected when oxygen is in excess. In this study, the NO concentration is fixed at 330 ppm or 0.033% while oxygen concentration varies from 0.1% to 3%. From the equation (13) it is clear that for the SCR four molecules of NO require only one molecule of oxygen hence at the minimum, the oxygen concentration is 12 times the stoichiometric value or a 1200% excess. Hence the water concentration would not affect the SCR rate i.e., d=0. Further discussion on the SCR rate dependencies on NO and water is done in section 8. By considering these factors, the rate expression reduces to:

$$r = k_T[NH_3]^a[O_2]^b \tag{56}$$

Mathematically the modeling problem for this method can be described as:

$$\min(z) = \sum (r - r_{\exp})^2 \tag{57}$$

Where r is the reaction rate as predicted by the rate order expression given by equation 1 and r_{exp} is the rate of the reaction as obtained by the experiments.

By using the principles of statistics, for z to be minimized:

$$\frac{\partial z_{T,i}}{\partial k_T} = 0 \tag{58}$$

Where T denotes an operating temperature and $Z_{T,j}$ denotes all the terms from the data set for that temperature.

$$\frac{\partial z}{\partial c_j} = 0 \tag{59}$$

Where c_j denotes the reaction order for the species j.

This will result in (i + j) linear equations which can be solved simultaneously to obtain the numerical values for the rate constants and exponents.

The resulting linear equations can be written in a convenient matrix form. This matrix system of equations will be solved using 'Matlab' (a technical computing software from The Mathwork, Inc.). The solution of the resulting system of equations will provide the rate constants for all the temperatures and the exponents for the ammonia and oxygen concentrations.

The activation energy for the SCR process can be determined by the expression: $k_T = Ae^{\frac{-E_a}{RT}}$ (60). R is the universal gas constant, and the rate constant, k_T will be determined for all temperatures, T, once the process modeling is complete. The slope of the $\ln(k_T)$ versus 1/T gives the value for the activation energy, E_a.

The experimental data for the each catalyst will be examined for NO, N_2O, NO_2 and NH_3 concentration in the exhaust for all data sets. Based on this analysis, an operating temperature range and ammonia and oxygen concentration will be recommended that correspond to satisfactory conversion performance (high reaction rate and low emission of all the above mentioned species).

After an operating temperature range has been determined, the regression analysis will be repeated for the new data set and new rate expressions will be obtained that would predict the conversion performance. It is expected that the model prediction will be sufficiently accurate for practical application. A sensitivity analysis will be performed to estimate the effect of probable error in the ammonia and oxygen concentrations in the simulated exhaust used for the experimentation.

6. SCR PROCESS MODELING – ALL TEMPERATURES

The results of the SCR process modeling for the four catalysts are presented in this section. The four catalyst considered in this study are a Copper exchanged form of the zeolite ZSM-5 honeycomb monolith catalyst (Cu-ZSM-5), Vanadium oxide based honeycomb monolith catalyst (V) and Vanadium, Titanium and Tungsten oxide based honeycomb monolith catalyst (V-Ti-W) and a Vanadium and Titanium based pillared inter layered clay catalyst (V-Ti PLIC). These catalysts were chosen based on their ability to selectively reduce NO_x with ammonia in presence of oxygen, as required for controlling NO_x from power plants and modern lean burn engines which contain significant amount of oxygen in the combustion exhaust.

Beginning with a brief introduction of each of the catalyst, formatted experimental data would be reported followed by the proposed rate order expression and the representative plots that illustrate the effect of the change in parameters on the reaction rate. The model performance can be judged by the "fit", close match between the experimentally obtained values with expression predicted values.

Modeling the data from entire temperature range provides information for determining the SCR rate constants for all temperatures, information that is needed to calculate the activation energy and to construct a continuous rate expression applicable to intermediate temperature as well.

In the next section, the data corresponding to the temperatures where the catalyst performance is not satisfactory in terms of the NO_x conversion, ammonia slip, N_2O and NO_2 generation would be omitted to come up with a more accurate SCR rate expression for the applicable range.

6.1 Cu-ZSM-5 Catalyst

Cu-exchanged form of the ZSM-5 shows some of the highest known activities for the SCR of NO. Cu-ZSM-5 has the advantage of being able to reduce NO both with and without the addition of a reducing agent.

Zeolites are one of the most well known inorganic molecular sieves [29] The word 'zeolite' comes from the roots *zeo* (for boil) and *lithos* (for stone) in Greek. Water molecules in the zeolite pores are readily lost when the zeolites are heated. The word was coined by Cronstedt, a Swedish mineralogist, who observed a mineral that gave off steam and appeared to boil when heated [30]

Zeolites are a well-defined class of naturally occurring crystalline aluminosilicate minerals. They have a three-dimensional structure arising from a framework of $[SiO_4]^{4-}$ and $[AlO_4]^{5-}$ coordination polyhedra linked by all their corners [31] The frameworks are generally very

open and contain channels and cavities in which cations and molecules are located, both of which have enough freedom of movement to permit cation exchange and reversible dehydration. Water molecules are located in these channels and cavities, as are the cations that neutralize the negatively charged framework.

Many different zeolite structures exist, but the one that will be discussed in the present study is ZSM-5 (Zeolite Socony Mobil-5) [32] ZSM-5 is a high silica zeolite with Si:Al ratio usually greater than 10. Detailed catalyst characteristics are provided in the appendix.

The experimental data for the Cu-ZSM-5 catalyst is presented in tables 6.1 – 6.9. The term SV represents space velocity, ratio of the volumetric flow rate through the catalyst to the volume of the catalyst itself; all other terms are self explanatory, for example NO_{in} represents NO concentration at the inlet. NO concentration was fixed at 330 ppm and space velocity at 42,000 per hour. Three cases with inlet ammonia concentration of 264, 330 and 660 ppm for corresponding beta values (ratio of inlet ammonia concentration to that of inlet NO concentration) of 0.8, 1 and 2 were considered. Three cases with inlet oxygen concentration of 0.1, 0.5 and 3.0% were considered.

Table 6.1 Experimental Data at 100^{o}C for Cu-ZSM-5 Based Catalyst [27]

NO_{in} (ppm)	NH_{3in} (ppm)	SV (h^{-1})	NO_{out} (ppm)	NH_{3out} (ppm)	N_2O_{out} (ppm)	NO_{2out} (ppm)	O_{2in} (%)
330	330	42000	323	319	0	2	0.1
330	330	42000	326	317	1	3	0.5
330	330	42000	322	316	0	2	3.0
330	264	42000	330	256	1	3	0.1
330	264	42000	327	255	1	1	3.0
330	660	42000	326	642	1	1	0.1
330	660	42000	325	641	1	1	0.5
330	660	42000	325	641	1	1	3.0

Table 6.2 Experimental Data at 150°C for Cu-ZSM-5 Based Catalyst [27]

NO_{in} (ppm)	NH_{3in} (ppm)	SV (h^{-1})	NO_{out} (ppm)	NH_{3out} (ppm)	N_2O_{out} (ppm)	NO_{2out} (ppm)	O_{2in} (%)
330	330	42000	319	309	1	2	0.10
330	330	42000	308	294	2	2	0.50
330	330	42000	291	275	3	1	3.00
330	264	42000	321	244	1	1	0.10
330	264	42000	313	232	2	2	0.50
330	264	42000	316	239	1	1	3.00
330	660	42000	324	638	1	1	0.10
330	660	42000	316	613	1	2	0.50
330	660	42000	316	645	2	1	3.00

Table 6.3 Experimental Data at 200°C for Cu-ZSM-5 Based Catalyst [27]

NO_{in} (ppm)	NH_{3in} (ppm)	SV (h^{-1})	NO_{out} (ppm)	NH_{3out} (ppm)	N_2O_{out} (ppm)	NO_{2out} (ppm)	O_{2in} (%)
330	330	42000	282	267	2	1	0.10
330	330	42000	174	147	13	2	0.50
330	330	42000	141	104	22	3	3.00
330	264	42000	271	198	2	0	0.10
330	264	42000	238	130	5	2	0.50
330	264	42000	196	100	11	1	3.00
330	660	42000	280	596	2	2	0.10
330	660	42000	189	543	4	1	0.50
330	660	42000	194	530	14	1	3.00

Table 6.4 Experimental Data at 225°C for Cu-ZSM-5 Based Catalyst [27]

NO_{in} (ppm)	NH_{3in} (ppm)	SV (h^{-1})	NO_{out} (ppm)	NH_{3out} (ppm)	N_2O_{out} (ppm)	NO_{2out} (ppm)	O_{2in} (%)
330	330	42000	129	90	14	2	0.50
330	330	42000	103	47	22	6	3.00
330	264	42000	184	84	7	5	0.50
330	264	42000	144	54	14	4	3.00
330	660	42000	135	444	12	0	0.50

Table 6.5 Experimental Data at 250°C for Cu-ZSM-5 Based Catalyst [27]

NO_{in} (ppm)	NH_{3in} (ppm)	SV (h^{-1})	NO_{out} (ppm)	NH_{3out} (ppm)	N_2O_{out} (ppm)	NO_{2out} (ppm)	O_{2in} (%)
330	330	42000	180	148	5	1	0.10
330	330	42000	104	51	13	0	0.50
330	330	42000	92	16	20	11	3.00
330	264	42000	170	118	4	5	0.10
330	264	42000	133	49	9	9	0.50
330	264	42000	109	19	15	7	3.00
330	660	42000	157	424	4	1	0.10
330	660	42000	94	316	19	0	0.50
330	660	42000	69	324	33	0	3.00

Table 6.6 Experimental Data at 300°C for Cu-ZSM-5 Based Catalyst [27]

NO_{in} (ppm)	NH_{3in} (ppm)	SV (h^{-1})	NO_{out} (ppm)	NH_{3out} (ppm)	N_2O_{out} (ppm)	NO_{2out} (ppm)	O_{2in} (%)
330	330	42000	115	34	7	3	0.10
330	330	42000	88	8	10	9	0.50
330	330	42000	97	3	13	21	3.00
330	264	42000	122	17	6	7	0.10
330	264	42000	107	7	7	14	0.50
330	264	42000	100	6	11	30	3.00
330	660	42000	76	225	6	0	0.10
330	660	42000	49	90	18	0	0.50
330	660	42000	37	50	30	0	3.00

Table 6.7 Experimental Data at 350°C for Cu-ZSM-5 Based Catalyst [27]

NO_{in} (ppm)	NH_{3in} (ppm)	SV (h^{-1})	NO_{out} (ppm)	NH_{3out} (ppm)	N_2O_{out} (ppm)	NO_{2out} (ppm)	O_{2in} (%)
330	330	42000	83	3	4	3	0.10
330	264	42000	109	0	4	7	0.10
330	660	42000	39	68	4	0	0.10

Table 6.8 Experimental Data at 400°C for Cu-ZSM-5 Based Catalyst [27]

NO_{in} (ppm)	NH_{3in} (ppm)	SV (h^{-1})	NO_{out} (ppm)	NH_{3out} (ppm)	N_2O_{out} (ppm)	NO_{2out} (ppm)	O_{2in} (%)
330	330	42000	81	0	3	4	0.10
330	330	42000	98	0	5	13	0.50
330	330	42000	130	0	7	43	3.00
330	264	42000	106	0	3	6	0.10
330	264	42000	134	0	4	21	0.50
330	264	42000	162	0	7	63	3.00
330	660	42000	26	9	3	0	0.10
330	660	42000	31	7	5	1	0.50
330	660	42000	81	0	15	23	3.00

Table 6.9 Experimental Data at 500°C for Cu-ZSM-5 Based Catalyst [27]

NO_{in} (ppm)	NH_{3in} (ppm)	SV (h^{-1})	NO_{out} (ppm)	NH_{3out} (ppm)	N_2O_{out} (ppm)	NO_{2out} (ppm)	O_{2in} (%)
330	330	42000	96	0	1	3	0.10
330	330	42000	140	0	2	9	0.50
330	330	42000	195	0	3	28	3.00
330	264	42000	123	0	1	4	0.10
330	264	42000	176	0	1	11	0.50
330	264	42000	224	0	5	41	3.00
330	660	42000	33	0	1	0	0.10
330	660	42000	52	6	1	0	0.50
330	660	42000	133	0	7	16	3.00

Regression analysis of the above data provides the values for the SCR rate constants for all temperatures and the exponents for ammonia and oxygen as listed in table 6.10.

Table 6.10 Rate Constants and Ammonia and Oxygen Exponents for Cu-ZSM-5

ln k_{100}	1.8461
ln k_{150}	2.8612
ln k_{200}	4.5267
ln k_{225}	5.1123
ln k_{250}	5.2684
ln k_{300}	5.5496
ln k_{350}	5.7683
ln k_{400}	5.5937
ln k_{500}	5.5494
Ammonia exponent	0.4349
Oxygen exponent	0.0758

Hence the rate order expression is given by $r = k_T[NH_3]^{0.435}[O_2]^{.076}$.

The ammonia exponent is 0.4349. This indicates that the reaction rate increases with inlet ammonia concentration while the oxygen exponent is much smaller at 0.0758 indicating a weak positive dependence of reaction rate on inlet oxygen concentration.

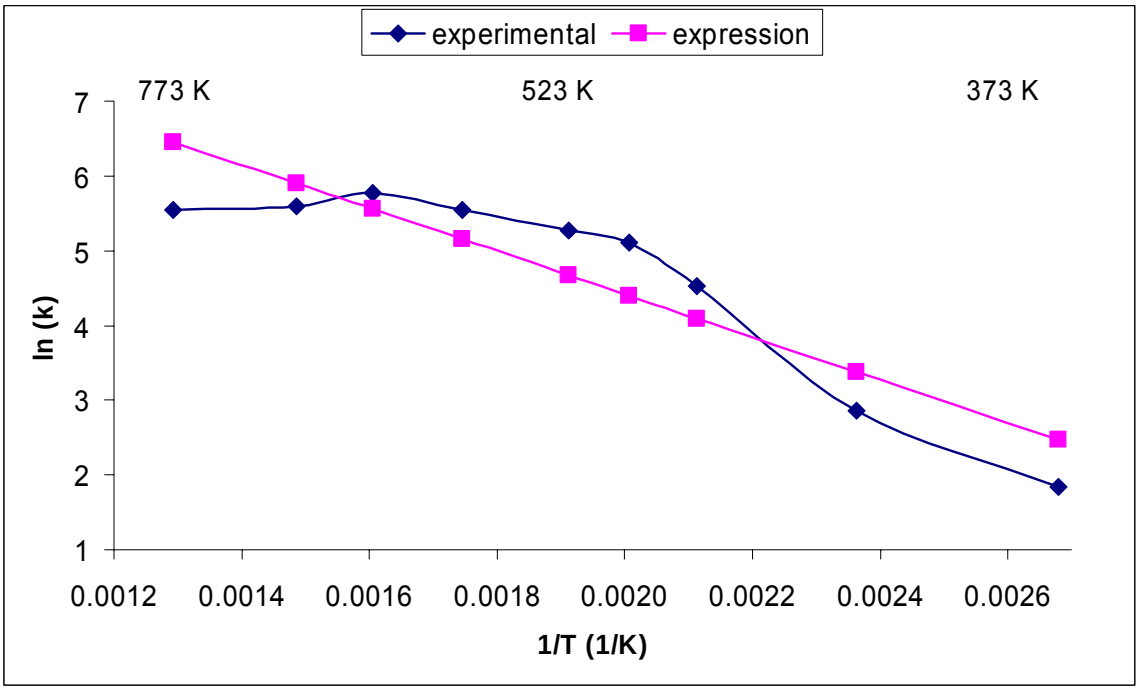

Fig 6.1 ln (k) versus 1/T for Cu-ZSM-5 Based Catalyst

Figure 6.1 shows that rate constant increases with temperature and reaches a maximum value at 350°C. The rate constant flattens out after 225°C. The value of the activation energy depends on the temperature range selected. The average activation energy for the complete temperature range turns out to be 23.845 KJ/mol. The SCR rate constant can be expressed as:

$$k_T = 25766e^{\frac{-23.845}{8.31434*T}}$$

This relation can be used to estimate the SCR rate constant (k_T) for intermediate temperature values.

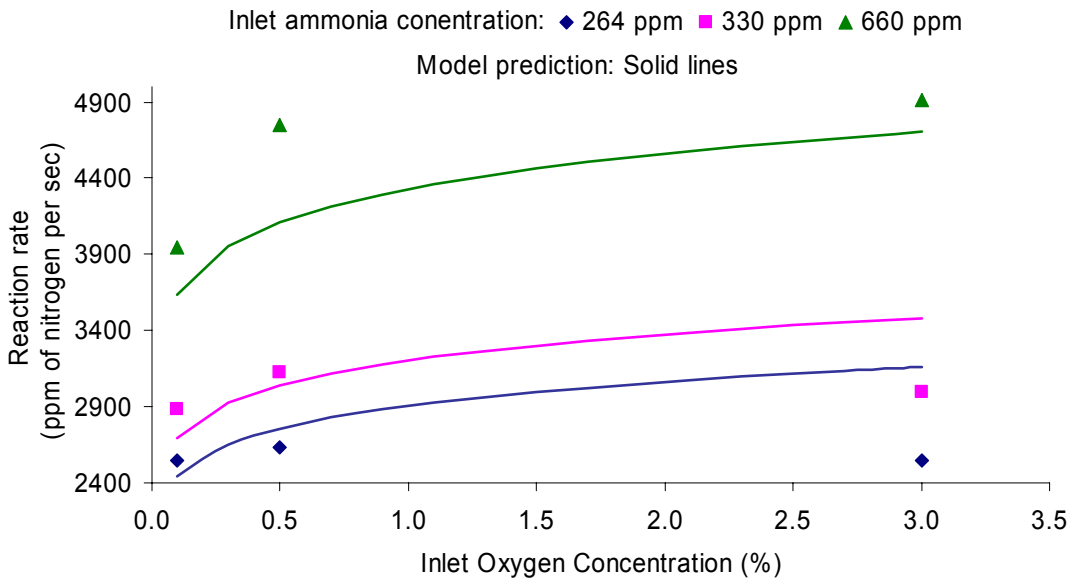

Fig 6.2 SCR Rate as a Function of Inlet Oxygen Concentration for Ammonia Concentrations of 264, 330 and 660 ppm at 300°C

Fig 6.2 illustrates the model performance for 0.1% to 3.0% inlet oxygen concentration for inlet ammonia concentrations of 264, 330 and 660 ppm at 300°C. The experimental values are shown with points while the solid lines indicate the model predictions. The reaction rate increase with inlet oxygen concentration for all inlet ammonia concentration.

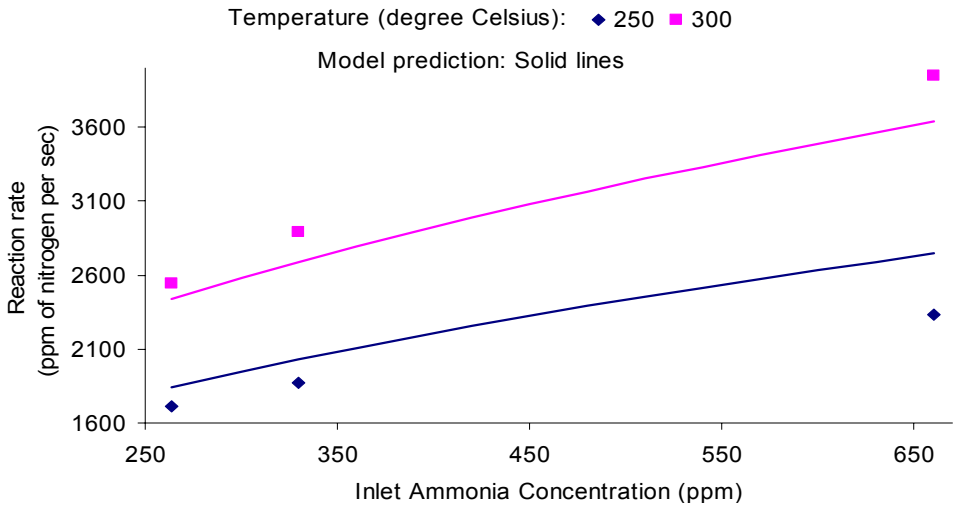

Fig 6.3 SCR Rate as a Function of Inlet Ammonia Concentrations at 250 °C and 300°C and 0.1% Inlet Oxygen Concentration

Fig 6.3 illustrates the model performance for 264 to 660 ppm inlet ammonia concentration at 250°C and 300°C and 0.1% inlet oxygen concentration. The experimental values are shown with points while the solid lines indicate the model predictions. The reaction rate increases with inlet ammonia concentration for all temperatures.

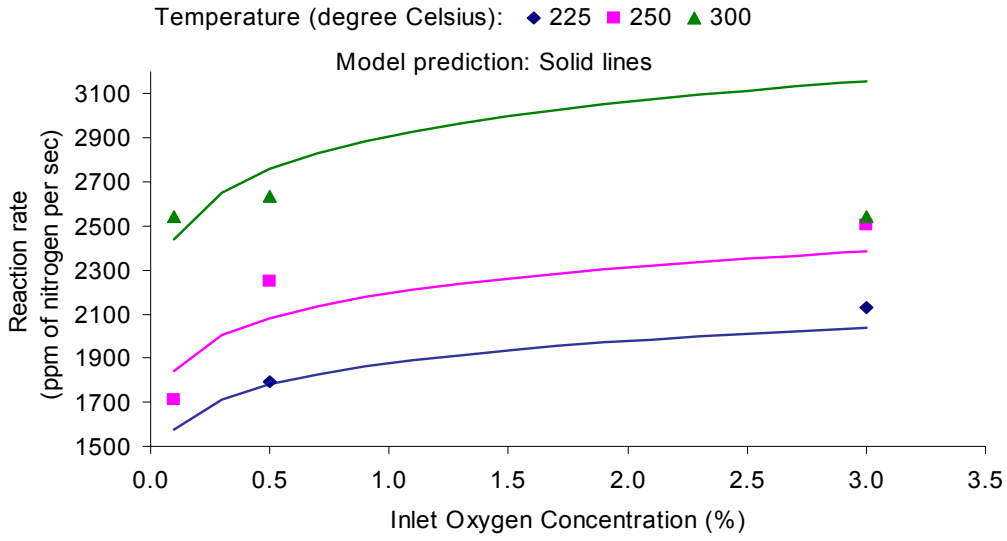

Fig 6.4 SCR Rate as a Function of Inlet Oxygen Concentration at 225°C, 250°C and 300°C and 264 ppm Inlet Ammonia Concentration

Fig 6.4 illustrates the model performance for 0.1 to 3.0% inlet oxygen concentrations at 225^{o}C, 250^{o}C and 300^{o}C and 264 ppm Inlet ammonia Concentration. The experimental values are shown with points while the solid lines indicate the model predictions. The reaction rate increases with inlet oxygen concentration for all temperatures.

6.2 Vanadium Based Catalyst

Vanadium oxide may be deposited onto the surface of a wide variety of supports (including alumina, silica, zirconia, and titania) [33] Such supported vanadium oxide materials find numerous applications, including their use as catalysts for the selective reduction reactions. Several studies in the past have investigated the structure and properties of supported vanadia. Of particular interest to the present study is their application to the selective catalytic reduction of NO. Supported vanadia catalysts show a high degree of effectiveness in selectively reducing NO in the presence of ammonia [34] Detailed catalyst characteristics are provided in the appendix.

The experimental data for the V catalyst is presented in tables 6.11 – 6.18. The term SV represents space velocity, ratio of the volumetric flow rate through the catalyst to the volume of the catalyst itself; all other terms are self explanatory for example NO_{in} represents NO concentration at the inlet. NO concentration was fixed at 330 ppm and space velocity at 42,000 per hour. Three cases for inlet ammonia concentration of 264, 330 and 660 ppm for corresponding beta values (ratio of inlet ammonia concentration to that of inlet NO concentration) of 0.8, 1 and 2 were considered. Three cases with inlet oxygen concentration of 0.1, 0.5 and 3.0% were considered.

Table 6.11 Experimental Data at 100^{o}C for V Based Catalyst [27]

NO_{in} (ppm)	NH_{3in} (ppm)	SV (h^{-1})	NO_{out} (ppm)	NH_{3out} (ppm)	N_2O_{out} (ppm)	NO_{2out} (ppm)	O_{2in} (%)
330	264	42000	324	238	0	0	0.1
330	264	42000	318	234	0	5	0.5
330	264	42000	321	232	0	1	3
330	330	42000	329	325	0	3	0.1
330	330	42000	324	317	0	0	0.5
330	330	42000	321	312	0	0	3
330	660	42000	322	640	0	1	0.1
330	660	42000	324	639	0	1	0.5
330	660	42000	322	636	0	1	3

Table 6.12 Experimental Data at 150°C for V Based Catalyst [27]

NO_{in} (ppm)	NH_{3in} (ppm)	SV (h^{-1})	NO_{out} (ppm)	NH_{3out} (ppm)	N_2O_{out} (ppm)	NO_{2out} (ppm)	O_{2in} (%)
330	264	42000	320	236	0	0	0.1
330	264	42000	310	222	1	4	0.5
330	264	42000	300	216	0	1	3
330	330	42000	321	314	1	2	0.1
330	330	42000	318	306	0	0	0.5
330	330	42000	316	304	0	1	3
330	660	42000	313	633	0	0	0.1
330	660	42000	316	625	0	3	0.5
330	660	42000	311	621	0	2	3

Table 6.13 Experimental Data at 200°C for V Based Catalyst [27]

NO_{in} (ppm)	NH_{3in} (ppm)	SV (h^{-1})	NO_{out} (ppm)	NH_{3out} (ppm)	N_2O_{out} (ppm)	NO_{2out} (ppm)	O_{2in} (%)
330	264	42000	289	206	1	1	0.1
330	264	42000	250	159	1	3	0.5
330	264	42000	221	132	1	0	3
330	330	42000	296	291	1	2	0.1
330	330	42000	240	222	1	0	0.5
330	330	42000	242	226	1	0	3
330	660	42000	276	597	1	0	0.1
330	660	42000	252	564	1	1	0.5
330	660	42000	219	561	1	0	3

Table 6.14 Experimental Data at 250°C for V Based Catalyst [27]

NO_{in} (ppm)	NH_{3in} (ppm)	SV (h^{-1})	NO_{out} (ppm)	NH_{3out} (ppm)	N_2O_{out} (ppm)	NO_{2out} (ppm)	O_{2in} (%)
330	264	42000	226	122	2	1	0.1
330	264	42000	171	81	2	3	0.5
330	264	42000	152	62	2	0	3
330	330	42000	221	219	3	3	0.1
330	330	42000	146	116	3	0	0.5
330	330	42000	151	122	3	0	3
330	660	42000	192	522	5	0	0.1
330	660	42000	154	485	5	1	0.5
330	660	42000	120	451	5	0	3

Table 6.15 Experimental Data at 300°C for V Based Catalyst [27]

NO_{in} (ppm)	NH_{3in} (ppm)	SV (h^{-1})	NO_{out} (ppm)	NH_{3out} (ppm)	N_2O_{out} (ppm)	NO_{2out} (ppm)	O_{2in} (%)
330	264	42000	149	60	8	2	0.1
330	264	42000	144	55	6	2	0.5
330	264	42000	132	43	4	0	3
330	330	42000	152	128	10	3	0.1
330	330	42000	119	67	7	0	0.5
330	330	42000	123	71	5	0	3
330	660	42000	127	439	22	0	0.1
330	660	42000	108	397	18	0	0.5
330	660	42000	91	367	16	0	3

Table 6.16 Experimental Data at 350°C for V Based Catalyst [27]

NO_{in} (ppm)	NH_{3in} (ppm)	SV (h^{-1})	NO_{out} (ppm)	NH_{3out} (ppm)	N_2O_{out} (ppm)	NO_{2out} (ppm)	O_{2in} (%)
330	264	42000	133	42	32	0	0.1
330	264	42000	148	39	28	3	0.5
330	264	42000	143	32	18	0	3
330	330	42000	134	85	26	1	0.1
330	330	42000	122	54	21	0	0.5
330	330	42000	151	45	15	0	3
330	660	42000	92	309	86	0	0.1
330	660	42000	93	269	60	3	0.5
330	660	42000	88	255	49	0	3

Table 6.17 Experimental Data at 400°C for V Based Catalyst [27]

NO_{in} (ppm)	NH_{3in} (ppm)	SV (h^{-1})	NO_{out} (ppm)	NH_{3out} (ppm)	N_2O_{out} (ppm)	NO_{2out} (ppm)	O_{2in} (%)
330	264	42000	147	31	54	1	0.1
330	264	42000	165	27	48	3	0.5
330	264	42000	180	24	34	1	3
330	330	42000	141	61	55	2	0.1
330	330	42000	141	43	36	0	0.5
330	330	42000	190	36	25	0	3
330	660	42000	108	183	139	0	0.1
330	660	42000	120	141	125	2	0.5
330	660	42000	125	128	101	1	3

Table 6.18 Experimental Data at 500°C for V Based Catalyst [27]

NO_{in} (ppm)	NH_{3in} (ppm)	SV (h^{-1})	NO_{out} (ppm)	NH_{3out} (ppm)	N_2O_{out} (ppm)	NO_{2out} (ppm)	O_{2in} (%)
330	264	42000	228	13	90	0	0.1
330	264	42000	238	12	84	5	0.5
330	264	42000	267	12	76	5	3
330	330	42000	197	23	105	2	0.1
330	330	42000	201	19	97	0	0.5
330	330	42000	273	20	90	3	3
330	660	42000	208	45	190	0	0.1
330	660	42000	241	36	176	0	0.5
330	660	42000	246	38	163	0	3

Regression analysis of the above data provides the values for the SCR rate constants for all temperatures and the exponents for ammonia and oxygen as listed in table 6.19.

Table 6.19 Rate Constants and Ammonia and Oxygen Exponents for V Catalyst

ln k_{100}	3.4860
ln k_{150}	4.1582
ln k_{200}	5.4155
ln k_{250}	6.1595
ln k_{300}	6.4183
ln k_{350}	6.4300
ln k_{400}	6.3350
ln k_{500}	5.8595
Ammonia exponent	0.2427
Oxygen exponent	0.1133

Hence the rate order expression is given by $r = k_T[NH_3]^{0.2427}[O_2]^{0.1133}$.

The ammonia exponent is 0.2427 that indicates that reaction rate increases with inlet ammonia concentration while the oxygen exponent is comparable at 0.1133 indicating a positive dependence of reaction rate on inlet oxygen concentration.

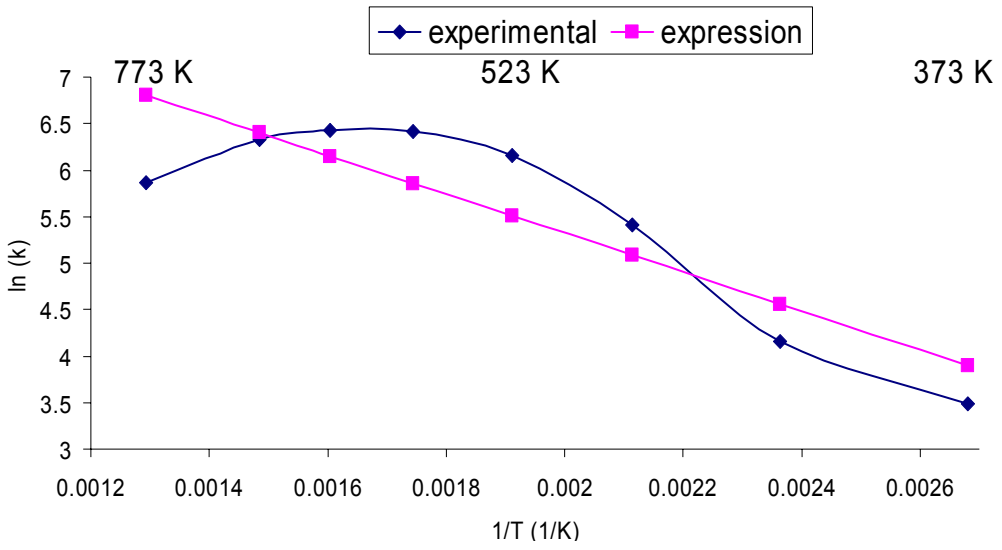

Fig 6.5 ln (k) versus 1/T for Vanadium Based Catalyst

Figure 6.5 shows that rate constant increases with temperature and reaches a maximum value at 350°C. The rate constant flattens out after 200°C. The value of the activation energy depends on the temperature range selected. The average activation energy for the complete temperature range turns out to be 17.4 KJ/mol. The SCR rate constant can be expressed as $k_T = 13533.6e^{\frac{-17.421}{8.31434*T}}$. This relation can be used to estimate the SCR rate constant k_T for intermediate temperature values.

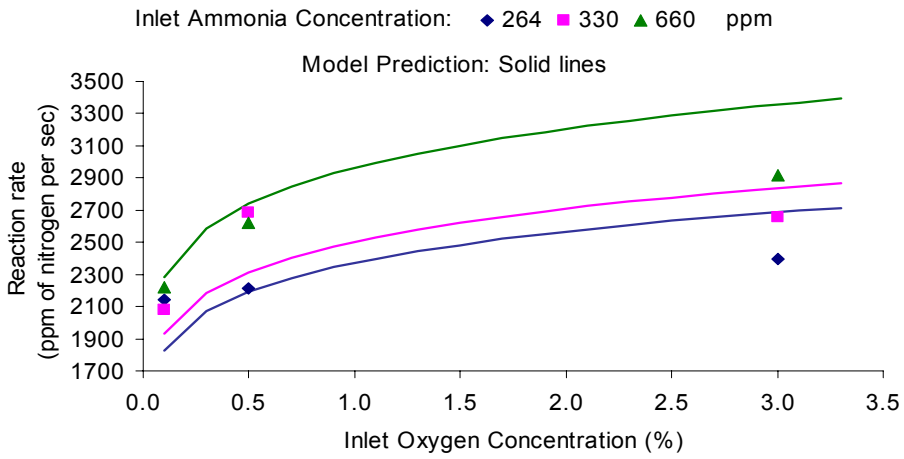

Fig 6.6 SCR Rate as a Function of Inlet Oxygen Concentration for Inlet Ammonia Concentrations of 264, 330 and 660 ppm at 300°C

Fig 6.6 illustrates the model performance for 0.1-3.0% inlet oxygen concentration for inlet ammonia concentrations of 264, 330 and 660 ppm at 300°C. The experimental values are shown with points while the solid lines indicate the model predictions. The reaction rate increase with inlet oxygen concentration for all inlet ammonia concentration.

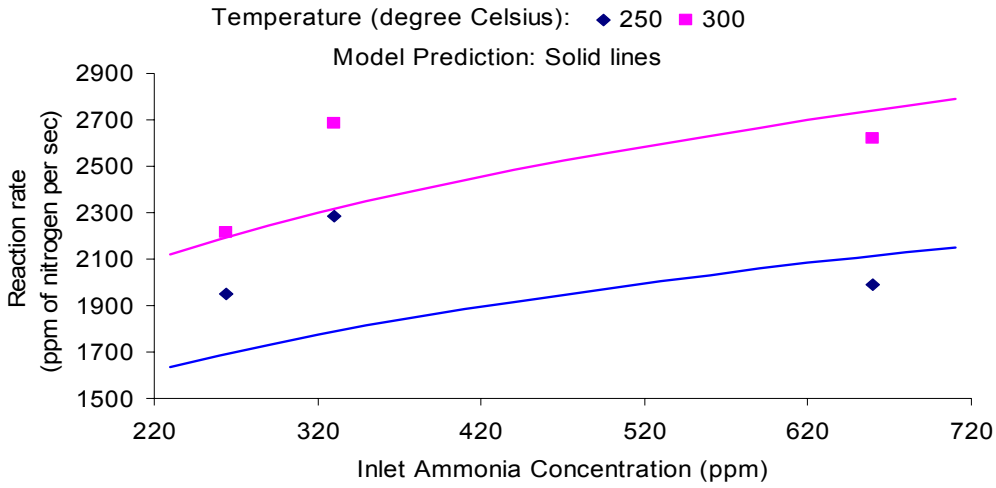

Fig 6.7 SCR Rate as a Function of Inlet Ammonia Concentrations at 250°C and 300°C and 0.5% Inlet Oxygen Concentration

Fig 6.7 illustrates the model performance for 264 to 660 ppm inlet ammonia concentrations at 250 and 300°C and 0.5% inlet oxygen concentration. The experimental values are shown with points while the solid lines indicate the model predictions. The reaction rate increases with inlet ammonia concentration for all temperatures.

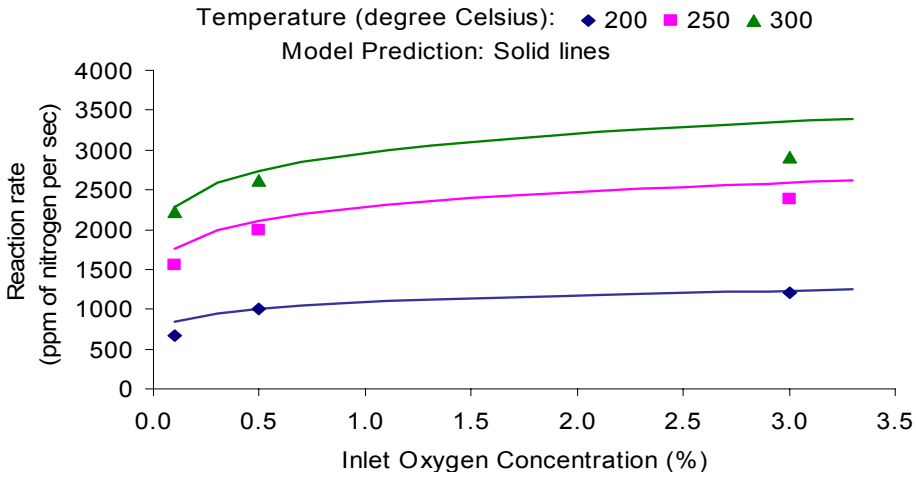

Fig 6.8 SCR Rate as a Function of Inlet Oxygen Concentration at 200°C, 250°C and 300°C and 660 ppm Inlet Ammonia Concentration

Fig 6.8 illustrates the model performance for 0.1-3.0% inlet oxygen concentrations at 200^{o}C, 250^{o}C and 300^{o}C and 660 ppm inlet ammonia concentration. The experimental values are shown with points while the solid lines indicate the model predictions. The reaction rate increases with inlet oxygen concentration for all temperatures.

6.3 V-Ti Based Pillared Inter Layered Clay (PLIC) Catalyst

New catalyst supports are being developed to overcome the disadvantages of titania such as limited surface area, a low sintering resistance, a high cost, and poor mechanical strength [35] PILCs with titania as a pillar (Ti-PILC) has been extensively investigated recently because of its characteristics that overcome the abovementioned limits of titania [36, 37] PILCs are a unique two-dimensional zeolite-like material [37] Ti-PILC catalyst has large surface area, strong mechanical strength, high resistance to SO_2, hydrothermal stability and multimodal pore size distribution [36, 37]

One of the advantages of PILCs support is the variety of physical and structural characteristics depending upon the technique of the catalyst preparation. The modification of the pore structure of the catalyst influences catalytic activity and sulfur tolerance for NO reduction with NH_3 [37] The pillaring of titania on the catalyst enhances the surface acidity and acid sites that improves the catalytic activity [38]

It was reported that the catalytic activity increased in the order Al_2O_3-PILC < ZrO_2-PILC < TiO_2-PILC < Fe_2O_3-PILC < Cr_2O_3-PILC as a SCR catalyst support [24] Due to the most active catalyst Cr_2O_3-PILC is severely weak by SO_2, TiO_2-PILC and Fe_2O_3-PILC catalysts have been widely used for commercial catalysts. Vanadia shows good performance for the SCR of NO_x with ammonia, and therefore, V_2O_5/Ti-PILC catalyst has been examined recently [36]

The experimental data for the V-Ti PLIC catalyst is presented in tables 6.20 – 6.26. The term SV represents space velocity, ratio of the volumetric flow rate through the catalyst to the volume of the catalyst itself; all other terms are self explanatory for example NO_{in} represents NO concentration at the inlet. NO concentration was fixed at 330 ppm and space velocity at 10,500 per hour. Three cases for inlet ammonia concentration of 264, 330 and 660 ppm for corresponding beta values (ratio of inlet ammonia concentration to that of inlet NO concentration) of 0.8, 1 and 2 were considered. Three cases with inlet oxygen concentration of 0.1, 0.5 and 3.0% were considered.

Table 6.20 Experimental Data at 150°C for V-Ti Based PILC Catalyst [28]

NO_{in} (ppm)	NH_{3in} (ppm)	SV (h^{-1})	NO_{out} (ppm)	NH_{3out} (ppm)	N_2O_{out} (ppm)	NO_{2out} (ppm)	O_{2in} (%)
330	264	10500	303	222	1	12	0.1
330	330	10500	280	303	0	11	0.1
330	660	10500	297	626	0	21	0.1
330	264	10500	269	198	0	9	3.0
330	330	10500	263	274	0	12	3.0
330	660	10500	278	608	0	22	3.0

Table 6.21 Experimental Data at 200°C for V-Ti Based PILC Catalyst [28]

NO_{in} (ppm)	NH_{3in} (ppm)	SV (h^{-1})	NO_{out} (ppm)	NH_{3out} (ppm)	N_2O_{out} (ppm)	NO_{2out} (ppm)	O_{2in} (%)
330	264	10500	224	151	0	10	0.1
330	330	10500	200	214	0	9	0.1
330	660	10500	220	556	0	19	0.1
330	264	10500	182	115	0	8	3.0
330	330	10500	169	182	0	10	3.0
330	660	10500	182	513	0	20	3.0

Table 6.22 Experimental Data at 250°C for V-Ti Based PILC Catalyst [28]

NO_{in} (ppm)	NH_{3in} (ppm)	SV (h^{-1})	NO_{out} (ppm)	NH_{3out} (ppm)	N_2O_{out} (ppm)	NO_{2out} (ppm)	O_{2in} (%)
330	264	10500	164	94	1	9	0.1
330	330	10500	132	151	1	8	0.1
330	660	10500	136	468	2	17	0.1
330	264	10500	123	64	0	7	3.0
330	330	10500	103	118	0	9	3.0
330	660	10500	99	427	1	16	3.0

Table 6.23 Experimental Data at 300°C for V-Ti Based PILC Catalyst [28]

NO_{in} (ppm)	NH_{3in} (ppm)	SV (h^{-1})	NO_{out} (ppm)	NH_{3out} (ppm)	N_2O_{out} (ppm)	NO_{2out} (ppm)	O_{2in} (%)
330	264	10500	136	63	3	9	0.1
330	330	10500	96	110	5	8	0.1
330	660	10500	82	408	10	16	0.1
330	264	10500	115	41	1	7	3.0
330	330	10500	72	84	2	8	3.0
330	660	10500	56	372	4	15	3.0

Table 6.24 Experimental Data at 350°C for V-Ti Based PILC Catalyst [28]

NO_{in} (ppm)	NH_{3in} (ppm)	SV (h^{-1})	NO_{out} (ppm)	NH_{3out} (ppm)	N_2O_{out} (ppm)	NO_{2out} (ppm)	O_{2in} (%)
330	264	10500	133	51	12	9	0.1
330	330	10500	83	84	22	7	0.1
330	660	10500	62	339	33	14	0.1
330	264	10500	110	34	6	7	3.0
330	330	10500	65	63	13	8	3.0
330	660	10500	39	286	19	13	3.0

Table 6.25 Experimental Data at 400°C for V-Ti Based PILC Catalyst [28]

NO_{in} (ppm)	NH_{3in} (ppm)	SV (h^{-1})	NO_{out} (ppm)	NH_{3out} (ppm)	N_2O_{out} (ppm)	NO_{2out} (ppm)	O_{2in} (%)
330	264	10500	145	44	39	8	0.1
330	330	10500	99	57	67	7	0.1
330	660	10500	55	227	89	11	0.1
330	264	10500	124	30	22	7	3.0
330	330	10500	88	40	43	7	3.0
330	660	10500	43	178	53	10	3.0

Table 6.26 Experimental Data at 500°C for V-Ti Based PILC Catalyst [28]

NO_{in} (ppm)	NH_{3in} (ppm)	SV (h^{-1})	NO_{out} (ppm)	NH_{3out} (ppm)	N_2O_{out} (ppm)	NO_{2out} (ppm)	O_{2in} (%)
330	264	10500	183	29	78	8	0.1
330	330	10500	141	29	110	6	0.1
330	660	10500	84	102	170	8	0.1
330	264	10500	179	21	50	7	3.0
330	330	10500	151	23	76	7	3.0
330	660	10500	85	81	121	8	3.0

Regression analysis of the above data provides the values for the SCR rate constants for all temperatures and the exponents for ammonia and oxygen as listed in table 6.27.

Table 6.27 Rate Constants and Ammonia and Oxygen Exponents for V-Ti PLIC Catalyst

ln k_{150}	3.4496
ln k_{200}	4.6393
ln k_{250}	5.0863
ln k_{300}	5.2454
ln k_{350}	5.2885
ln k_{400}	5.2019
ln k_{450}	4.9415
Ammonia exponent	0.2175
Oxygen exponent	0.0770

Hence the rate order expression is given by $r = k_T [NH_3]^{0.218} [O_2]^{0.077}$.

The ammonia exponent is 0.218 that indicates that reaction rate increases with inlet ammonia concentration while the oxygen exponent is much smaller at 0.077 indicating a weak positive dependence of reaction rate on inlet oxygen concentration.

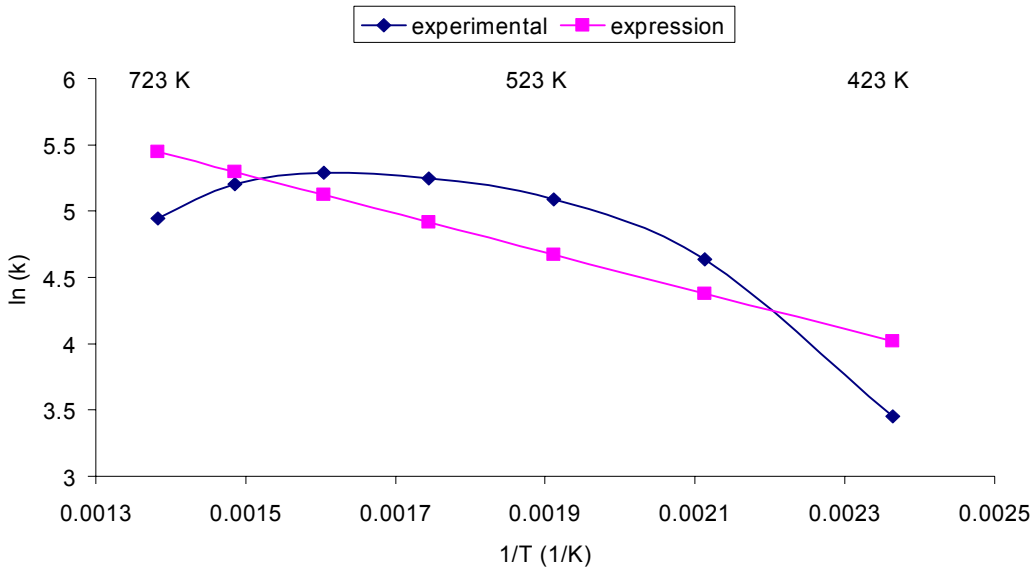

Fig 6.9 ln (k) versus 1/T for V-Ti Based PLIC Catalyst

Figure 6.9 shows that rate constant increases with temperature and reaches a maximum value at 350°C. The rate constant flattens out after 200°C. The value of the activation energy depends on the temperature range selected. The average activation energy for the complete temperature range turns out to be 12.1 KJ/mol.

The SCR rate constant can be expressed as:

$$k_T = 1740.7 e^{\frac{-12.123}{8.31434 * T}}$$

This relation can be used to estimate the SCR rate constant k_T for intermediate temperature values.

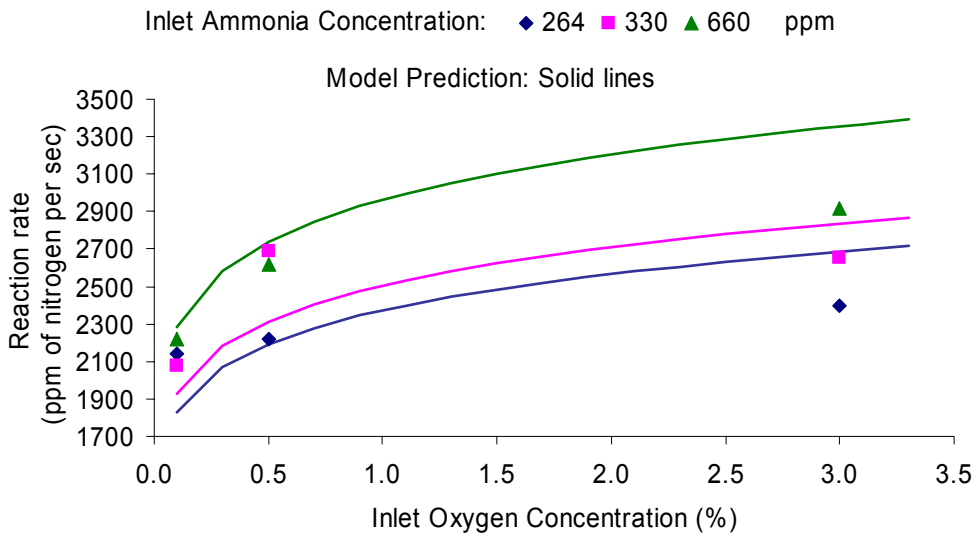

Fig 6.10 SCR Rate as a Function of Inlet Oxygen Concentration for Ammonia Concentrations of 264, 330 and 660 ppm at 250°C

Fig 6.10 illustrates the model performance for 0.1-3.0% inlet oxygen concentrations for inlet ammonia concentrations of 264, 330 and 660 ppm at 250°C. The experimental values are shown with points while the solid lines indicate the model predictions. The reaction rate increase with inlet oxygen concentration for all inlet ammonia concentration.

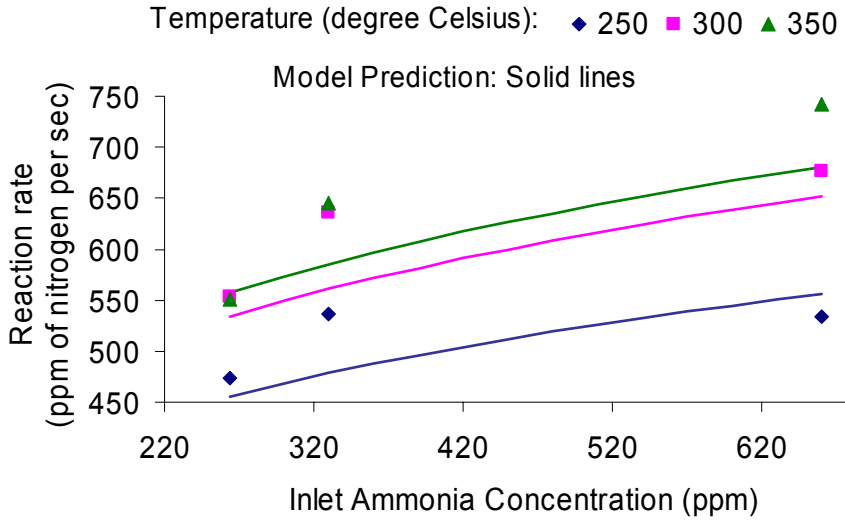

Fig 6.11 SCR Rate as a Function of Inlet Ammonia Concentrations at 250°C, 300°C and 350°C and 0.1% Inlet Oxygen Concentration

Fig 6.11 illustrates the model performance for 264 to 660 ppm ammonia concentrations at 250, 300 and 350^{o}C and 0.1% Inlet oxygen concentration. The experimental values are shown with points while the solid lines indicate the model predictions. The reaction rate increases with inlet ammonia concentration for all temperatures.

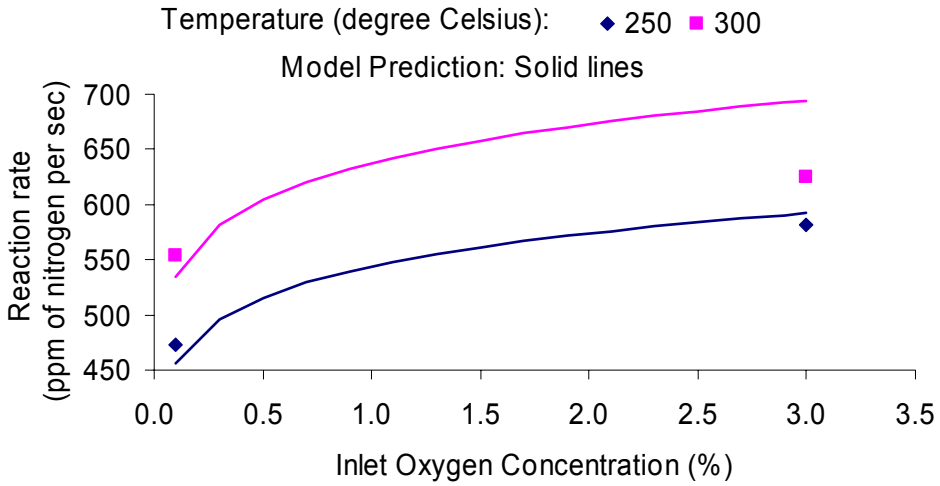

Fig 6.12 SCR Rate as a Function of Inlet Oxygen Concentration at 225^{o}C, 250^{o}C and 300^{o}C and 264 ppm Inlet Ammonia Concentration

Fig 6.12 illustrates the model performance for 0.1-3.0% inlet oxygen concentrations at 225^{o}C, 250^{o}C and 300^{o}C and 264 ppm Inlet ammonia concentration. The experimental values are shown with points while the solid lines indicate the model predictions. The reaction rate increases with inlet oxygen concentration for all temperatures.

6.4 V-Ti-W Based Catalyst

Selective catalytic reduction of NO_x with ammonia (NH_3) has been used for over 20 years for NO_x abatement from the industrial boiler flue gas and power plants. The most common catalysts in commercial material today are vanadia-based catalysts. The supports including alumina, silica, zirconia, and titania were commonly used for vanadia-based catalysts. Alumina has a higher specific surface area, superior mechanical strength, and is highly resistant to sintering, compared to titania. However, for the SCR of NO_x with NH_3 using alumina support (Al_2O_3), SO_2 in the flue gas reacts with ammonia and then deactivates the catalytic activity. It indicates that Al_2O_3 is weakly poisoned by sulfur components [35]

Among the many metal oxide supports, the TiO_2 support exhibits is the most effective for the selective catalytic reduction of NO_x with NH_3 because of its durability to sulfur compounds.

The sulfation of the TiO_2 supported catalyst even enhances the level of NO removal. Therefore, due to its high activity and durability to sulfur compounds, V_2O_5 supported on TiO_2 is well known to be the most effective and widely used commercial catalyst for the SCR processes [39]

A ternary catalyst, V_2O_5-WO_3/TiO_2, was also recently introduced. Promoters such as WO_3, SiO_2 and MoO_3 are usually added to V_2O_5/TiO_2 catalyst [36, 37] The promoters create acid sites on the catalyst surface, and the catalysts exhibit a higher catalytic activity than that of a single TiO_2 supported vanadium catalyst [36] The addition of WO_3 provides some poison resistance and improves NH_3 oxidation. There are still many studies to promote the activity of vanadia-based catalysts, but V_2O_5-WO_3/TiO_2 indicates more reliable results for removal of NO_x.

The experimental data for the V-Ti PLIC catalyst is presented in tables 6.28 – 6.35. The term SV represents space velocity, ratio of the volumetric flow rate through the catalyst to the volume of the catalyst itself; all other terms are self explanatory for example NO_{in} represents NO concentration at the inlet. NO concentration was fixed at 330 ppm and space velocity at 10,500 per hour. Three cases for inlet ammonia concentration of 264, 330 and 660 ppm for corresponding beta values (ratio of inlet ammonia concentration to that of inlet NO concentration) of 0.8, 1 and 2 were considered. Three cases with inlet oxygen concentration of 0.1, 0.5 and 3.0% were considered.

Table 6.28 Experimental Data at 100^{o}C for V-Ti-W Based Catalyst [28]

NO_{in} (ppm)	NH_{3in} (ppm)	SV (h^{-1})	NO_{out} (ppm)	NH_{3out} (ppm)	N_2O_{out} (ppm)	NO_{2out} (ppm)	O_{2in} (%)
330	264	10500	321	252	1	11	0.1
330	330	10500	318	322	1	14	0.1
330	660	10500	301	662	0	21	0.1
330	264	10500	284	231	0	9	0.5
330	330	10500	279	296	0	10	0.5
330	660	10500	293	648	0	21	0.5
330	264	10500	256	201	0	9	3.0
330	330	10500	281	281	0	13	3.0
330	660	10500	290	648	0	23	3.0

Table 6.29 Experimental Data at 150°C for V-Ti-W Based Catalyst [28]

NO_{in} (ppm)	NH_{3in} (ppm)	SV (h^{-1})	NO_{out} (ppm)	NH_{3out} (ppm)	N_2O_{out} (ppm)	NO_{2out} (ppm)	O_{2in} (%)
330	264	10500	217	143	2	12	0.1
330	330	10500	201	208	1	12	0.1
330	660	10500	199	575	0	20	0.1
330	264	10500	139	84	0	7	0.5
330	330	10500	139	157	0	9	0.5
330	660	10500	147	517	0	17	0.5
330	264	10500	96	39	0	7	3.0
330	330	10500	109	117	0	10	3.0
330	660	10500	105	473	0	20	3.0

Table 6.30 Experimental Data at 200°C for V-Ti-W Based Catalyst [28]

NO_{in} (ppm)	NH_{3in} (ppm)	SV (h^{-1})	NO_{out} (ppm)	NH_{3out} (ppm)	N_2O_{out} (ppm)	NO_{2out} (ppm)	O_{2in} (%)
330	264	10500	71	20	3	10	0.1
330	330	10500	56	56	2	11	0.1
330	660	10500	43	416	1	18	0.1
330	264	10500	30	11	0	6	0.5
330	330	10500	31	39	0	8	0.5
330	660	10500	22	386	0	15	0.5
330	264	10500	46	8	1	9	3.0
330	330	10500	26	32	1	9	3.0
330	660	10500	23	385	1	19	3.0

Table 6.31 Experimental Data at 250^{o}C for V-Ti-W Based Catalyst [28]

NO_{in} (ppm)	NH_{3in} (ppm)	SV (h^{-1})	NO_{out} (ppm)	NH_{3out} (ppm)	N_2O_{out} (ppm)	NO_{2out} (ppm)	O_{2in} (%)
330	264	10500	45	9	5	10	0.1
330	330	10500	28	28	6	11	0.1
330	660	10500	8	331	8	16	0.1
330	264	10500	49	0	1	6	0.5
330	330	10500	13	21	4	9	0.5
330	660	10500	1	342	5	14	0.5
330	264	10500	64	0	3	10	3.0
330	330	10500	9	20	2	8	3.0
330	660	10500	15	357	6	20	3.0

Table 6.32 Experimental Data at 300^{o}C for V-Ti-W Based Catalyst [28]

NO_{in} (ppm)	NH_{3in} (ppm)	SV (h^{-1})	NO_{out} (ppm)	NH_{3out} (ppm)	N_2O_{out} (ppm)	NO_{2out} (ppm)	O_{2in} (%)
330	264	10500	76		8	15	0.1
330	330	10500	24	14	25	11	0.1
330	660	10500	7	202	32	14	0.1
330	264	10500	51	0	9	7	0.5
330	330	10500	12	11	20	9	0.5
330	660	10500	0	213	30	11	0.5
330	264	10500	64	0	8	11	3.0
330	330	10500	10	0	11	8	3.0
330	660	10500	13	209	30	17	3.0

Table 6.33 Experimental Data at 350^{o}C for V-Ti-W Based Catalyst [28]

NO_{in} (ppm)	NH_{3in} (ppm)	SV (h^{-1})	NO_{out} (ppm)	NH_{3out} (ppm)	N_2O_{out} (ppm)	NO_{2out} (ppm)	O_{2in} (%)
330	264	10500	81	8	52	9	0.1
330	330	10500	31	8	76	11	0.1
330	660	10500	7	45	117	11	0.1
330	264	10500	58	0	35	8	0.5
330	330	10500	21	0	63	9	0.5
330	660	10500	0	29	121	7	0.5
330	264	10500	70	0	28	13	3.0
330	330	10500	20	0	35	9	3.0
330	660	10500	13	30	112	13	3.0

Table 6.34 Experimental Data at 400^{o}C for V-Ti-W Based Catalyst [28]

NO_{in} (ppm)	NH_{3in} (ppm)	SV (h^{-1})	NO_{out} (ppm)	NH_{3out} (ppm)	N_2O_{out} (ppm)	NO_{2out} (ppm)	O_{2in} (%)
330	264	10500	116	0	100	9	0.1
330	330	10500	78	0	133	11	0.1
330	660	10500	13	0	249	10	0.1
330	264	10500	95	0	86	10	0.5
330	330	10500	66	0	113	12	0.5
330	660	10500	7	0	243	6	0.5
330	264	10500	101	0	69	19	3.0
330	330	10500	66	0	85	15	3.0
330	660	10500	19	0	221	12	3.0

Table 6.35 Experimental Data at 500^{o}C for V-Ti-W Based Catalyst

NO_{in} (ppm)	NH_{3in} (ppm)	SV (h^{-1})	NO_{out} (ppm)	NH_{3out} (ppm)	N_2O_{out} (ppm)	NO_{2out} (ppm)	O_{2in} (%)
330	264	10500	187	0	130	12	0.1
330	330	10500	161	8	160	15	0.1
330	660	10500	70	0	300	11	0.1
330	264	10500	162	0	113	16	0.5
330	330	10500	154	0	144	19	0.5
330	660	10500	70	0	285	10	0.5
330	264	10500	162	0	98	32	3.0
330	330	10500	162	0	120	32	3.0
330	660	10500	86	0	253	22	3.0

Regression analysis of the above data provides the values for the SCR rate constants for all temperatures and the exponents for ammonia and oxygen as listed in table 6.36.

Table 6.36 Rate Constants and Ammonia and Oxygen Exponents for V-Ti-W Catalyst

ln k_{100}	2.8870
ln k_{150}	5.3140
ln k_{200}	5.8635
ln k_{250}	5.9218
ln k_{300}	5.9426
ln k_{350}	5.8490
ln k_{400}	5.4933
ln k_{450}	4.9774
Ammonia exponent	0.1517
Oxygen exponent	0.1416

Hence the rate order expression is given by $r = k_T[NH_3]^{0.152}[O_2]^{0.142}$.

The ammonia exponent is 0.152 that indicates that reaction rate increases with inlet ammonia concentration while the oxygen exponent is comparable at 0.142 indicating a positive dependence of reaction rate on inlet oxygen concentration.

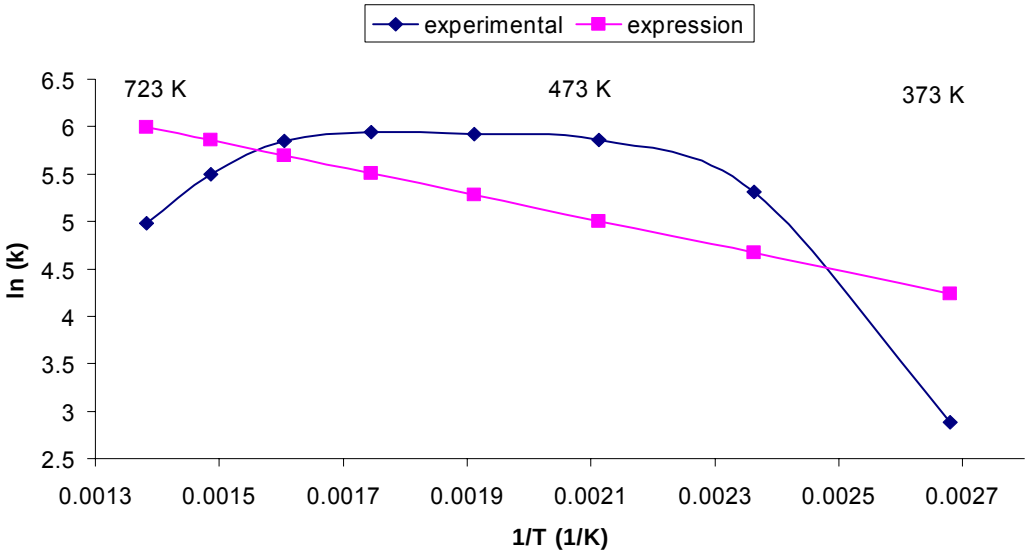

Fig 6.13 ln (k) versus 1/T for V-Ti-W Based Catalyst

Figure 6.13 shows that rate constant increases with temperature and reaches a maximum value at 300°C. The rate constant flattens out after 150°C. The value of the activation energy depends on the temperature range selected. The average activation energy for the complete temperature range turns out to be 11.27 KJ/mol. As can be seen from the figure, the rate constant does not vary for most of the temperature range. The SCR rate constant can be expressed as $k_T = 2618.8e^{\frac{-11.268}{8.31434*T}}$. This relation can be used to estimate the SCR rate constant (k_T) for intermediate temperature values.

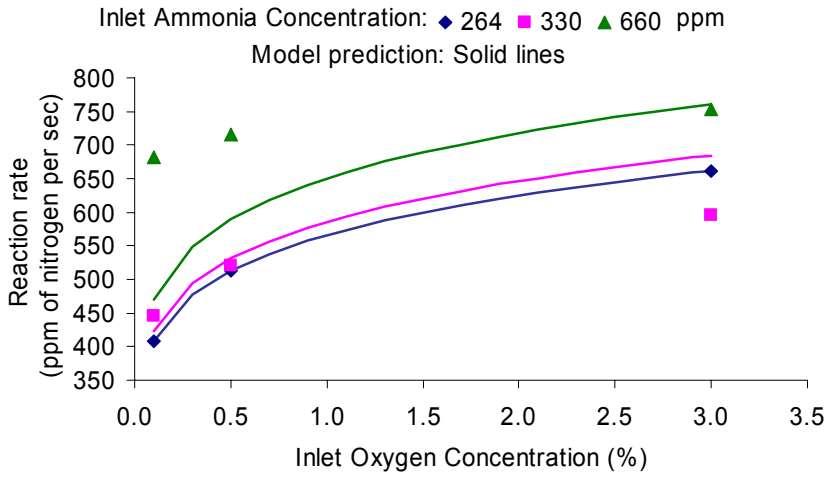

Fig 6.14 SCR Rate as a Function of Inlet Oxygen Concentration for Ammonia Concentrations of 264, 330 and 660 ppm at 400°C

Fig 6.14 illustrates the model performance for 0.1-3.0% inlet oxygen concentration for inlet ammonia concentrations of 264, 330 and 660 ppm at 400°C. The experimental values are shown with points while the solid lines indicate the model predictions. The reaction rate increase with inlet oxygen concentration for all inlet ammonia concentration.

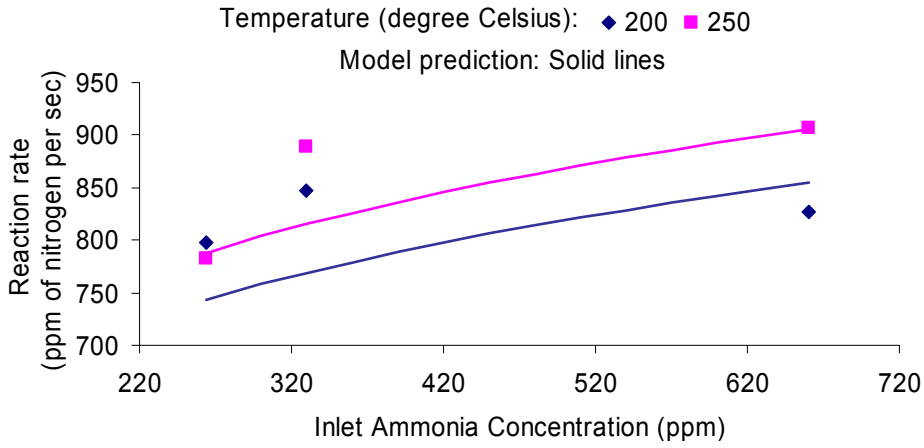

Fig 6.15 SCR Rate as a Function of Inlet Ammonia Concentrations at 250°C and 300°C and 0.5% Inlet Oxygen Concentration

Fig 6.15 illustrates the model performance for 264-660 ppm inlet ammonia concentrations at 250 and 300°C and 0.5% Inlet Oxygen Concentration. The experimental values are shown with points while the solid lines indicate the model predictions. The reaction rate increases with inlet ammonia concentration for all temperatures.

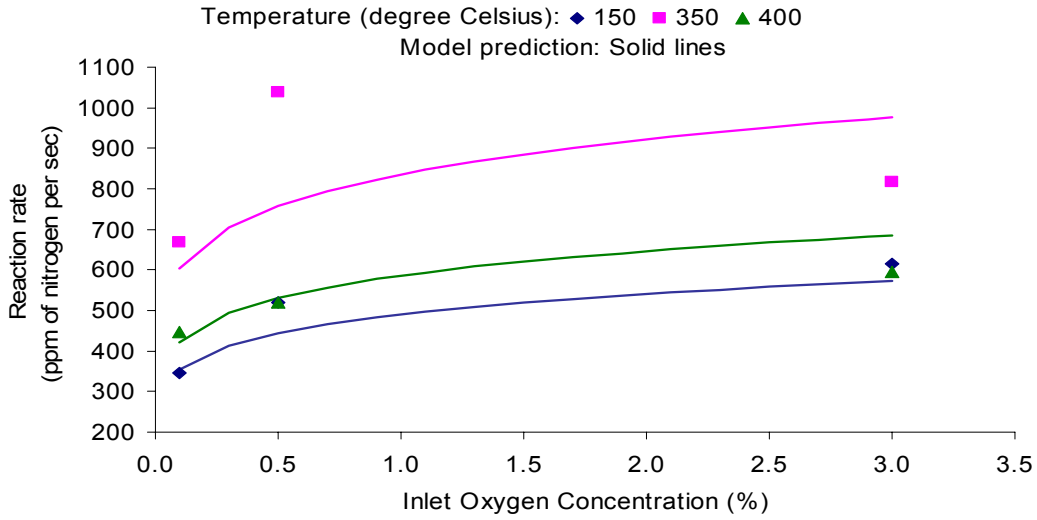

Fig 6.16 SCR Rate as a Function of Inlet Oxygen Concentration at 225°C, 250°C and 300°C and 330 ppm Inlet Ammonia Concentration

Fig 6.16 illustrates the model performance for 0.1 to 3.0% inlet oxygen concentrations at 225^{o}C, 250^{o}C and 300^{o}C and 330 ppm inlet ammonia concentration. The experimental values are shown with points while the solid lines indicate the model predictions. The reaction rate increases with inlet oxygen concentration for all temperatures.

Summarizing this section, for CU-ZSM-5, the ln K versus 1/T profile is quite linear as the reaction rate increases with temperature except for the 500^{o}C. The reaction rate increases significantly with ammonia concentration as indicated by the rate order of 0.4349 and weakly with oxygen (rate order of 0.0758). For V, the ln K versus 1/T profile increases sharply and then flattens out after 250^{o}C. The reaction rate increases with ammonia concentration as indicated by the rate order of 0.2427 and with oxygen (rate order of 0.1133). For V-Ti PLIC, a trend similar to V is observed as the ln K versus 1/T profile increases sharply and then flattens out after 200^{o}C. The reaction rate increases with ammonia concentration as indicated by the rate order of 0.2175 and with oxygen (rate order of 0.077). For V-Ti-W, the ln K versus 1/T is very flat throughout the temperature range except at 100^{o}C. The reaction rate increases with ammonia concentration as indicated by the rate order of 0.1517 and with oxygen (rate order of 0.1416).

7. SCR PROCESS MODELING – APPLICABLE RANGE

For practical applications, the SCR process with a particular catalyst would only be applicable for a certain temperature range, limited by the concentrations of NO, NO_2, N_2O and NH_3 in the exhaust. The NO reduction should be sufficiently high to meet the requirements, and at the same time the emission of NO_2, N_2O and NH_3 should be within the specified limits. Hence, the experimental results for each of the catalyst would be analyzed to determine the range of application and a rate order expression would be obtained for this recommended range. The model performance would be presented in the form of graphs for different operating conditions.

7.1 Cu-ZSM-5 Catalyst

For Cu-ZSM-5 the NO conversion reaches a value of 70% at 225°C and increases thereafter with temperature to up to 90%. The NH_3 slip for this range decreases with temperature from about 20% at 225°C to almost 0% at temperatures above 300°C. The N_2O emission for the Cu-ZSM-5 catalyst is very low for all operating conditions, the maximum value being 30ppm and average value being about 7 ppm. The NO_2 emission for the catalyst is also unnoticeable (except for the 400°C operating temperature) with the average value being about 7ppm. Hence, a temperature range of 225-500°C is reasonable for the Cu-ZSM-5 catalyst. The best performance was observed for 400°C, 660ppm and inlet oxygen concentrations of 0.1% and 0.5%. The results are summarized in table 7.1.

Table 7.1 Results for the Recommended Range

ln k_{225}	4.2369
ln k_{250}	4.3322
ln k_{300}	4.6134
ln k_{350}	4.7106
ln k_{400}	4.6574
ln k_{500}	4.6131
Ammonia exponent	0.5844
Oxygen exponent	0.0031

Hence, the rate order expression is given by $r = k_T[NH_3]^{0.584}[O_2]^{.003}$. The ammonia exponent is 0.584 that indicates that reaction rate increases with inlet ammonia concentration while the oxygen exponent is much smaller at 0.003 indicating that reaction rate is independent of inlet oxygen concentration.

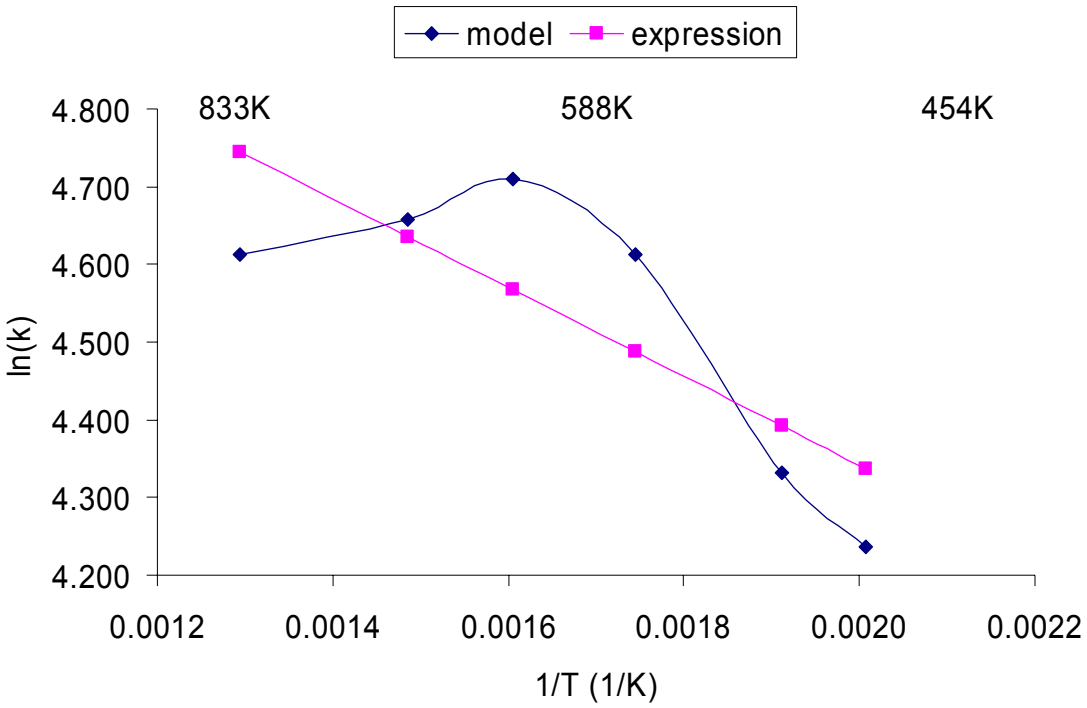

Fig 7.1 ln (k) versus 1/T for Cu-ZSM-5 Catalyst

The ln (k) versus 1/T graph shows a similar profile to the case when the whole of temperature range was considered. Figure 7.1 shows that rate constant increases with temperature and reaches a maximum value at 350^{o}C. The rate constant flattens out after 250^{o}C. The value of the activation energy depends on the temperature range selected. The average activation energy for the complete temperature range turns out to be 4.74 KJ/mol. The SCR rate constant can be expressed as $k_T = 240.5e^{\frac{-4.744}{8.31434*T}}$. This relation can be used to estimate the SCR rate constant (k_T) for intermediate temperature values.

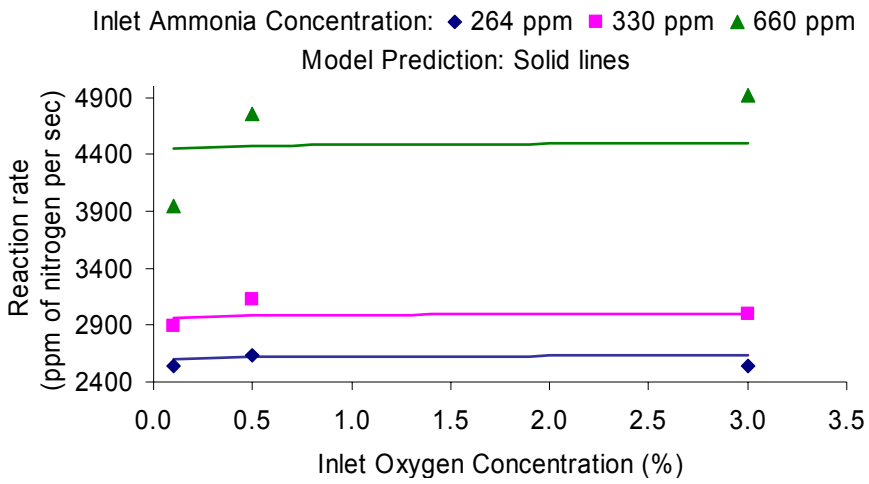

Fig 7.2 SCR Rate as a Function of Inlet Oxygen Concentration for Ammonia Concentrations of 264, 330 and 660 ppm at 300°C

Fig 7.2 illustrates the model performance for 0.1-3.0% inlet oxygen concentration for inlet ammonia concentrations of 264, 330 and 660 ppm at 300°C. The experimental values are shown with points while the solid lines indicate the model predictions. The reaction rate increase with inlet oxygen concentration for all inlet ammonia concentration.

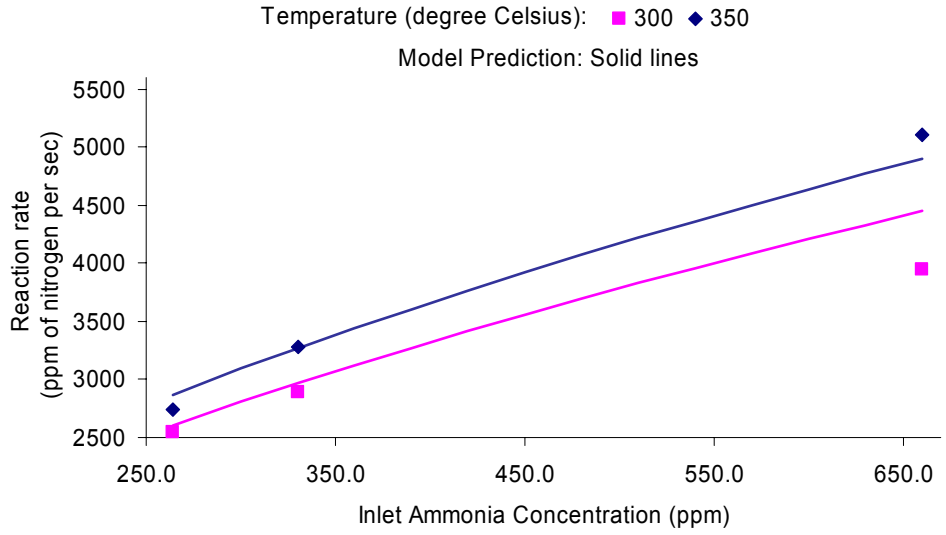

Fig 7.3 SCR Rate as a Function of Inlet Ammonia Concentrations at 300°C and 350°C and 0.5% Inlet Oxygen Concentration

Fig 7.3 illustrates the model performance for 264-660 ppm inlet ammonia concentrations at 300 and 350°C and 0.5% Inlet Oxygen Concentration. The experimental values are shown with

points while the solid lines indicate the model predictions. The reaction rate increases with inlet ammonia concentration for all temperatures.

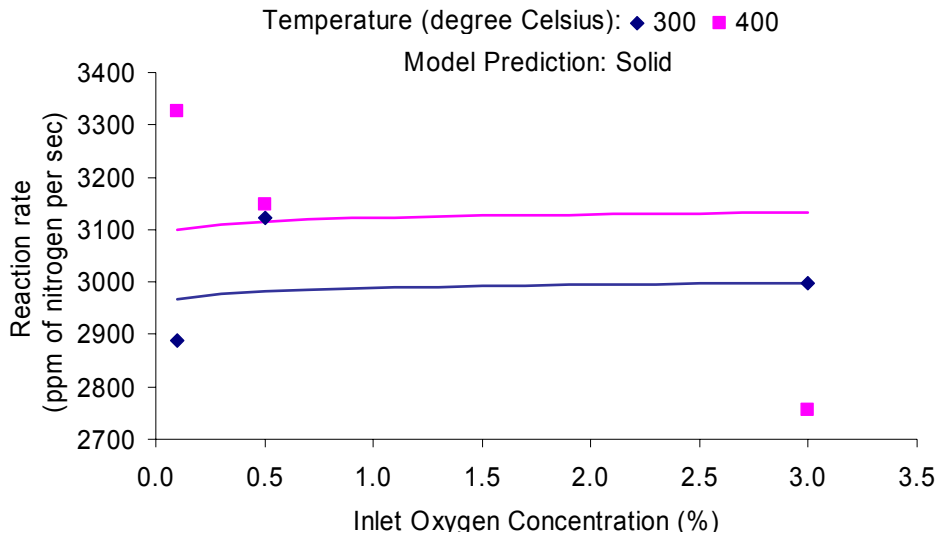

Fig 7.4 SCR Rate as a Function of Inlet Oxygen Concentration at 300°C and 400°C and 330 ppm Inlet Ammonia Concentration

Fig 7.4 illustrates the model performance for 0.1 to 3.0% inlet oxygen concentrations at 300°C and 400°C and 330 ppm inlet ammonia concentration. The experimental values are shown with points while the solid lines indicate the model predictions. The reaction rate increases with inlet oxygen concentration for all temperatures.

Table 7.2 Sensitivity Analysis for Ammonia and Oxygen Exponents

Parameter	Ammonia exponent	Oxygen exponent
Original	0.5844	0.0031
Inlet NO (-1%)	0.5878 (0.58%)	0.0031 (0%)
Inlet NO (+1%)	0.5810 (0.58%)	0.0030 (3.23%)
Inlet NH_3 (-1%)	0.5804 (0.68%)	0.0032 (3.23%)
Inlet NH_3 (+1%)	0.5882 (0.65%)	0.0029 (6.45%)

The table 7.2 indicates that the ammonia exponent changes by less than 0.7%, between the values of 0.5804-0.5882 while the oxygen exponent changes by up to 6.5%, between the values of 0.0029-0.0032 when the inlet nitric oxide or the inlet ammonia concentration is decreased and increased by 1%.

7.2 Vanadium Based Catalyst

For V the NO conversion reaches a value of 64% at 250°C and increases to 74% for 350°C. The NH_3 slip for this range decreases with temperature from about 24% at 250°C to 9% at 400°C. The N_2O emission for the V catalyst increases with temperature, from almost zero concentration to above 100ppm at 500°C. The NO_2 emission for the catalyst is unnoticeable with maximum value being 5ppm. Hence a temperature range of 250-400°C is resonable for the V catalyst. The best performance was observed for 300°C, 264 ppm and 3% inlet oxygen concentration. The results are summarized in table 7.3.

Table 7.3 Results for the Recommended Range

ln k_{250}	6.1926
ln k_{300}	6.4514
ln k_{350}	6.4631
ln k_{400}	6.3680
Ammonia exponent	0.2327
Oxygen exponent	0.0714

Hence, the rate order expression is given by $r = k_T[NH_3]^{0.2327}[O_2]^{0.0714}$. The ammonia exponent is 0.2327 that indicates that reaction rate increases with inlet ammonia concentration while the oxygen exponent is much smaller at 0.0714 indicating a weak dependence of reaction rate on inlet oxygen concentration.

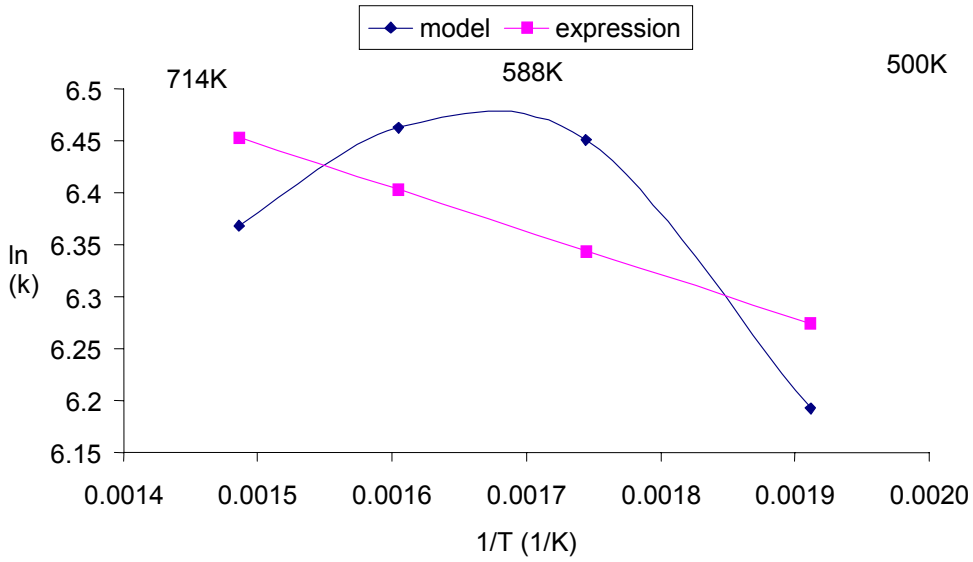

Fig 7.5 ln(k) versus 1/T for V Based Catalyst

The ln (k) versus 1/T graph shows a similar profile to the case when the whole of temperature range was considered. Figure 7.5 shows that rate constant increases with temperature and reaches a maximum value at 300°C. The rate constant flattens out after 150°C. The value of the activation energy depends on the temperature range selected. The average activation energy for the complete temperature range turns out to be 3.5 KJ/mol. The SCR rate constant can be expressed as $k_T = 1183.1e^{\frac{-3.486}{8.31434*T}}$. This relation can be used to estimate the SCR rate constant (k_T) for intermediate temperature values.

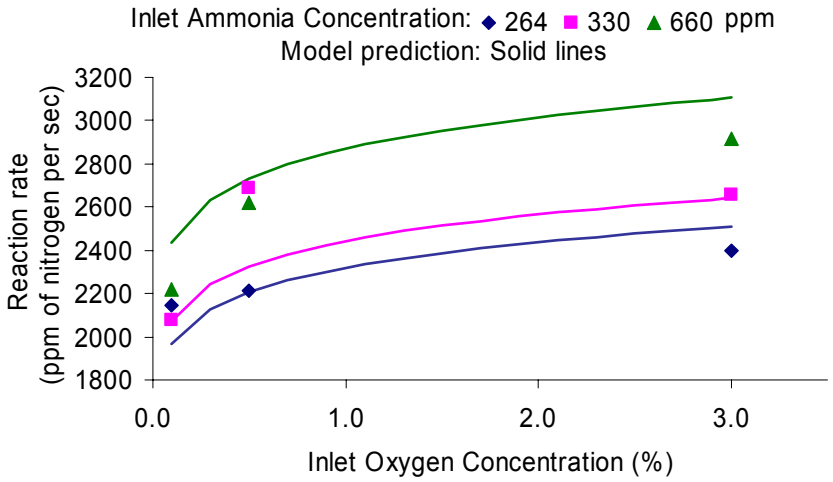

Fig 7.6 SCR Rate as a Function of Inlet Oxygen Concentration for Ammonia Concentrations of 264, 330 and 660 ppm at 300°C

Fig 7.6 illustrates the model performance for 0.1-3.0% inlet oxygen concentration for inlet ammonia concentrations of 264, 330 and 660 ppm at 300°C. The experimental values are shown with points while the solid lines indicate the model predictions. The reaction rate increase with inlet oxygen concentration for all inlet ammonia concentration.

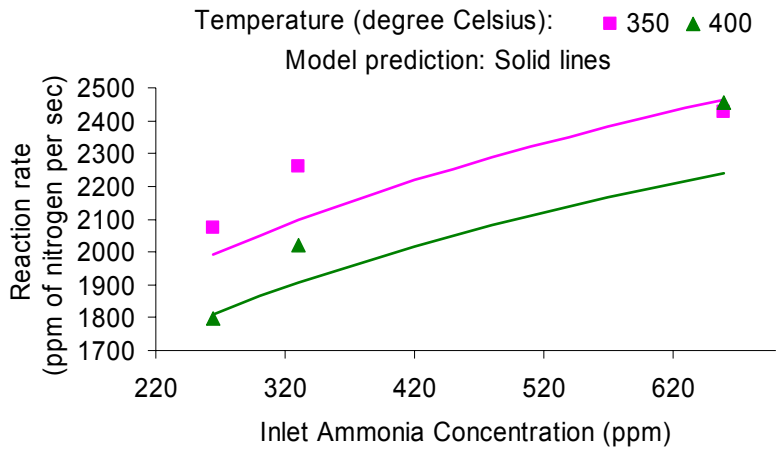

Fig 7.7 SCR Rate as a Function of Inlet Ammonia Concentrations at 350°C and 400°C and 0.1% Inlet Oxygen Concentration

Fig 7.7 illustrates the model performance for 264-660 ppm inlet ammonia concentrations at 350 and 400°C and 0.1% Inlet Oxygen Concentration. The experimental values are shown with points while the solid lines indicate the model predictions. The reaction rate increases with inlet ammonia concentration for all temperatures.

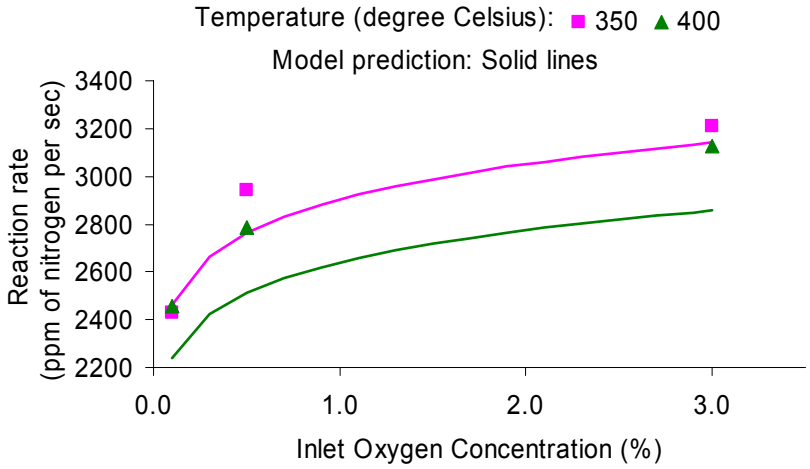

Fig 7.8 SCR Rate as a Function of Inlet Oxygen Concentration at 350°C and 400°C and 330 ppm Inlet Ammonia Concentration

Fig 7.8 illustrates the model performance for 0.1 to 3.0% inlet oxygen concentrations at 350°C and 400°C and 330 ppm inlet ammonia concentration. The experimental values are shown

with points while the solid lines indicate the model predictions. The reaction rate increases with inlet oxygen concentration for all temperatures.

Table 7.4 Sensitivity Analysis for Ammonia and Oxygen Exponents

Parameter	Ammonia exponent	Oxygen exponent
Original	0.2327	0.0714
Inlet NO (-1%)	0.2347 (0.86%)	0.0721 (1%)
Inlet NO (+1%)	0.2308 (0.82%)	0.0707 (1%)
Inlet NH_3 (-1%)	0.2237 (3.9%)	0.0723 (1.26%)
Inlet NH_3 (+1%)	0.2415 (3.8%)	0.0705 (1.26%)

The table 7.4 indicates that the ammonia exponent changes by up to 3.9%, between the values of 0.2237-0.2415 while the oxygen exponent changes by 1.26%, between the values of 0.0705-0.0723 when the inlet nitric oxide or the inlet ammonia concentration is decreased and increased by 1%.

7.3 Vanadium-Titanium Based PLIC Catalyst

For the V-Ti based PLIC catalyst, the NO conversion reaches a value of 70% at 250^{o}C and increases thereafter with temperature to up to 89%. The NH_3 slip for this range decreases with temperature from about 24% at 250^{o}C to 11% at 400^{o}C. The N_2O emission for the catalyst increases with temperature, from almost zero concentration to above 50ppm at 400^{o}C. The NO_2 emission for the catalyst is very low with maximum value being 17ppm. Hence a temperature range of 250-400^{o}C is reasonable for the catalyst. The best performance was observed for 350^{o}C, 330ppm and 3% inlet oxygen concentration. The results are summarized in table 7.5.

Table 7.5 Results for the Recommended Range

ln k_{250}	4.6051
ln k_{300}	4.7642
ln k_{350}	4.8073
ln k_{400}	4.7208
Ammonia exponent	0.2955
Oxygen exponent	0.0493

Hence the rate order expression is given by $r = k_T[NH_3]^{0.2955}[O_2]^{.0493}$. The ammonia exponent is 0.2955 that indicates that reaction rate increases with inlet ammonia concentration

while the oxygen exponent is much smaller at 0.0493 indicating a weak dependence of reaction rate on inlet oxygen concentration.

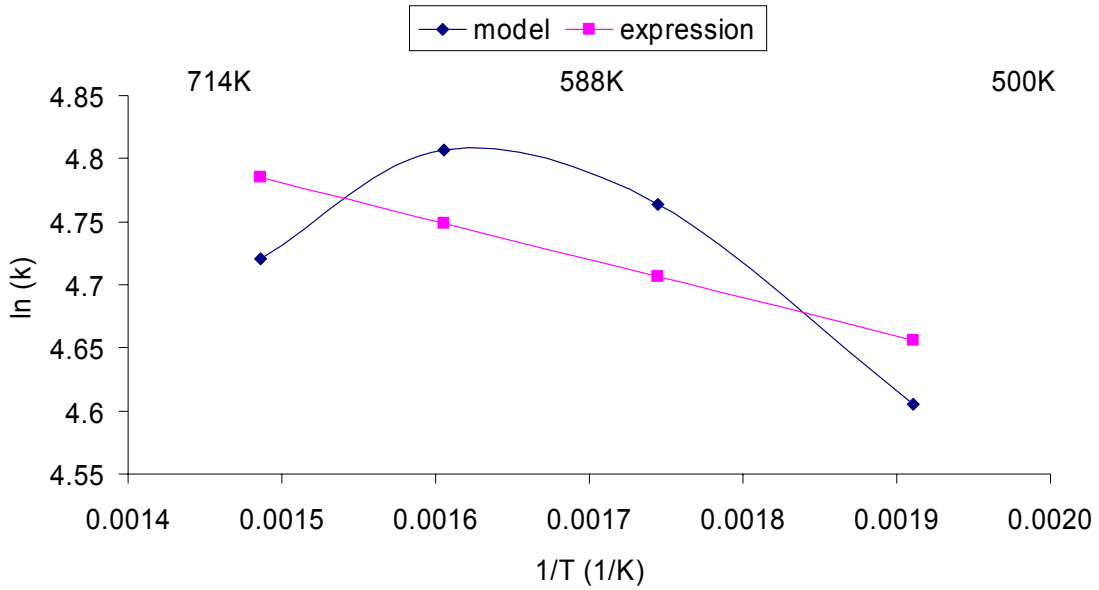

Fig 7.9 ln(k) versus 1/T for V-Ti Based PLIC Catalyst

The ln (k) versus 1/T graph shows a similar profile to the case when the whole of temperature range was considered. Figure 7.9 shows that rate constant increases with temperature and reaches a maximum value at 300^{o}C. The rate constant flattens out after 150^{o}C. The value of the activation energy depends on the temperature range selected. The average activation energy for the complete temperature range turns out to be 2.5 KJ/mol. The SCR rate constant can be expressed as $k_T = 187.7e^{\frac{-2.515}{8.31434*T}}$. This relation can be used to estimate the SCR rate constant (k_T) for intermediate temperature values.

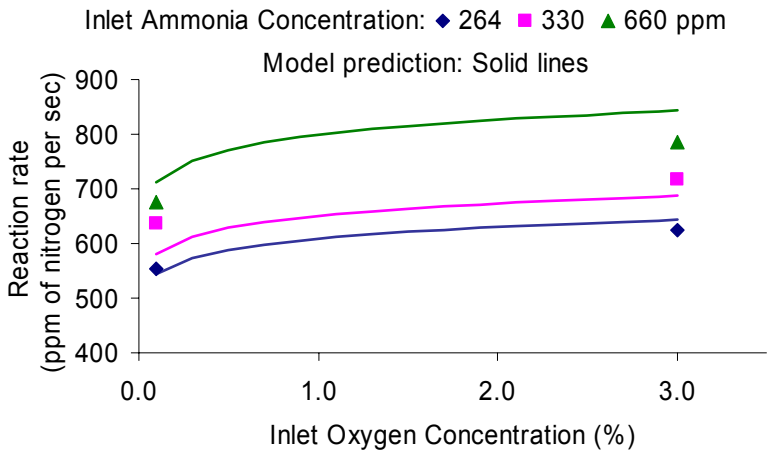

Fig 7.10 SCR Rate as a Function of Inlet Oxygen Concentration for Ammonia Concentrations of 264, 330 and 660 ppm at 300°C

Fig 7.10 illustrates the model performance for 0.1-3.0% inlet oxygen concentration for inlet ammonia concentrations of 264, 330 and 660 ppm at 300°C. The experimental values are shown with points while the solid lines indicate the model predictions. The reaction rate increase with inlet oxygen concentration for all inlet ammonia concentration.

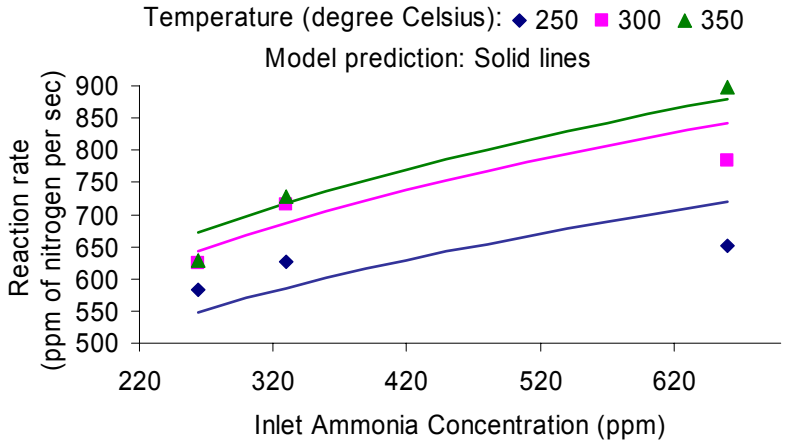

Fig 7.11 SCR Rate as a Function of Inlet Ammonia Concentrations at 250°C, 300°C and 350°C and 3% Inlet Oxygen Concentration

Fig 7.11 illustrates the model performance for 264-660 ppm inlet ammonia concentrations at 250, 300 and 350°C and 3% Inlet Oxygen Concentration. The experimental values are shown

with points while the solid lines indicate the model predictions. The reaction rate increases with inlet ammonia concentration for all temperatures.

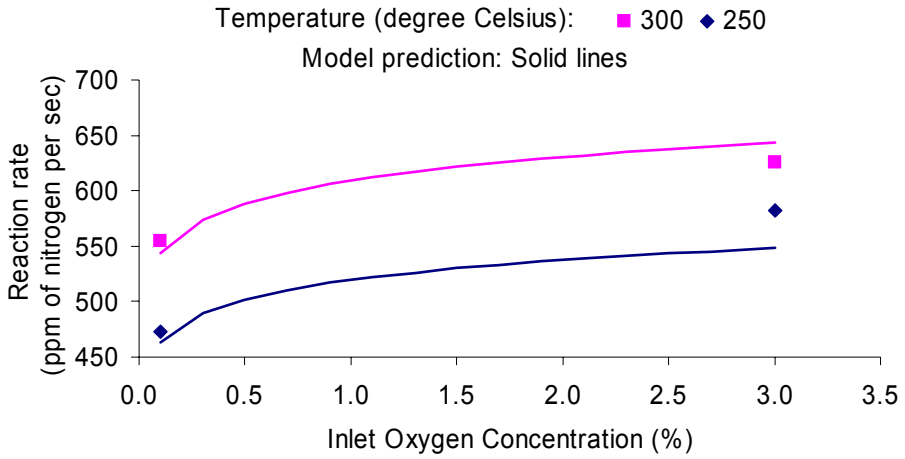

Fig 7.12 SCR Rate as a Function of Inlet Oxygen Concentration at 250°C and 300°C and 264 ppm Inlet Ammonia Concentration

Fig 7.12 illustrates the model performance for 0.1 to 3.0% inlet oxygen concentrations at 250°C and 300°C and 264 ppm inlet ammonia concentration. The experimental values are shown with points while the solid lines indicate the model predictions. The reaction rate increases with inlet oxygen concentration for all temperatures.

Table 7.6 Sensitivity Analysis for Ammonia and Oxygen Exponents

Parameter	Ammonia exponent	Oxygen exponent
Original	0.2955	0.0493
Inlet NO (-1%)	0.2976 (0.71%)	0.0496 (0.61%)
Inlet NO (+1%)	0.2933 (0.74%)	0.0489 (0.81%)
Inlet NH_3 (-1%)	0.2883 (2.44%)	0.0497 (0.81%)
Inlet NH_3 (+1%)	0.3025 (2.37%)	0.0488 (1.01%)

The table 7.6 indicates that the ammonia exponent changes by up to 2.44%, between the values of 0.2883-0.3025 while the oxygen exponent changes by 1.01%, between the values of 0.0488-0.0497 when the inlet nitric oxide or the inlet ammonia concentration is decreased and increased by 1%.

7.4 Vanadium-Titanium-Tungsten Based Catalyst

For V-Ti-W catalyst, the NO conversion reaches a value of 70% at 150°C and increases thereafter with temperature to up to 100%. The NH_3 slip for this range decreases with temperature from about 50% at 150°C to almost 0% at temperatures above 300°C. The N_2O emission for the catalyst increases with temperature, from almost zero concentration to above 50ppm at 350°C. The NO_2 emission for the catalyst is very low with maximum value being 20ppm. Hence a temperature range of 200-350°C is reasonable for the catalyst. The best performance was observed for 300°C, 330 ppm ammonia and 3% inlet oxygen concentration. The results are summarized in table 7.7.

Table 7.7 Results for the Recommended Range

ln k_{200}	5.1735
ln k_{250}	5.2318
ln k_{300}	5.2527
ln k_{350}	5.1591
Ammonia exponent	0.2546
Oxygen exponent	0.0192

Hence the rate order expression is given by $r = k_T[NH_3]^{0.2546}[O_2]^{0.0192}$. The ammonia exponent is 0.255 that indicates that reaction rate increases with inlet ammonia concentration while the oxygen exponent is much smaller at 0.019 indicating a weak dependence of reaction rate on inlet oxygen concentration.

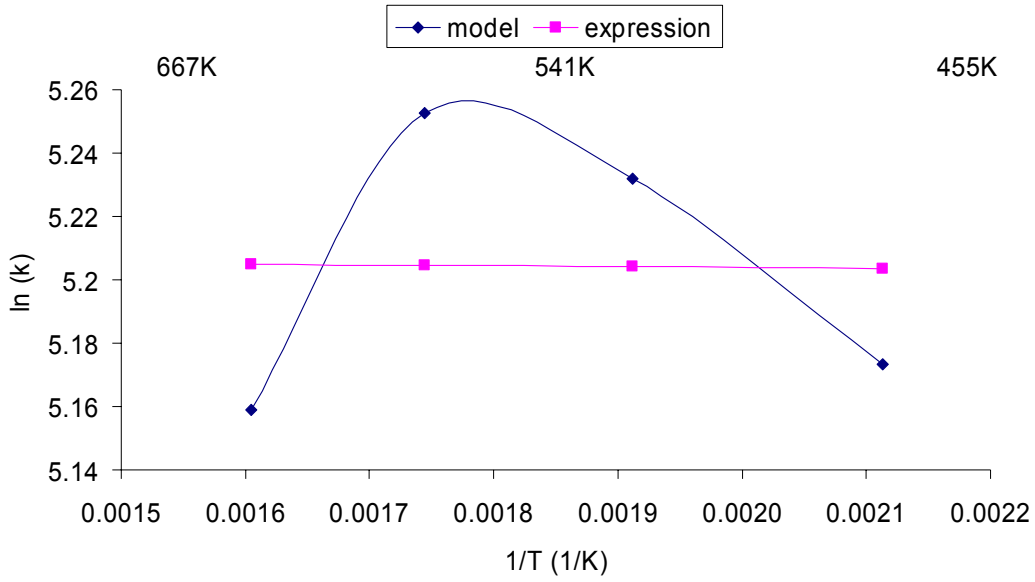

Fig 7.13 ln(k) versus 1/T for V-Ti-W Based Catalyst

The ln (k) versus 1/T graph shows a similar profile to the case when the whole of temperature range was considered. Figure 7.13 shows that rate constant increases with temperature and reaches a maximum value at 300°C. The rate constant flattens out after 150°C. The value of the activation energy depends on the temperature range selected. The average activation energy for the complete temperature range turns out to be 0.025 KJ/mol. The SCR rate constant can be expressed as $k_T = 183.1e^{\frac{-0.0249}{8.31434*T}}$. This relation can be used to estimate the SCR rate constant (k_T) for intermediate temperature values.

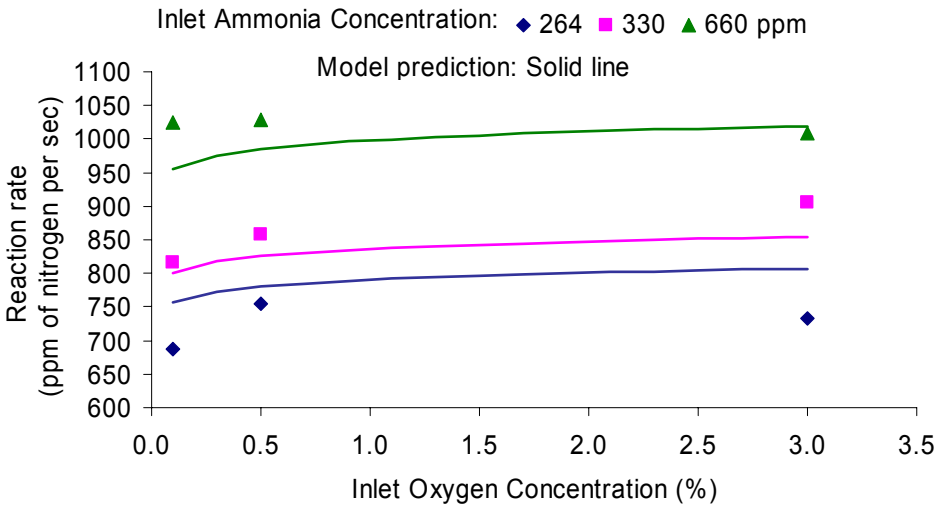

Fig 7.14 SCR Rate as a Function of Inlet Oxygen Concentration for Ammonia Concentrations of 264, 330 and 660 ppm at 300°C

Fig 7.14 illustrates the model performance for 0.1-3.0% inlet oxygen concentration for inlet ammonia concentrations of 264, 330 and 660 ppm at 300°C. The experimental values are shown with points while the solid lines indicate the model predictions. The reaction rate increase with inlet oxygen concentration for all inlet ammonia concentration.

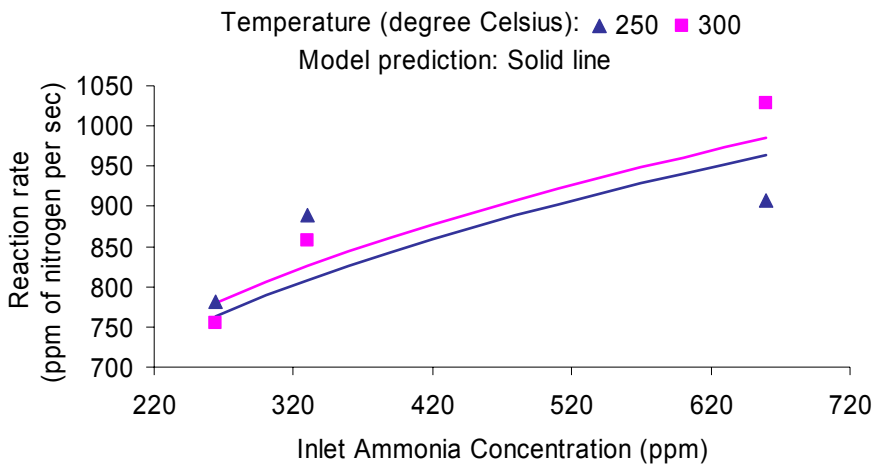

Fig 7.15 SCR Rate as a Function of Inlet Ammonia Concentrations at 250°C and 300°C and 0.5% Inlet Oxygen Concentration

Fig 7.15 illustrates the model performance for 264-660 ppm inlet ammonia concentrations at 250 and 300°C and 0.5% Inlet Oxygen Concentration. The experimental values are shown with points while the solid lines indicate the model predictions. The reaction rate increases with inlet ammonia concentration for all temperatures.

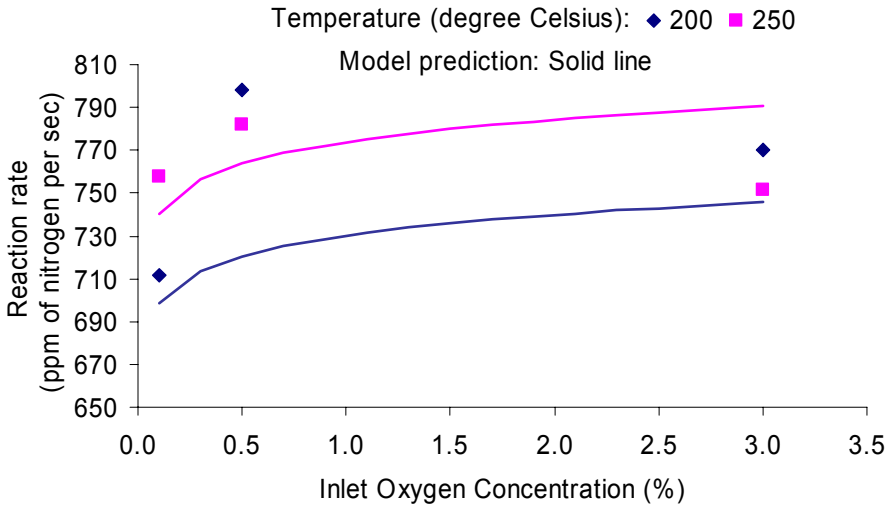

Fig 7.16 SCR Rate as a Function of Inlet Oxygen Concentration at 200°C and 250°C and 264 ppm Inlet Ammonia Concentration

Fig 7.16 illustrates the model performance for 0.1 to 3.0% inlet oxygen concentrations at 200^{o}C and 250^{o}C and 264 ppm inlet ammonia concentration. The experimental values are shown with points while the solid lines indicate the model predictions. The reaction rate increases with inlet oxygen concentration for all temperatures.

Table 7.8 Sensitivity Analysis for Ammonia and Oxygen Exponents

Parameter	Ammonia exponent	Oxygen exponent
Original	0.2546	0.0192
Inlet NO (-1%)	0.2561 (0.59%)	0.0194 (1.04%)
Inlet NO (+1%)	0.2531 (0.59%)	0.0191 (0.52%)
Inlet NH_3 (-1%)	0.2488 (2.28%)	0.0194 (1.04%)
Inlet NH_3 (+1%)	0.2603 (2.24%)	0.0191 (0.52%)

The table 7.8 indicates that the ammonia exponent changes by up to 2.28%, between the values of 0.2488-0.2603 while the oxygen exponent changes by 1.04%, between the values of 0.0191-0.0194 when the inlet nitric oxide or the inlet ammonia concentration is decreased and increased by 1%.

Summarizing this section, for CU-ZSM-5, the ln K versus 1/T profile increases linearly and then flattens out after 300^{o}C. The reaction rate increases significantly with inlet ammonia concentration as indicated by the rate order of 0.5844 and is independent of inlet oxygen concentration (rate order of 0.0031). The sensitivity analysis indicated that for ±1% error in measuring inlet NO concentration or inlet NH_3 concentration, the ammonia rate order could be off by up to 0.7% and the oxygen rare order by up to 6.4. For V, the ln K versus 1/T profile increases linearly and then flattens out after 300^{o}C. The reaction rate increases with inlet ammonia concentration as indicated by the rate order of 0.2327 and weakly with inlet oxygen concentration (rate order of 0.0714). The sensitivity analysis indicated that for ±1% error in measuring inlet NO concentration, the rate orders could be off by up to 1% and by up to 3.9% for ±1% error in measuring inlet NH_3 concentration. For V-Ti PLIC, a trend similar to V is observed as the ln K versus 1/T increases linearly and then flattens out after 350^{o}C. The reaction rate increases with inlet ammonia concentration as indicated by the rate order of 0.2955 and very weakly with inlet oxygen concentration (rate order of 0.0493). The sensitivity analysis indicated that for ±1% error in measuring inlet NO concentration, the rate orders could be off by up to 0.8% and by up to 2.4% for ±1% error in measuring inlet NH_3 concentration. For V-Ti-W, the ln K versus 1/ increases linearly with a sharp drop at 350^{o}C. The reaction rate increases with inlet ammonia concentration as indicated by the rate order of 0.2546 and is independent of inlet oxygen concentration (rate

order of 0.0192).). The sensitivity analysis indicated that for ±1% error in measuring inlet NO concentration, the rate orders could be off by up to 1% and by up to 2.3% for ±1% error in measuring inlet NH_3 concentration.

8. DISCUSSION

In this section, the rate order expressions obtained by the regression analysis will be discussed. An attempt will be made to understand the reaction kinetics based on the mechanistic information obtained from such kinetic models. The probable reactions, processes and the mechanisms would be briefly explained.

8.1 Comparisons to Previous Works

Many kinetic studies have been reported for the SCR reaction. These are based on both merely empirical expressions (e.g. power-law kinetics) and/or mechanistic approaches (e.g. Langmuir-Hinshelwood or Eley-Rideal models). The NO conversion rate for the SCR process can be supposed to depend on the concentrations of the reactants C_{NO}, C_{NH_3} and C_{O_2}, and also from the concentration of water, C_{H_2O}, which is a reaction product and is also present in the feed under actual SCR conditions. Accordingly, the following more general empirical power kinetic equation, similar to ones obtained in this work, can be used to model kinetic data:

$$r = k_c C_{NO}^{\alpha} C_{NH_3}^{\beta} C_{O_2}^{\gamma} C_{H_2O}^{\delta}$$

In this work, the NO order is assumed to be 1. The reaction order with respect to NO on V based catalysts has been measured to be 1 by many research groups [40-47]

The reaction order of 1 with respect to NO on CuZSM5 has also been found [48] that justifies the assumption in this study.

According to Inomata et al. [41] (for pure V_2O_5) and to Wong and Nobe [42] (for V_2O_5/TiO_2), for cases of excess oxygen and in the absence of water vapor, or with water contents above 5%, the rate dependencies from water can be neglected. All authors, with few exceptions [49], agree that water hinders the SCR reaction [50-55] although this effect is no more evident, on industrial catalysts, for H_2O levels above 5% (v/v) [56], and hence this rate dependency was not considered in this work.

Also, according to Inomata et al. [41] (for pure V_2O_5) and to Wong and Nobe [42], the reaction order with respect to ammonia was estimated to be 0 for cases with excess oxygen and in the absence or excess of water. According to Orlik et al. [40] working on monolithic 15% V_2O_5-TiO_2 the reaction rate is first order in ammonia at very low concentrations and becomes zero order with increasing ammonia concentration. No effect of ammonia concentration on the reaction rate has been reported by several other authors on vanadia-based catalysts [57-60] For SCR monolith reactors working in excess of NH_3, the reaction rate depends only on the NO concentration [61]

According to some authors, working with a substoichiometric NH_3/NO ratio (as actually occurs in industrial reactors to minimize ammonia slip) the rate dependence from ammonia concentration appears. In this case values near 0.2 have been measured [52-54] These agree well with the ammonia exponent values of 0.2427 for V, 0.2175 for V-TI based PLIC and 0.1517 for the V-Ti-W catalyst determined by this work. The reaction order with respect to ammonia changed to 0.2327 for V, 0.2955 for V-TI based PLIC and 0.2546 for the V-Ti-W catalyst when only the data in the recommended range was used to model the process.

Zero order with respect to ammonia has also been measured on Cu-ZSM5 [48] while this study suggests a value of 0.4349 (and 0.5844 for the recommended range).

Conflicting data are reported on the reaction order with respect to oxygen, generally found in the range 0-0.5 [45-48], which has however been neglected by many authors because, in practical conditions, oxygen is in large excess. The reaction order with respect to oxygen obtained in this study were 0.0758 for CuZSM5, 0.1133 for V, 0.0770 for V-Ti based PLIC and 0.1416 for V-Ti-W which are in the range mentioned above and closer to 0. The reaction order with respect to oxygen changed to 0.0031 for CuZSM5, 0.0714 for V, 0.0493 for V-TI based PLIC and 0.0192 for the V-Ti-W catalyst when only the data in the applicable range was used to model the process. These values are much closer to zero and that suggests independence of reaction rate with respect to inlet oxygen concentration, as proposed by many research groups.

8.2 Mechanistic Interpretations

8.2.1 Reactions

It has been concluded that NO is the actual reactant in SCR [41] and that oxygen does participate in the reaction [63, 64], though in the past, it was supposed that the true reactant for the SCR process could be NO_2 [62] Today, most authors agree that the reaction stoichiometry in typical SCR conditions is the following:

$$4NH_3 + 4NO + O_2 \rightarrow 4N_2 + 6H_2O \quad (60)$$

Using isotopically labeled reactants, it has been demonstrated that both on vanadia-based catalysts [65-67] and on noble metals [68], the two nitrogen atoms of N_2 arise, one from NO and the other from ammonia.

V_2O_5-based catalysts also catalyze the reduction of NO_2 in the presence of oxygen [69, 70]:

$$4NH_3 + 2NO_2 + O_2 \rightarrow 3N_2 + 6H_2O \quad (61)$$

In the absence (or defect) of O_2, the reaction stoichiometry(13) converts [63, 64] into the following:

$4NH_3 + 6NO \rightarrow 5N_2 + 6H_2O$ (62)

This reaction can be formally considered as the combination of the reverse of reaction (1) plus reaction(13). In this case, four N_2 molecules arise from a reaction between NO and NH_3 (through reaction (13)) one arises from two molecules of NO. The reaction between NO and ammonia can also proceed in a different way, giving rise to the unwanted product N_2O:

$4NH_3 + 4NO + 3O_2 \rightarrow 4N_2O + 6H_2O$ (63)

In general, authors agree that under typical SCR conditions, with NH_3/NO near 1, a few percent oxygen and T<400^oC, reaction (13) accounts for the overall stoichiometry on the best catalysts [71, 72, 56], a conclusion which supports the applicable range determined in this thesis. Accordingly, the SCR process occurs when N_2 is produced with selectivity close to 100% and the ratio of converted moles of NO and NH_3 is 1. Non-selective behavior occurs when products other than N_2 (namely N_2O) are formed (e.g. via reaction (63)) and/or when the ratio of converted NO and NH_3 moles is lower than 1. This implies that ammonia is converted by ways other than reaction (13), i.e., it is in part oxidized by oxygen instead of NO through one of the following ways:

$2NH_3 + 3/2O_2 \rightarrow N_2 + 3H_2O$ (64)

$2NH_3 + 2O_2 \rightarrow N_2O + 3H_2O$ (65)

$2NH_3 + 5/2O_2 \rightarrow 2NO + 3H_2O$ (66)

Reaction (64) is being studied, because in principle it helps to minimize any ammonia slip after the SCR reactors (if working with excess of ammonia), without introducing other reactants into the gas mixture and without producing further pollutants [73-75] This is the so-called SCO process (selective catalytic oxidation of ammonia). Several active SCR catalysts are also active in SCO, although at slightly higher temperatures. Reactions (64) and (66) account for an unbalanced conversion of NO and NH_3 molecules, even in the absence of N_2O among the products. Reactions (64)-(66) have been shown to occur on most transition metal oxides [76-78], and, in particular, over systems which are active in SCR [73-75,76-81] In general, reaction (64) is favored with respect to reaction (66) at lower temperatures, while the reverse is found at higher temperatures. Due to the higher thermodynamic stability of N_2 with respect to NO and N_2O, its is obvious that reactions (65) and (66) must be parallel more than in series with respect to reaction (64). All of them are also parallel to reaction (13), although they can have intermediates in common. N_2O can arise from NH_3.NO (reaction (63)), from NH_3 oxidation (reaction (65)) and from NO alone, without participation of ammonia, i.e. through reactions such as:

$2NO \rightarrow N_2O + 1/2O_2$ (67)

$3NO \rightarrow N_2O + NO_2$ (68)

Reaction (67) can be mediated by the dimeric species of NO, i.e. N_2O_2. It can be an intermediate step in NO decomposition (the reverse of reaction (1)). In fact, transition metal oxide catalysts, like those active in the SCR [82] can also be active as catalysts for the decomposition of N_2O:

$N_2O \rightarrow N_2 + 1/2O_2$ (69)

Reaction (68) is the disproportionation of NO and is a gas-phase reaction, favored at high pressures [83] As it will be further discussed below, isotopic labeling experiments [65, 84] showed that under typical SCR conditions and over SCR metal oxide catalysts, reaction(63) is the main one for N_2O production and reactions (67) and (68) do not occur.

It is obvious that on SCR catalysts reaction (13) must be faster than the competitive reactions (63)-(66). In typical SCR conditions NO conversion approaches to be total with converted NH_3/NO ratios of 1 already near 550 K and upon a working window up to 650-700 K. This behavior implies that reaction (13) occurs selectively and no N_2O is formed in this working window.

However, at temperatures higher than those corresponding to the working window, the NO conversion decreases progressively. This is due to the onset of reactions (63)-(66) that become competitive with reaction (13) and both subtract the reactant NH_3 (the case of reactions (64) and (65)) and/or produce back NO (reaction (66)). When (with feed NH_3/NO ratios'1) the NO conversion starts to decrease, in general N_2O appears and the ratio of converted NH_3/NO is higher than 1. Accordingly on industrial catalysts in the working temperature window reaction (13) is faster than reactions (63)-(66). The observation that over SCR catalysts the presence of NO favors NH_3 consumption via route (13) instead through the competitive reactions (63)-(66) indicates that the SCR reaction and the NH_3 oxidation reaction involve different rate-determining steps.

The complex chemistry of the SCR systems has also been studied by investigating the ammonia oxidation reaction [73-81,85] These studies showed that reactions (64)-(66) are actually competitive reactions.

Parallel behaviors, with a temperature range with maximum NO conversion upon SCR and the competition of SCR and ammonia oxidation reactions, have been found on any vanadia-based catalyst [86] For other catalysts, the maximum conversion obtained is frequently lower than on industrial catalysts at a given temperature, the working window for the SCR is smaller, the selectivity to nitrogen is lower than 1 with signifcant N_2O production also at low temperature, and the ratio of converted NH_3 and NO is frequently higher than 1. This implies that Cu-, Fe-, Cr- and Mn-based oxides efficiently catalyze reactions (63)-(66), so that they are less selective than V_2O_5-based catalysts. In any case, the observed parallelism in the catalytic behavior of these catalysts suggests that the basic mechanistic features of the reactions on these different metal oxide samples should be the same. This is in line with the observation that in oxidation catalysis the basic mechanistic features are usually mainly determined by the chemistry of the reactants [87]

8.2.2 Adsorption and Desorption

Kinetic data strongly suggest that on all active catalysts ammonia reacts from a strongly adsorbed state, whereas different opinions are available concerning the interaction of NO with the catalytic surface. The adsorption characteristics of the SCR reactants over various oxide-based catalysts have been extensively investigated. All authors agree in indicating that ammonia adsorbs on pure V_2O_5, on V_2O_5-TiO_2 and on V_2O_5-WO_3/TiO_2 in two different strongly held species [88-100] They are: (i) molecularly adsorbed ammonia, through a Lewis-type interaction on coordinatively unsaturated cations; and (ii) ammonia adsorbed as ammonium ions, over Brùnsted acidic -OH surface hydroxyl groups.

Adsorption on Lewis sites is predominant in V_2O_5-TiO_2 [101] The TiO_2-anatase supports, if pure, only show Lewis acidity [102], whereas ammonium ions are formed on V-OH sites. These data suggest that vanadyl sites are Lewis acidic and can convert into Brùnsted sites by water adsorption

ESR (Electron Spin Resonance) and XPS (X-ray Photoelectron Spectroscopy) data also showed that NH_3 can reduce the vanadia sites over V_2O_5/TiO_2 [103] while conductance measurements [104] showed that ammonia adsorption caused a significant increase in the conductance of V_2O_5/SiO-TiO_2 catalysts, so confirming a catalyst reduction by ammonia, in agreement with TPR (Temperature Programmed Reduction) data [105]

It has been found that a simple Langmuir approach could not represent the NH_3 adsorption-desorption data accurately. A nice fit of the data could be obtained by assuming a non-activated NH_3 adsorption and a Temkin-type desorption kinetics [106]

Lewis bonded and Brùnsted bonded ammonia species have also been found on Cu-ZSM5, even if overexchanged [41, 107] In these cases it has been supposed that the Brùnsted acid sites are residual nonexchanged OHs of the zeolite, that are retained in spite of the cation over-exchange.

The chemistry of nitrogen oxide at the interface of oxide materials is very complex [108-113] In principle, NO can adsorb to form surface nitrosyls where it interacts with a lone pair of the N atom to the surface metal cationic centers, and can be oxidized by oxide surfaces, giving rise to species like nitrosonium ion (NO^+), nitrite ions (NO_2^-), adsorbed nitrogen dioxide (NO_2), nitronium ion, (NO_2^+), and nitrate ions (NO_3^-). However, it can also act as an oxidizing agent, reducing itself to (NO^-) and to its dimeric form, the hyponitrite anion ($N_2O_2^{2-}$), as well as to N_2O and N_2. Moreover, it can dimerize to dinitrogen dioxide N_2O_2 (which is possibly an intermediate in its reduction and/ or in its oxidation) and to disproportionate giving rise to both reduced and oxidized species. It has been shown that over catalysts like pure V_2O_5 [94, 114], on V_2O_5-TiO_2 [94, 106, 115-118], on V_2O_5 -WO_3-TiO_2 [116], the interaction of NO is very weak In any case, adsorption is usually negligible at the reaction temperature, particularly in the presence of ammonia. These data allowed some authors to interpret the kinetic data on vanadia-based catalysts (and in

particular the apparent first order kinetics with respect NO due to slow step involving the reaction of gas-phase NO with adsorbed NH_3.

8.3 Mechanisms

The surface species that are supposed to be involved in the most popular reaction schemes among those proposed in the literature for SCR are summarized in table 8.1:

Table 8.1 Proposed Reactant Species, Intermediates and Active Sites in Different Mechanisms and/or Kinetic Schemes for SCR on Vanadia Based Catalysts [41, 63, 66, 119, 94, 61, 120-122, 86]

Reactant species		Intermediate	Catalyst	Supposed active site
From NH_3	From NO			
NH_4^+	O-N-O |		V_2O_5	
NH_4^+	NO gas	H-bonded complex	V_2O_5	O OH ‖ | -O-V-O-V-O
O-NH_2 | V	NO gas		V_2O_5/supp	O O ‖ ‖ -O-V-O-V-O
NH_4^+	NO gas		V_2O_5	OH | V + V-O-V
NH_2 | V	NO gas	NH_2NO | V	V_2O_5/TiO_2	O ‖ V
NH_3ads NH_2	N_2Oads adsorbed NO		V_2O_5/supp V_2O_5/TiO_2	Lewis sites
O^- H_3N^+ HO | | V V	NO gas	O^- ^+H_3N-N=O HO | | V V	V_2O_5/TiO_2	O HO ‖ | -V- -V-
NH_4^+	O-NO_2 | V^{4+}	NH_4NO_2	V_2O_5/TiO_2	O ‖ V^{5+}
$Cu(NH_3)_nNO_2$			Cu-ZSM5	Dimers Cu^{2+} $(NH_3)_n$

Ramis et al. [94] proposed the reaction pathway shown in Fig. 8.1 for V oxide based catalysts. This mechanism consists of the following steps:

$$NH_3 + M^{n+} + O^{=} \rightarrow M^{(n-1)+}\text{-}NH_2 + {}^{-}OH \quad (70)$$

$$M^{(n-1)+}\text{-}NH_2 + NO \rightarrow M^{(n-1)+}\text{-}NH_2NO \quad (71)$$

$$M^{(n-1)+}\text{-}NH_2NO \rightarrow M^{(n-1)+} + N_2 + H_2O \quad (72)$$

$$2\ M^{(n-1)+} + 1/2\ O_2 \rightarrow 2M^{n+} + O^{=} \quad (73)$$

$$2\ {}^{-}OH \rightarrow H_2O + O^{=} \quad (74)$$

Accordingly, ammonia is adsorbed over a Lewis acid site that activates ammonia to an amide NH_2 species (step 70), resulting in catalyst reduction. This activated ammonia species then react with gas-phase NO giving rise to a nitrosamide intermediate (step 71), that then decomposes to nitrogen and water (step 72).

The reduced catalyst sites are then regenerated by gas-phase oxygen (step 73). The proper sum of these equations gives the reaction stoichiometry (3). The key reaction step is supposed to involve a radical coupling between the $[M^{(n-1)+}\text{-}NH_2]$ surface species with the radical molecule NO. This is the first mechanism proposed for vanadia-based catalyst implying an activation of ammonia on Lewis acid sites.

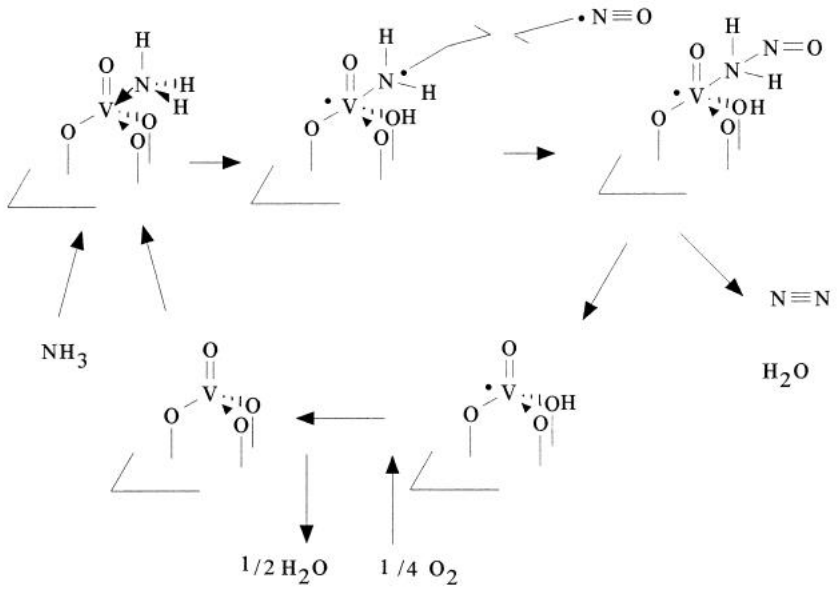

Fig 8.1 Mechanism of the NO-NH_3 Reaction on Supported Vanadium Oxide Catalysts Proposed by Ramis et al. [94] in the Presence of Oxygen.

On the basis of in situ on-line FTIR studies under steady-state conditions, Topsùe et al. [122] proposed the mechanistic scheme shown in Fig. 8.2 for V-Ti catalysts. In this mechanism, the catalytic activity is found to be related to the ammonia adsorbed on the Bronsted acid sites

associated with V^{5+}-OH sites. V^{5+}=O groups are also involved in the reaction, and specifically in the activation of adsorbed ammonia. This activation process involves the transfer or partial transfer of a hydrogen from the NH_3 molecule and accordingly reduced V^{4+}-OH sites are produced. Once ammonia has been activated, NO from the gas-phase reacts with the activated ammonia complex leading to the formation of an intermediate that then decomposes to nitrogen and water. Regeneration of the active sites (i.e., oxidation of the reduced VOH sites to V^{5+}=O groups) occurs by gas-phase oxygen. Accordingly, the proposed catalytic cycle consists of both acid-base and redox functions.

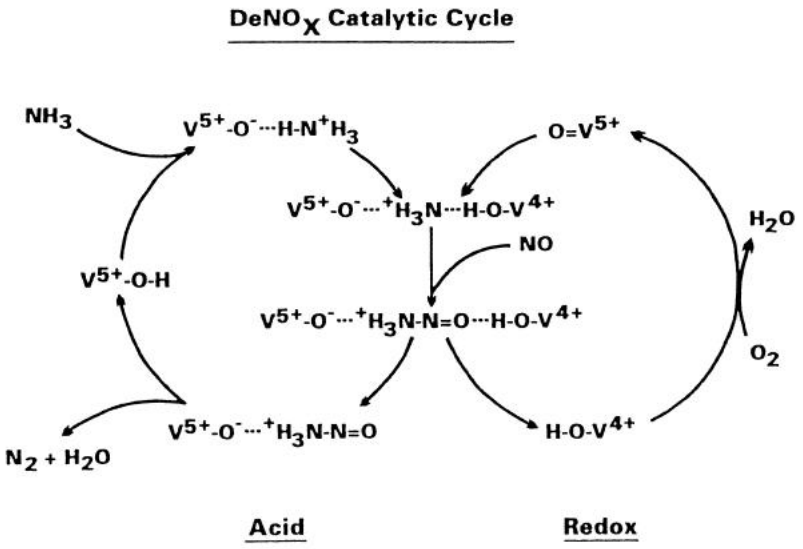

Fig 8.2 Scheme Illustrating the Catalytic Cycle of the SCR Reaction Over Vanadia/Titania Catalyst in the Presence of Oxygen Proposed by Topsùe et al. [122]

A more complex mechanism has been proposed by Komatsu et al. [48] for Cu-zeolite catalysts (Fig. 8.3). In this mechanism, a molecule of NO and a dissociated oxygen atom react with the oxygen atom of a suggested active NH_3 -Cu dimer species (species (a)), thus resulting in the formation of a bridging NO_3 species. To explain the observed first order rate in NO and half order in O_2, the step from (a) to (b) has been considered as the rate-determining step. Then another NO molecule attacks the NO_3 species to form two NO_2 molecules, each attacked to a Cu atom (species (c)). Finally, the reactive NO_2 species and one of the NH_3 ligands bound to the same Cu ion react to produce nitrogen and water. Although these authors do not count explicitly the electrons, the proposed reaction intermediate is necessarily a nitrite species NO_2^-, formed by reaction of a nitrate species, NO_3^-, with NO and Cu. However this complex chemistry should be supported by more data.

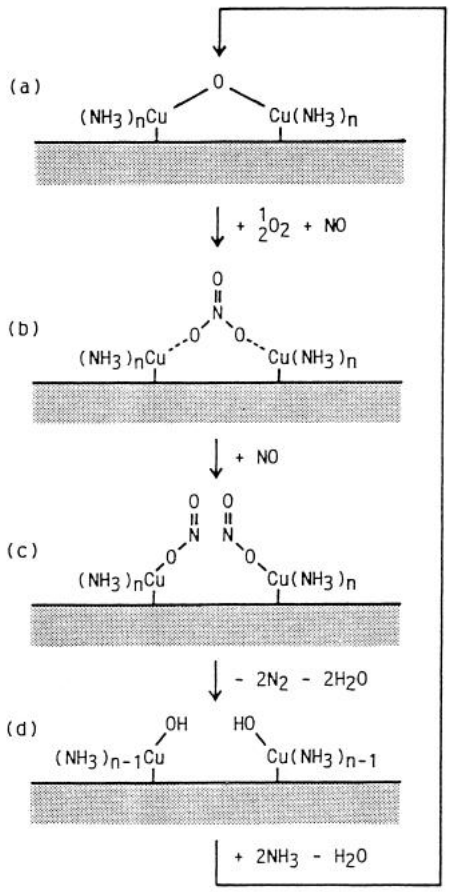

Fig 8.3 Scheme Illustrating the Catalytic Cycle of the SCR Reaction Over Cu-ZSM5 Catalyst in the Presence of Oxygen Proposed by Komatsu et al. [48]

Different research groups have been proposing different reaction mechanisms and have been able to explain most of the observations in a SCR process. Though the exact validated reduction mechanisms with their reacting species, intermediates and actives sites have not been found, a general understanding of the complex catalytic process has been established. However for the purpose of detailed and exact SCR process modeling, kinetic data (such as Arrhenius constant and activation energy) is required for each individual reaction and also exact values of adsorption and desorption coefficients, diffusivity and pore dimensions needs to be determined. That along with the coupling between the chemical and thermal problem and the variables such as flow profile, contaminants, aging makes the SCR process modeling a very challenging task.

9. SUMMARY

The SCR process was investigated and different modeling approaches were studied in order to select the one most suited to the scope of this study. The experimental data was analyzed to determine the applicable range of operation for each of the catalyst based on their NO_x conversion and ammonia, N_2O and NO_2 emission.

Analysis of the experimental data revealed that for the Cu-ZSM-5 based catalyst, the best performance was observed for 400^oC, 660 ppm inlet ammonia concentration and 0.1%/0.5% inlet oxygen concentration. For the Vanadium based honeycomb monolith catalyst (V), the best performance was observed for 300^oC, 264 ppm inlet ammonia concentration and 3% inlet oxygen concentration. For the Vanadium-Titanium based PLIC catalyst (V-Ti PLIC), the best performance was observed for 350^oC, 330 ppm inlet ammonia concentration and 3% inlet oxygen concentration. For the Vanadium-Titanium-Tungsten based honeycomb monolith catalyst (V-Ti-W), the best performance was observed for 300^oC, 330 ppm inlet ammonia concentration and 3% inlet oxygen concentration.

At the suggested point of operation, the Cu-ZSM-5 and the V-Ti-W catalysts have minimal ammonia slip while for the V and V-Ti PILC catalysts the ammonia slip is much higher throughout the temperature range which limits their potential.

At the operating conditions listed above, the N_2O emission is less than 20 ppm and the NO_2 emission is less than 10 ppm for all the catalysts.

For the Cu-ZSM-5 catalyst, the performance deteriorates with increasing oxygen concentrations which is a serious drawback since most of the modern lean burn engine exhaust and turbine exhaust has high concentrations of oxygen. These observations are summarized in table 9.1.

Table 9.1 Summary of Catalyst Performance

Catalyst	Emission	Suggested Operation	Comments
Cu-ZSM-5	- Ammonia slip 0-20% - N_2O emmision ~10 ppm - NO_2 emission ~10 ppm	400^oC, 660 ppm NH_3 and 0.1%/0.5% O_2	Decreased performance for higher O_2 concentrations
V	- Ammonia slip 9-24% - N_2O emmision upto 100 ppm - NO_2 emission ~5 ppm	300^oC, 264 ppm NH_3 and 3% O_2	Low NO conversion, high ammonia slip
V-Ti PILC	- Ammonia slip 11-24% - N_2O emmision upto 50 ppm - NO_2 emission ~10 ppm	350^oC, 330 ppm NH_3 and 3% O_2	Low NO conversion, high ammonia slip
V-Ti-W	- Ammonia slip 0-50% - N_2O emmision upto 50 ppm - NO_2 emission ~10 ppm	300^oC, 330 ppm NH_3 and 3% O_2	Satisfactory performance

Considering the overall performance, the V-Ti-W catalyst stands out. Though Cu-ZSM-5 does have marginally lower ammonia slip and N_2O and NO_2 emission, the NO_x conversion drops

with increasing inlet oxygen concentration in the applicable range. For the V-Ti PLIC catalyst, increase in NO_x conversion is accompanied by an unacceptable increase in ammonia slip, which is also the case with the V catalyst.

The expressions obtained for each of the catalysts predict the conversion performance satisfactorily. The average error for the applicable range is computed as 12.8% for CU-ZSM-5 catalyst, 8.8% for V catalyst, 6.2% for V-Ti PLIC catalyst and 8% for V-Ti-W catalyst that is acceptable for industrial applications.

The expression provides a way to control the catalytic converter operation by varying the operating parameters such as temperature, reducing agent concentration (ammonia in this case) and the oxygen concentration. The concentrations and the temperature can be controlled to reduce the NO_x emission to acceptable levels without causing secondary emissions, and with minimum use of reducing agent. The expression also provides a way to efficiently design the catalytic converter. The catalytic converters use precious metals and are prone to aging, contamination and poisoning hence it is imperative to design the converter optimally with as little use of the precious metals as possible. Here it may be noted that Cu-ZSM-5 is a copper based catalyst and is relatively inexpensive. The results of the modeling are summarized in table 9.2.

Table 9.2 Summary of Modeling Results

Catalyst	Temperature range	Rate Expression	Average Error
Cu-ZSM-5	(225-500^{o}C)	$R = 240.5\ e^{(-4.744/RT)}\ [NH_3]^{0.584}\ [O_2]^{0.003}$	12.8%
V	(250-400^{o}C)	$R = 1183.1\ e^{(-3.486/RT)}\ [NH_3]^{0.233}\ [O_2]^{0.071}$	8.8%
V-Ti PILC	(250-400^{o}C)	$R = 187.7\ e^{(-2.515/RT)}\ [NH_3]^{0.584}\ [O_2]^{0.003}$	6.2%
V-Ti-W	(200-350^{o}C)	$R = 183.1\ e^{(-0.0249/RT)}\ [NH_3]^{0.255}\ [O_2]^{0.019}$	8%

It is recommended that the reaction mechanism for the SCR process be investigated in detail. A thorough understanding of the reaction mechanism would facilitate higher NO_x reduction without increasing the secondary emissions such as ammonia, N_2O or NO_2. This would be achieved by altering the catalyst and the process so as to promote some reactions and inhibit some of them. Also if the kinetic data (rate constant, activation energy, heat of the reaction etc.) for all the reactions is available, a comprehensive modeling of the SCR process can be performed.

NOMENCLATURE

ΔH	Heat of the reaction
a(x)	Catalytic surface area per unit reactor volume
BET	Brunauer_/Emmett_/Teller
C	Concentration
D	Diffusion constant
E_a	Activation energy for a reaction
g	Acceleration due to gravity
h	Heat transfer coefficient
HC	Hydrocarbons
j	Rate of diffusion
Le	Lewis number
M	Molecular weight
n	Number of moles
N_2O_{out}	N_2O concentration after SCR
NH_{3in}	Inlet NH_3 concentration
NH_{3out}	NH_3 concentration after SCR
NO_{2out}	NO_2 concentration after SCR
NO_{in}	Inlet NO concentration
NO_{out}	NO concentration after SCR
NO_x	Oxides of Nitrogen (NO, NO_2)
Nu	Nusselt number
O_{2in}	Inlet O_2 concentration
p	Partial pressure
PM	Particulate matter
Pr	Prandlt number
R	Universal gas constant
r	Rate of reaction, radial co-ordinate
Re	Reynolds number
S	Geometric surface area per unit reactor volume
Sh	Sherwood number
SV	Space velocity (ratio of volumetric flow rate to the catalyst volume)
T	Temperature
t	Time
u	Velocity

V	Volume
w	Mass flow of exhaust gas
X*	Graetz number
x,y	Planar co-ordinate at any z
Y	Mass fraction
z	Axial co-ordinate
ε	Void fraction of the monolith
λ	Conductivity
ρ	Density

Subscripts:	
c	Convection
g	Gas
h	Hydraulic
i, k	for any species, variable
In	At the inlet of the catalytic converter
m	Mass-transfer
Out	At the outlet of the catalytic converter
r	Radiation
s	Solid
w	Wall
x,y,z,r	Co-ordinates
Superscripts:	
i	For a cell under consideration

REFERENCES

[1] T. Cheung, S. K. Bhargava, M. Hobday, K. Foger, Journal of Catalysis, 158 (1996) 301.

[2] J. E. Mincy, in: Fourteenth National Industrial Energy Technology Conference, Houston, TX (1992) 173.

[3] National Aeronautics and Space Administration (NASA) Facts, Cape Girardeau, MO (1998) NF–198.

[4] Chemical Information Manual, U.S. Department of Labour [sic], Occupational Safety and Health Administration, Directorate of Technical Support, Government Institutes, Inc., May 1988.

[5] Environmental Protection Agency, http://www.epa.gov/air/clearskies/basic.html, Accessed: 04/05/2004.

[6] A. G. Clarke, M. Radojevic, R. M. Harrison, Atmospheric acidity : sources, consequences, and abatement, Elsevier, London (1992).

[7] J. B. Heywood, Internal Combustion Engine Fundamentals, McGraw-Hill, New York (1988).

[8] Process Simulations Ltd., http://www.psl.bc.ca/downloads/ftp/kilns/Model-NOx.pdf , Accessed: 02/08/2003.

[9] P. Glarborg, J. A. Miller, R. J. Kee, Combust. Flame, 65 (1986) 177.

[10] The Edinburgh Collection of Open Software for Simulation and Education, http://ecosse.org/jack/Projects/proj2000/degussa/degussa.html , Accessed: 04/05/2004.

[11] J. A. Miller, C. T. Bowman, Prog. Energy Combust. Sci., 15 (1989) 287.

[12] P. Eastwood, Critical Topics in Exhaust Gas After-treatment, Research Studies Press, London (2000).

[13] European Fertilizer Manufacturers Association, http://www.efma.org/Publications/BAT%202000/Bat02/section06.asp, Accessed: 04/05/2004.

[14] R. K. Lyon, J. E. Hardy, Ind. Eng. Chem. Fundam. 25 (1986) 19.

[15] C. D. Holland, R. G. Anthony, Fundamentals of chemical reaction engineering, Prentice-Hall (1979).

[16] D. K. S. Chen, E. J. Bissett, S. H. Oh, D. L. V. Ostrom, SAE 880282 (1998).

[17] R. H. Heck, J. Wei, J. R. Katzer, American Institute of Chemical Engineers 22-3 (1976) 477.

[18] J. C. W. Kuo, C. R. Morgan, H. G. Larson, SAE, Automotive Engineering Congress 710289 (1991).

[19] Reaction Design Inc., http://chemkin.com/support/members/documents/chemkin/creslaf.pdf, Accessed: 04/05/2004.

[20] J. Eng, C. H. Bartholomew, Journal of Catalysis 171 (1997) 14.

[21] K. C. Byong, Journal of Catalysis 142 (1993) 418.

[22] E. Tronconi, P. Forzatti, M. J. P. Gomes, S. Malloggi, Chemical Engineering Science 47 (192) 2401.

[23] H. J. Chae, S. T. Choo, H. Choi, I. Nam, Industrial Engineering Chemical Resources *39* (2000) 1159.

[24] E. S. Borisova, A. S. Noskov, L. N. Bobrova, Catalysis Today 38 (1997) 97.

[25] R. Willi, M. Maciejewski, U. Gobel, R. A. Koppel, A. Baiker, Journal of Catalysis 166 (1997) 356.

[26] S. A. Stevenson, J. C. Vartuli, C. F. Brooks, Journal of Catalysis 190 (2000) 228.

[27] S. Gupta, M.S. Thesis, Texas A&M University, College Station, Texas, 2003.

[28] H. Oh, M.S. Thesis, Texas A&M University, College Station, Texas, 2004.

[29] D. W. Breck, Zeolite Molecular Sieves: Structure, Chemistry and Use, Wiley, New York (1974).

[30] S. C. Larsen, A. Aylor, A. T. Bell, J. A. Reimer, J. Phys. Chem. 98 (1994) 11533.

[31] T. Sun, M. D. Fokema, J. Y. Ying, Catalysis Today 33 (1997) 251.

[32] M. Konno, T. Chikahisa, T. Murayama, M. Iwamoto, Society of Automotive Engineers, SAE 920091 (1992).

[33] F. Roozeboom, J. A. Moulijn, J. Medema, P. J. Gellings, J. Phys. Chem., 84 (1980) 2783.

[34] I .E. Wachs, B. M. Weckhuysen, Applied Catalysis A: General 157 (1997) 67.

[35] Sung-Won Ham, In-Sik Nam, The Royal Society of Chemistry 2002, “Catalysis,” Volume 16, senior reporter, C. Kemball; reporters A. D. Caunt, London: Chemical Society, c1977.

[36] R. Q. Long, R. T. Yang, Applied Catalysis B: Environmental, 24 (2000) 13.

[37] Ho J. Chae, In-Sik Nam, Hee S. Yang, S. L. Song,, Ik Do Hur, Journal of Chemical Engineering of Japan 34 No 2, (2001) 148.

[38] R. M. Heck, R. J. Farrauto, with S. T. Gulati, “Catalytic Air Pollution Control: Commercial Technology,” New York: Wiley-Interscience, c2002.

[39] S. T. Choo, Y. Gil Lee, In-Sik Nam, Sung-Won Ham,, Jeong-Bin Lee, Applied Catalysis A: General 200 (2000) 177.

[40] S. N. Orlik, V. A. Ostapyuk, M. G. Martsenyuk-Kurkharuk, Kinet. Katal 36 (1995) 284.

[41] (a) M. Inomata, A. Miyamoto, Y. Murakami, J. Catal. 62 (1980) 140; (b) A. Miyamoto, K. Kobayashi, M. Inomata, Y. Murakami, J. Phys. Chem. 86 (1982) 2945; (c) M. Inomata, A. Miyamoto, T. Ui, K. Kobayashi, Y. Murakami, Ind. Eng. Chem. Prod. Res. Dev. 21 (1982) 424.

[42] W. C. Wong, K. Nobe, Ind. Eng. Chem. Prod. Res. Dev. 23 (1984) 564.

[43] I. Nam, J. W. Eldridge, I. R. Kittrell, Ind. Eng. Chem. Prod. Res. Dev. 25 (1986) 1186.

[44] J. W. Beekman, L. L. Hegedus, Ind. Eng. Chem. Res. 30 (1991) 969.

[45] L. J. Pinoy, B.G. Massart, L. H. Hosten, in: Proceedings of the First World Congress on Environmental Catalysis, Pisa, 1995, SCI, Rome 1995, p. 215.

[46] L. J. Pinoy, L. H. Hosten, Catal. Today 17 (1993) 151.

[47] J. Marangozis, Ind. Eng. Chem. Res. 31 (1992) 987.

[48] T. Komatsu, M. Nunokawa, S. Moon, T. Takahara, S. Namba, T. Yashima, J. Catal. 148 (1994) 427.

[49] D. J. Cole, C. F. Cullis, D. J. Hucknall, J. Chem. Soc., Farady Trans. 1 72 (1976) 2185.

[50] G. Tuenter, W. F. van Leeuwen, L.J.M. Snepvangers, Ind. Eng. Chem. Prod. Res. Dev. 25 (1986) 633.

[51] C. U. I. Odenbrand, S. T. Lundin, L. A. H. Andersson, Appl. Catal. 18 (1985) 335.

[52] H. G. Lintz, T. Turek, Appl. Catal. A 85 (1992) 13.

[53] V. Tufano, M. Turco, Appl. Catal. B 2 (1993) 9; M. Turco, L. Lisi, R. Pirone, P. Ciambelli, Appl. Catal. B 3 (1994) 133.

[54] C. U. I. Odenbrand, P. L. T. Gabrielsson, J. G. M. Brandin, L.A.H. Andersson, Appl. Catal. 78 (1991) 109.

[55] N. Y. Topsùe, T. Slabiak, B. S. Clausen, T. Z. Srnak, J. A. Dumesic, J. Catal. 134 (1992) 742.

[56] P. Forzatti, L. Lietti, Heterogeneous Chem. Rev. 3 (1996) 33.

[57] J. W. Beekman, L. L. Hegedus, Ind. Eng. Chem. Res. 30 (1991) 969.

[58] L. J. Pinoy, B. G. Massart, L. H. Hosten, in: Proceedings of the First World Congress on Environmental Catalysis, Pisa, 1995, SCI, Rome, 1995, p. 215.

[59] L. J. Pinoy, L. H. Hosten, Catal. Today 17 (1993) 151.

[60] J. Marangozis, Ind. Eng. Chem. Res. 31 (1992) 987.

[61] E. Tronconi, P. Forzatti, AIChE J. 38 (1992) 201.

[62] M. Takagi, T. Kowai, M. Soma, T. Onishi, K. Tamaru, J. Catal. 50 (1977) 441.

[63] H. Bosch, F. J. J. G. Janssen, F. M. G. van den Kerkhof, J. Oldenziel, J. G. van Ommen, J. R. H. Ross, Appl. Catal. 25 (1986) 239.

[64] E. T. C. Vogt, A. J. van Dillen, J. W. Geus, F. J. J. G. Janssen, F. van den Kerkhof, J. Catal. 119 (1989) 269.

[65] (a) F. Janssen, F. Van den Kerkhof, H. Bosch, J.J. Ross, Phys. Chem. 91 (1987) 5931; (b) F. Janssen, F. Van den Kerkhof, H. Bosch, J.J. Ross, Phys. Chem. 91 (1987) 6633; (c) G. Busca, L. Lietti, G. Ramis, F. Berti, Applied Catalysis B: Environmental 18 (1998) 33

[66] B. L. D. Duffy, H. E. Curry Hyde, N. W. Cant, P. F. Nelson, J. Phys. Chem. 98 (1994) 7153.

[67] (a) U. S. Ozkan, Y. Cai, M. W. Kumthekar, J. Catal. 149 (1994) 375; (b) U.S. Ozkan, Y. Cai, M.W. Kumthekar, J. Catal. 149 (1994) 390; (c) U.S. Ozkan, Y. Cai, M.W. Kumthekarm, J. Phys. Chem. 99 (1995) 2363.

[68] K. Otto, M. Shelef, J. T. Kummer, J. Phys. Chem. 74 (1970) 2690.

[69] C. U. I. Odenbrand, L. A. H. Anderson, J. G. M. Brandin, S. T. Lundin, Appl. Catal. 27 (1986) 363.

[70] R. M. Heck, J. M. Chen, B. K. Speronello, L. Morris, in: J. N. Armor (Ed.), Environmental Catalysis, ACS Symposium Series, vol. 552, American Chemical Society, Washington, 1994, p. 215.

[71] (a) H. Bosch, F.J. Janssen, Catal. Today 2 (1988) 369; (b) F.J. Janssen, in: G. Ertl, H. KnoÈzinger, J. Weitkamp (Eds.), Handbook of Heterogeneous Catalysis, VCH Verlagsgesellschaft mbH, Weinheim, 1997, p. 1633.

[72] S. M. Cho, Chem. Eng. Prog. 90(I) (1994) 39.

[73] J. J. P. Biermann, F.J. J. P. G. Janssen, Appl. Catal. A 86 (1992) 165.

[74] M. de Boer, H. Huisman, R.J.M. Mos, R.G. Leliveld, A.J. van Dillen, J.W. Geus, Catal. Today 17 (1993) 189.

[75] A. Wollner, F. Lange, H. Schmelz, H. KnoÈzinger, Appl. Catal. A 94 (1993) 181.

[76] J. E. Germain, R. Perez, Bull. Soc. Chim. France (1972) 2042.

[77] N. I. Il'chenko, G.S. Golodets, J. Catal. 39 (1975) 57.

[78] Y. Kasaki, A. Kiyamoto, Y. Murakami, Bull. Chem. Soc. Jpn. 52 (1979) 617.

[79] W. B. Williamson, D. R. Flenige, J. H. Lunsford, J. Catal. 37 (1975) 258.

[80]] F. Cavani, F. TrifiroÁ , Catal. Today 4 (1989) 253.

[81] U. S. Ozkan, Y. Cai, M. W. Kumthekar, L. Zhang, J. Catal. 142 (1993) 182.

[82] K. V. Ramanujachari, C. S. Swamy, J. Catal. 93 (1985) 279.

[83] T. P. Melia, J. Inorg. Nucl. Chem. 27 (1965) 95.

[84] M. W. Kumthekar, U. S. Ozkan, Appl. Catal. A 151 (1997) 289.

[85] M. deBoer, A.J. vanDillen, D.C. Koningsberger, F.J.J.G. Janssen, T. Koerts, J.W. Geus, in: P. Ruiz, B. Delmon (Eds.), New Developments in Selective Oxidations by Heterogeneous Catalysis, Elsevier, Amsterdam, 1992, p. 133.

[86] V. Indovina, M. Occhiuzzi, P. Ciambelli, D. Sannino, G. Ghiotti, F. Prinetto, in: J.W. Hightower, W.N. Delgass, E. Iglesia, A.T. Bell (Eds.), Proceedings of the 11th International Congress on Catalysis - 40th Anniversary, Elsevier, Amsterdam, 1996, p. 691.

[87] G. Busca, Catal. Today 27 (1996) 457.

[88] L. Lietti, J.L. Alemany, P. Forzatti, G. Busca, G. Ramis, E. Giamello, F. Bregani, Catal. Today 29 (1996) 143.

[89] G. Busca, G. Centi, L. Marchetti, F. Trifiro, Langmuir 2 (1986) 568; G. Busca, Langmuir 2 (1986) 577; G. Busca, Mater. Chem. Phys. 19 (1988) 157.

[90] Yu.M. Belokopytov, K.M. Kolyvenko, S.V. Gerei, J. Catal. 60 (1979) 1.

[91] M. Inomata, K. Mori, A. Miyamoto, T. Ui, Y. Murakami, J. Phys. Chem. 87 (1983) 754.

[92] H. Miyata, Y. Nakagawa, T. Ono, Y. Kubokawa, Chem. Lett. (1983) 1141.

[93] R. A. Rajadhayaksha, H. KnoÈzinger, Appl. Catal. 51 (1989) 81.

[94] G. Ramis, G. Busca, F. Bregani, P. Forzatti, Appl. Catal. 64 (1990) 259; G. Ramis, G. Busca, F. Bregani, P. Forzatti, in: S. Yoshida, N. Takezawa, T. Ono (Eds.), Catalytic Science and Technology, vol. 1, Kondasha, Tokyo, 1991, p. 189

[95] N. Y. Topsùe, J. Catal. 128 (1991) 499.

[96] T. J. Dives, C. H. Rochester, A. M. Ward, J. Chem. Soc., Faraday Trans. 87 (1991) 1611.

[97] L. Lietti, P. Forzatti, G. Ramis, G. Busca, F. Bregani, Appl. Catal. B 3 (1993) 13.

[98] H. Schneider, S. Tschudin, M. Schneider, A. Wokaun, A. Baiker, J. Catal. 147 (1993) 5.

[99] R. J. Willey, C. T. Wang, J. B. Peri, J. Non-Cryst. Solids 186 (1995) 408.

[100] G. Ramis, Y. Li, G. Busca, Catal. Today 28 (1996) 373.

[101] S. Hu, S.P. Harris, J. Catal. 158 (1996) 199.

[102] (a) G. Busca, H. Saussey, O. Saur, J.C. Lavalley, V. Lorenzelli, Appl. Catal. 14 (1985) 245; (b) G. Ramis, G. Busca, V. Lorenzelli, P. Forzatti, Appl. Catal. 64 (1990) 243.

[103] J. A. Odriozola, J. Soria, G.A. Somorjai, H. Heinemann, J. F. Garcia de la Banda, M. Lopez Granados, J.C. Conesa, J. Phys. Chem. 95 (1991) 240.

[104] R. B. Bjorklund, C. U. I. Odenbrand, J. G. M. Brandin, L. A. H. Andersson, Bo Liedberg, J. Catal. 119 (1989) 187.

[105] F. J. J. G. Janssen, J. Therm. Anal. 37 (1991) 1281.

[106] T. Z. Srnak, J. A. Dumesic, B. S. Clausen, E. Tornquist, N.-Y. Topsùe, J. Catal. 135 (1991) 246.

[107] K. Hadjiivanov, D. Klissurski, G. Ramis, G. Busca, Appl. Catal. B 7 (1996) 251.

[108] M. Shelef, J. T. Kummer, Chem. Eng. Prog. Symp. Ser. No. 115 67 (1971) 74.

[109] D. V. Pozdnyakov, V. N. Filimonov, Kinet. Katal. 14 (1973) 760.

[110] H. C. Yao, M. Shelef, in: R. L. Klemesh, J. G. Larson (Eds.), The Catalytic Chemistry of Nitrogen Oxides, Plenum Press, New York, 1975, p. 45.

[111] G. Busca, V. Lorenzelli, J. Catal. 72 (1981) 303.

[112] E. Escalona, G. Platero, A. Spato, Zecchina, J. Chem. Soc., Faraday Trans. 1 81 (1985) 1283.

[113] M. C. Kung, H. H. Kung, Catal. Rev.-Sci. Eng. 27 (1985) 425.

[114] J. A. Odriozola, H. Heinemann, G. A. Somorjai, J. F. Garcia de la Banda, P. Pereira, J. Catal. 119 (1989) 71.

[115] L. Lietti, P. Forzatti, J. Catal. 147 (1994) 241.

[116] L. Lietti, Appl. Catal. B 10 (1996) 281.

[117] M. Takagi-Kawai, M. Soma, T. Onishi, K. Tamaru, Can. J. Chem. 58 (1980) 2132.

[118] H. Niiyama, K. Murata, H.V. Can, E. Echigoya, J. Catal. 62 (1980) 1.

[119] M. G. Gasior, J. Haber, T. Machej, T. Czeppe, J. Mol. Catal. 43 (1988) 359.

[120] G. T. Went. L.-J. Leu, A.T. Bell, J. Catal. 134 (1992) 479; G.T. Went, L.-J. Leu, S.J. Lombardo, A.T. Bell, J. Phys. Chem. 96 (1992) 2235; G.T. Went, L.-J. Leu, R.R. Rosin, A.T. Bell, J. Catal. 134 (1992) 492.

[121] M. Kantcheva, V. Bushev, D. Klissurski, J. Catal. 145 (1994) 96.

[122] (a) N. Y. Topsùe, Science 265 (1994) 1217; (b) N. Y. Topsùe, H. Topsùe, J. H. Dumesic, J. Catal. 151 (1995) 226; (c) N. Y. Topsùe, H. Topsùe, J. H. Dumesic, J. Catal. 151 (1995) 241.

[123] Postech Environmental Catalysis Laboratory (PECL), Department of Chemical Engineering Pohang University of Science and Technology, Korea, http://cedb.postech.ac.kr/~envcat/, Accessed: 04/05/2004.

[124] KWH Catalysts, Inc., http://www.k-w-h.com/start-e.html, Accessed: 04/05/2004.

APPENDIX

The Cu-ZSM-5 catalyst sample was obtained from Johnson Matthey Technology Center, UK, upon contacting Mr. Stan Golunski, Research Leader, Automotive and Process Catalysis. Table A.1 lists further details of the sample.

Table A.1 Cu-ZSM-5 Catalyst Sample Details

Material	Ceramic honeycomb with square-cells
Cell density (cells/in^2)	413
Sample density (Kg/m^3)	605
Cu-loading, % (by weight)	5
Si:Al ratio	80:1
BET surface area (m^2/gm)	345
Operating temperature (advised)	300–550°C

The vanadium based catalyst sample was obtained from Sud-Chemie Prototech Inc., USA, upon contacting Mr. Yinyan Huang, R&D Manager. Table A.2 lists further details of the sample.

Table A.2 Vanadium Based Catalyst Sample Details

Material	Cordierite ceramic honeycomb with square-cells Cordierite ceramic: 40–60 wt% Vanadium pentoxide (V_2O_5): <1 wt%
Cell density (cells/inch^2)	230
Sample density (Kg/m^3)	636
Geometric surface area / Geometric volume (cm^2/cm^3)	21.34
Operating temperature (advised)	< 500°C

V_2O_5/Ti-PILC honeycomb catalyst sample was provided by Postech Environmental Catalysis Laboratory (PECL) [123] in Department of Chemical Engineering Pohang University of Science and Technology in Korea. Table A.3 lists the details of the sample. Vanadium content in each catalyst was analyzed by Neutron Activation Analysis (NAA).

Table A.3 V_2O_5/Ti-PILC Honeycomb Monolithic Catalyst Sample Details

Material	Vanadia- titania-pillared interlayer clay (PILC) honeycomb monolithic catalyst
Ti content	35 wt.%
BET surface area	110 m2/g
Height × Width × Length	11 cm × 11 cm × 13 cm
Cell size	3.8 mm × 3.8 mm
Inorganic binder	10 wt.%
Vanadium content	2.35 wt. %

V_2O_5-WO_3/TiO_2 honeycomb monolithic catalyst sample was provided by KWH Catalysts, Inc. [124], USA. Table A.4 lists the details of the sample.

Table A.4 V_2O_5-WO_3/TiO_2 Honeycomb Monolithic Catalyst Sample Details

Material	Tetragonal-shaped square-channel titania-vanadia-tungsten based honeycomb monolithic catalyst
Appearance	Dark-green/gray color
Specific gravity	1.8
pH (potential of hydrogen)	5
Specific surface area	1,015 m2/m3
Height × Width × Length	6 inches × 6 inches × 11 inches
Cell size	(1/3) cm × (1/3) cm
Operating temperature (advised)	< 430 ˚C
Other properties	Toxic and odorless

VITA

Giriraj Sharma was born on April 23, 1980 in Gwalior, India. He enrolled in mechanical engineering at the Indian Institute of Technology (IIT), Bombay in the Fall of 1998 and received his Bachelor of Technology degree in the Summer of 2002. He worked as an Intern at the Indian Smelting and Refinery Company, Bombay in 2001. He enrolled at Texas A&M University in the Fall of 2002 and received a Master of Science in mechanical engineering in the summer of 2004. Giriraj Sharma can be reached at: giriraj_sharma@hotmail.com. His permanent address is: 37 Shakuntala Puri, Thatipur, Gwalior, India 474011.